Project Title:	ECOPOTENTIAL: IMPROVING FUTURE ECOSYSTEM BENEFITS THROUGH EARTH OBSERVATIONS
Project number:	641762
Project Acronym:	ECOPOTENTIAL
Proposal full title:	IMPROVING FUTURE ECOSYSTEM BENEFITS THROUGH EARTH OBSERVATIONS
Type:	Research and innovation actions
Work program topics addressed:	SC5-16-2014: "Making Earth Observation and Monitoring Data usable for ecosystem modelling and services"

Deliverable No: 6.1

Methods in Earth Observation-based modelling

Version:	v1
Main Authors:	CERTH, CNR, CREAF, DELTARES, EBD-CSIC, EPFL, FORTH, ICETA-INBIO, IST, POLIMI, UFZ, UNIVLEEDS

This project has received funding from the *European Union's Horizon 2020 research and innovation program* under grant agreement No

Table of Contents

1. Executive summary

Ecosystem models are fundamental tools to achieve a deeper understanding of the spatiotemporal dynamics of both marine and terrestrial environments. The development of mathematical models reproducing variables describing an ecosystem is useful to pursuit several different tasks, from improving the monitoring of the system filling the spatiotemporal gaps that are frequently present in the measured data to computing short- and long- term forecasts of the system dynamics, from assessing the uncertainty associated with the observations to evaluating the system response under different management strategies. Two major approaches to build the computational core of available models can be identified. Models in the first group are based on the statistical relationships between the simulated variables and the climatic and environmental measurements, also called predictors. Species Distribution Models (SDMs) and niche models are among these data-driven models. The second group of models is based on the reproduction of the physical processes governing the system, thus computing the output by processing the observed environmental data through dynamical equations, referred to as process-based models.

The complexity of natural ecosystems pushes toward the development of models that consider several levels of environmental predictors and interplaying mechanistic processes. For example, the dynamics of marine ecosystems descends from numerous interactions between multiple entities such as nutrient concentrations, solar radiation, primary production, and hydrodynamic processes [1]. An accurate mathematical description of these complex systems requires the consideration of diverse parameters and functions, as well as careful calibration and validation of the model [2]. Process-based ecological modelling of marine and terrestrial environments often relies on the simultaneous use of different models, which combined are able to reproduce the main ecosystem features and account for the wide array of parameters, including hydrodynamic, morphological, and ecological components relevant to an ecological assessment [3]–[5]. Thus, the setup of an ecosystem model requires the accurate spatiotemporal characterization of the ecosystem under study by way of past and present environmental measurements, which are fundamental to accurately characterize the input and forcing data, model predictors, as well as initial conditions. The need for the assimilation of environmental measurements is further intensified by the diversity of indicators that are related to the ecosystem dynamics in conjunction with the more refined spatial and temporal resolution typically required to tackle increasingly complex questions posed by researchers, managers and stakeholders [5]. Since collecting in-situ data proves quite time-, cost-, and labour-intensive, it is recommended to exploit the ever-expanding list of ready-to-use RS data products.

RS products estimating climatic data, such as precipitation, air temperature, radiance, soil and water surface temperature, together with information on land cover and use, and the estimation of canopy properties, constitute crucial information that can be incorporated into ecological models at different stages of the modelling process (see Figure 1). Inspired by the seminal work of Plummer [6], the present deliverable D6.1 focuses on analysing how RS-data have been used in the literature to:

1. Improve the spatial description of marine and terrestrial variables, with particular attention to the useful predictors for SDMs (**Section 2**). In this context, we performed a qualitative literature review to analyse some important aspects that ecologists must consider when combining RS products with models for local applications, which included:

    - An overview of the available RS-based climate datasets of temperature, precipitation and radiance (e.g., TRMM, PERSIANN-CDR, and Heliosat (SARAH)) and their possible downscaling for local ecological models requiring spatial resolutions higher than 1 km (**Section 2.1**, main contributors: CNR, FORTH).

    - The review of the approaches available in the literature to compute RS-based ecological products (**Sections 2.2 - 2.4** main contributors: CERTH, FORTH).

    - An analysis of the RS products to guide SDMs at local scale (**Section 2.5**, main contributors: EBD-CSIC, FORTH) with applications of multi-sensor/multi-platform approaches (**Section 2.6**, main contributor: UFZ).

2. Assess the reliability of spatially-distributed model outputs, thus validating the model results. This is a fundamental step in the development of ecological models, where the comparison with in-situ data might

be inappropriate due to local heterogeneities and model resolution. Here, D6.1 reviewed how ecological models outputs have been compared to RS data, with the goal to analyse the possible strategies available to link EO data and ecological models (**Section 3**, main contributors: EPFL, ICETA-INBIO, POLIMI).

3. Analyse model forecast and reduce their uncertainty through data assimilation (DA) techniques. When performing real-time applications, RS data are essential to operationalize ecosystem models through the use of DA [7]. The incorporation of RS products into ecological models through suitable DA techniques typically results in a drastic improvement of model results, reduction of model uncertainty and, thus more reliable forecasts of the system dynamics. **Section 4** describes the main DA techniques presented in the literature and their applications for ecological purposes, identifying the DA platforms that are currently available to the modeller community. Particular attention has been dedicated to the limitations of these DA techniques, in particular to the description of the model and measurement uncertainties (main contributors: DELTARES, EPFL).

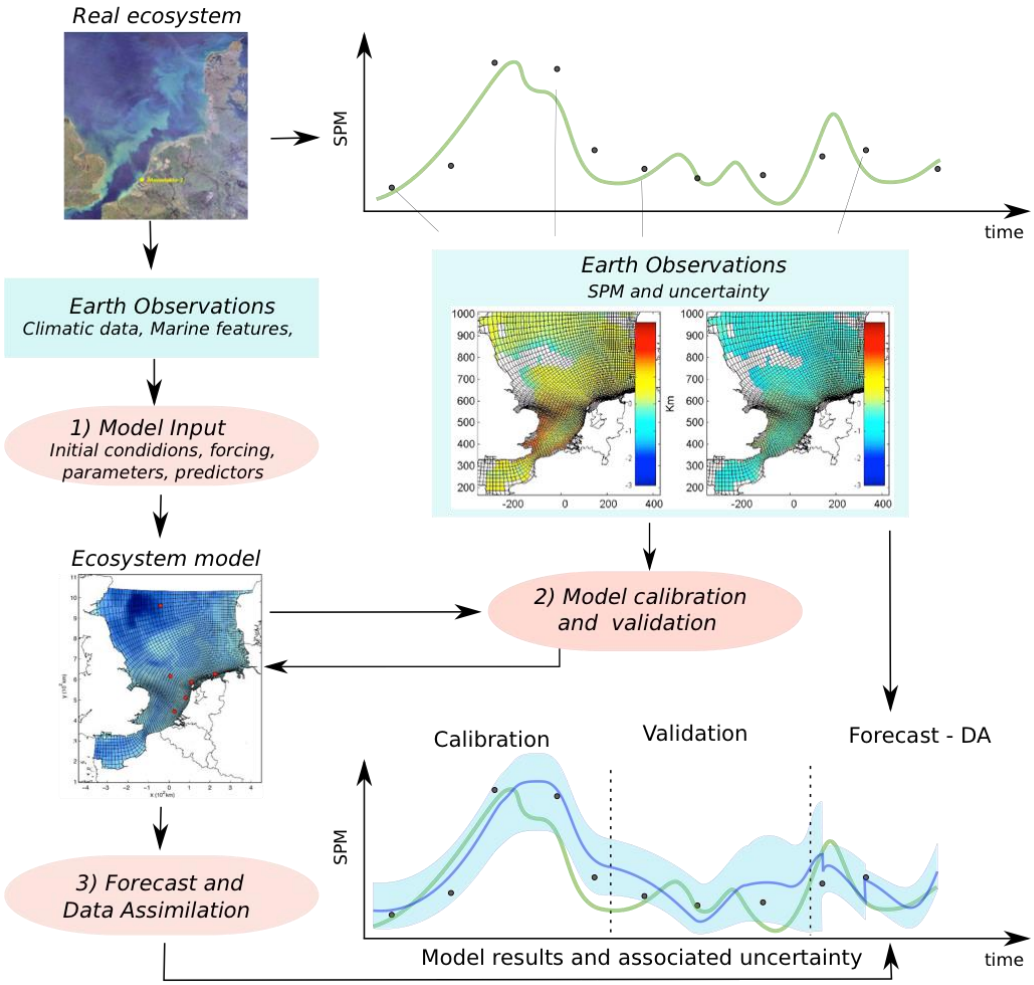

Figure 1 Schematic representation of the steps required when modeling the spatiotemporal variability of ecosystem variables, here represented by the suspended particulate matter (SPM) over the North Sea (see [8], [9]). EOs provide useful information at three levels of the modelling workflow: 1) EOs are input of the ecosystem model; 2) EO can be used to calibrate model parameters and in the validation phase, thus giving a feedback to the modeler; 3) during the operational forecast, the assimilation of EOs corrects the model prediction and reduce its uncertainty (maps from [8], [9]).

Table 1 Abbreviation and acronyms

AMSRE-E	Advanced Microwave Scanning Radiometer on the Earth Observing System
ANN	Artificial Neural Networks
ASAR	Advanced Synthetic Aperture Radar
ASCAT	Advanced SCATterometer
ALOS	Advanced Land Observing Satellite
ASTER	Advanced Spaceborne Thermal Emission and Reflection Radiometer
AVHRR	Advanced Very High Resolution Radiometer
BI	Brightness Index
BRDF	Bidirectional Reflectance Distribution Function
CASA	Carnegie-Ames-Stanford Approach
CAI	Cellulose Absorption Index
CCSM	Advanced Very High Resolution Radiometer Model
CMAP	Climate Prediction Center Merged Analysis of Precipitation
CMR	Clay Minerals Ratio
CI	Crust Index
CN	Carbon-Nitrogen model
ColI	Coloration Index
CRU	Climatic Research Unite
DAAC	Distributed Active Archive Centre
DART	Data Assimilation Research Testbed
DEM	Digital Elevation Model
DGVM	Dynamic Global Vegetation Model
ED2	Ecosystem Demography Biosphere model version 2
EO	Earth Observations
ECMWF	European Centre for Medium-Range Weather Forecasts
EnKF	Ensemble Kalman Filter
EOF	Empirical Orthogonal Function
ERS	European Remote Sensing
EVI	Enhanced Vegetation Index
EURO4M	European Reanalysis and Observations for Monitoring project
ET	Evapotranspiration
FAPAR/FPAR	Fraction of Absorbed Photosynthetically Active Radiation
FCover	Fraction of Vegetation Cover
FMR	Ferrous Minerals Ratio
GMED	Global Marine Environment Dataset
GMMS	Global Inventory Modelling and Mapping Studies
GORT	Geometric Optical Radiative Transfer model
GPCC	Global Precipitation Climatology Centre
GPCP	Global Precipitation Climatology Project
GPM	Global Precipitation Measurement
GPP	Gross primary production
HDVI	Hybrid Difference Vegetation Index
HLS	Harmonized Landsat-Sentinel-2 project
KF	Kalman Filter
IOR	Iron Oxide Ratio
LAI	Leaf Area Index
LIDAR	Light Detection and Ranging
LPJ	Lund-Potsdam-Jena model
LSM	Land Surface Model
LST	Land Surface Temperature
LUT	Look Up Tables
MARSPEC	Ocean Climate Layers for Marine Spatial Ecology project
MERRA	Modern-Era Retrospective Analysis for Research and Applications
MIMICS	Michigan Microwave Canopy Scattering model
MISR	Multi-angle Imaging SpectroRadiometer
MODIS	Moderate Resolution Imaging Spectroradiometer
NDII	Normalized Difference Infrared Index
NDLI	Normalized Difference Lignin Index
NDVI	Normalized Difference Vegetation Index
NDWI	Normalized Difference Water Index

NIR	Near Infrared
NPP	Net Primary Production
NSE	Nash-Sutcliffe Efficiency
OB	Ocean Biology
OpenDA	Open Data Assimilation
OpenMI	Open Model Interface
PALSAR	Phased Array type L-band Synthetic Aperture Radar
PCC	Phytoplankton Community Composition
PDAF	Parallel Data Assimilation Framework
PDF	Probability Density Function
PFT	Phytoplankton Functional Types
PFZ	Potential Fishing Zones
RI	Redness Index
RMSE	Root Mean Squared Error
RPV	Rahman-Pinty-Verstraete model
RS	Remotely sensed
RTnLS	RossThin-LiSparseReciprocal model
SAIL	Scattering by Arbitrary Inclined Leaves model
SAR	Synthetic Aperture Radar
SAVI	Soil-Adjusted Vegetation Index
SEVIRI	Spinning Enhanced Visible and InfraRed Imager
SIF	Solar-Induced chlorophyll Fluorescence
SMOS	Soil Moisture Ocean Salinity mission
SOM	Soil Organic Matter
SPM	Suspended Particulate Matter
SST	Sea Surface Temperature
SSS	Sea Surface Salinity
SWH	Significant Wave Height
SWI	Soil Water Index
SWIR	Short-wavelength infrared
TM	Thematic Mapper
TGI	Triangular Greenness Index
TRMM	Tropical Rainfall Measuring Mission
VegDRI	Vegetation Drought Response Index
VHR	Very High Resolution
VI	Vegetation Index
VIS	Visible
WDVI	Weighted Difference Vegetation Index

2. Remotely sensed products as drivers and predictors of ecological models

D. Pasetto[1], J. Bustamante[2], A. F. Cord[3], N. Chrysoulakis[4], A. Dittrich[3], C. Domingo[5], A. Karnieli[6], G. Kordelas[7], I. Manakos[7], E. Palazzi[8], D. Poursanidis[4], S. Terzago[8], G. Ziv[9]

[1]Laboratory of Ecohydrology, École Polytechnique Fédérale de Lausanne, Switzerland
[2]Estación Biológica de Doñana, Spanish National Research Council, Spain
[3]Department of computational Landscape Ecology, UFZ-Helmholtz Centre for Environmental Research, Leipzig, Germany
[4]Institute of Applied and Computational Mathematics, Foundation for Research and Technology Hellas, Greece
[5]CREAF, GRUMETS Research Group, Bellaterra, Barcelona, Spain
[6]Jacob Blaustein Institutes for Desert Research, Ben-Gurion University of the Negev, Israel
[7]Information Technologies Institute, Centre for Research and Technology Hellas, Greece
[8]Institute of Atmospheric Sciences and Climate, National Research Council, Turin, Italy
[9]School of Geography, University of Leeds, UK

Spatially-distributed ecological models for both terrestrial (e.g. SDMs, hydrological models, dynamic global vegetation models, carbon cycle models, …) and marine (hydrodynamic models, biogeochemical models, sediment transport models, …) applications require the accurate spatiotemporal characterization of the ecological system under study. Climatic data such as precipitation, air temperature, radiance, and soil surface temperature, together with information on land cover and use, and the estimation of canopy properties constitute crucial inputs for setting the initial conditions and dynamical forcing of ecological models. As highlighted by Plummer [6] at the beginning of the century, satellite based RS data have been of fundamental importance for the estimation of these system features, guaranteeing a global spatiotemporal coverage, long-term surveillance missions and since some years ago, for many missions (Landsat, Sentinel 1 and 2, Aqua, Terra, TRMM,…), free data access.

While several global process-based models are nowadays driven by RS data, especially in the field of climate forecasting, vegetation phenology and oceanography, the potentialities of combining ecological models and RS data for real-time monitoring and forecasting at local and regional scales are yet to be fully exploited. For example, vegetation indices (VIs), in particular the Normalized Difference Vegetation Index (NDVI), designed to allow spatial and temporal inter-comparisons of terrestrial photosynthetic activity and canopy structural variation, provide essential information to address a variety of research questions in ecology (see [10] and references therein). Many applications (e.g., modelling ecosystem dynamics), however, require such information at very high spatial and temporal resolution. This is certainly true in the case of the elaboration of vegetation maps based on RS data, a common area of research, in which, at least from a local perspective, it has been possible to use medium-resolution RS products since the launch of the Landsat-1 satellite in 1972. A simple search in Scopus with the term "vegetation map*" produced 3420 documents, of which 52% included terms related to RS data[1], and 22% included terms related to medium and high-resolution sensors (Landsat, MODIS, LIDAR). A similar search with "Species distribution model*", a topic that has received considerable attention in the ecological modelling scientific literature and that in general is quite specific and included in keywords, results in 3352 documents, but only 5% of these include terms related with RS data and less than 2% include terms related to medium or high resolution products.

In the literature, applications of RS data to terrestrial ecosystem models include the use of RS-derived maps of vegetation, land cover and land use into process-based models to improve estimates of primary production, for example through the Lund-Potsdam-Jena (LPJ) model [11], the Boreal Ecosystem Productivity Simulator (BEPS) [12], [13], and the Community Land Model (CLM) [14]. Coupled hydrological and vegetation models are frequently constrained by RS-based estimates of evapotranspiration, precipitation, soil moisture and snow cover to improve the system hydrological response (e.g. [15]–[18]), specially complex in semi-arid environments [19]. Nowadays RS VIs are becoming more and more used in SDMs (e.g., [20]–[23]) and in drought monitoring and forecasting on vegetation [24] for instance using the Vegetation Drought Response Index (VegDRI) [25] or the Vegetation Outlook [26].

[1] Research performed on 4 May 2017, with the terms “Remote sensing” or “Landsat” or “MODIS” or “AVHRR” or “LAI” or “NDVI” or “EVI” or “SAVI” or “LiDAR” or “SAR” or “Radar” or “Sentinel” or “SEVIRI”.

For marine ecosystems, the input required in marine models can range from wind velocities, atmospheric deposition of nutrients, wave height, a range of initialization conditions, and boundary fluxes; these are often as important as the numerical solvers which form the basis of process-based models [27]. Modellers often contend with interpreting spotty or extremely coarse data in order to introduce realistic boundary and forcing conditions for given model space, leading to the introduction of a substantial level of uncertainty into the model outputs [28]. Some of these boundary conditions can be generalized using averages or interpolations from long-term data sets and extrapolating system trends; however, increased measurement coverage would enhance the quality of such elements [29]. Alternatively, additional boundary information can be extracted from new sources of EO information and therefore can contribute to improving the model output. As highlighted by the detailed Klemas' review [30] about marine variables detectable from RS applications, several products are available on long temporal scales thanks to the longer-lived satellite programs (e.g. MODIS), with high resolution products being developed from the more recent missions (e.g. Sentinel-2 and Sentinel-3). This piece of information is essential when planning hind-casting activities, enabling one to ensure the availability of data with adequate temporal and spatial resolution, as well as forming the foundation for the planning of real-time operational or forecasting systems in the context of current and future planned satellite missions. An example of application is the use of RS measurements of SPM as input variable for various process-based ecological models which investigate primary and secondary production as well as nutrient cycling such as Delft-3D-GEM [31], MIRO&CO-3D, or ECO_MARS3D [32].

Although the availability of satellite-based Earth Observation (EO) data opens a wide range of possibilities for ecosystem modelling, some factors are still restricting research advances. This section analyses the following important topics that ecologists must consider when combining RS products with models for local applications:

1. *Climate products and downscaling*: while global RS climate datasets of temperature, precipitation and radiance exist (e.g., TRMM, PERSIANN-CDR [33], and Heliosat (SARAH) [34]), they are at resolutions that vary from 0.05 degree (about 5km at the equator) to 0.25 degree (27 km at the equator), which is still coarse for many local applications. In fact, ecological models at local scales usually require data at a spatial resolution higher than 1 km. Thus, the use of adequate downscaling techniques is in some cases mandatory, especially in mountain environments and in spatially-heterogeneous areas with regional to local climatic regimes affected by complex topography.
2. *RS-based ecological products*: several terrestrial and marine properties can be estimated from RS optical and radar data, and, thus, linked to the input components of ecological models. Modellers should be aware of the range of approaches available in the literature to translate the measured radiation in the input parameters for the model, their associated accuracy and the RS data required.
3. *RS data as predictors of SDMs*: RS products have been used to feed SDMs for both terrestrial and marine applications. For these goals, the use of multi-sensor/multi-platform approaches generating radiometrically homogeneous time series of data represent a crucial step to overcome some limitations of RS data, such as the scarcity of long time series (e.g., AVHRR, which started in 1981, requires a lot of pre-processing, few LANDSAT products are available since 1972, while MODIS series started only around 2000) and high temporal resolution (e.g. Landsat revisiting period is 16 days, Sentinel-2 revisiting period has been of 12 days up to now, but will improve to 5 days when combined with the data from Sentinel-2B).

2.1 Climate products and downscaling

Atmospheric data and climate variables are the main driving factors of most terrestrial ecological models, since they directly reflect the seasonality of the system and long-term trends, and they help quantifying the entity of extreme events. Several studies have been devoted to improve the estimation of surface climate variables from RS data, and the most relevant products are nowadays available in many repositories at a global scale with a near real-time release. For example, the Global Precipitation Measurement (GPM) project regularly issues near-real-time precipitation estimates. Land surface temperature/emissivity (LST), cloud cover [35], [36], and surface reflectance [37] can be obtained from MODIS database. Other climate products that can be estimated starting from MODIS reflectance data are the solar and net radiation [38], surface solar irradiance [39], relative humidity [40], surface water pressure and air temperature [41]. Potential and actual Evapotranspiration (ET) are key parameters for the

characterization of the water cycle, and has been estimated following different approaches, such as involving surface temperature and vegetation indexes from MODIS [42], [43]. ET estimates from 2000 to 2010 are available in the MODIS website, but at a coarse resolution. Ke et al. [44] proposed a possible approach to downscale MODIS ET products from 1 km to 30 m resolution using machine learning and data fusion techniques, maintaining a good agreement with in-situ measured ET.

In the following we focus our attention on the estimation of precipitation and LST.

2.1.1 Precipitation

Precipitation is one of the most dynamic components of the climate system and plays a key role in matter and energy exchange in Earth's water, atmosphere, and soil cycles. The amount of precipitation influences soil moisture, vegetation growth, and stream flow [45], [46] and quantifications of it are essential. Conventional ground measurements and RS estimates are two ways to accomplish this task. On the one hand, spatial interpolation of precipitation data from irregularly spaced weather stations is frequently used to obtain spatially continuous, gridded dataset. When available at a regional scale, as the Digital climatic atlas of the Iberian Peninsula [47], these datasets achieve a resolution lower than 200 m, while at global scale the resolution is about 1 km. Examples of rainfall datasets are DAYMET, PRISM and WorldClim, which have been compared in [48] as well as Chealsa, which is a satellite-based dataset [49]. Note that, especially at a global scale, the average distance among the surface stations used in gridded datasets such as WorldClim is much larger than 1 km, so the dataset resolution is derived by downscaling the data from a coarser grid through strong statistical assumptions (for example based on the relationship between precipitation and elevation) that can be satisfied locally but not necessarily globally. As a consequence, the reliability of such datasets depends on the density of surface observations, and it can be poor in areas where the network is sparse, mainly natural regions with difficult accessibility, far from urban and agricultural environments, and restrict temporal availability. In addition, datasets such as WorldClim provide only the average climatology on a give multi-annual time window, and they do not provide any information on temporal variability. On the other hand, satellite rainfall measurements are designed to cope with this limitation and can be used to generate spatially continuous precipitation datasets over large areas. A range of global and regional precipitation databases including rain gauge stations, satellites, and other observations exist, such as the merged in-situ and satellite Global Precipitation Climatology Project (GPCP) [50] providing data from 1979 until 2015 and its continuation, the Climate Prediction Center Merged Analysis of Precipitation (CMAP) [51] extending from 1979 to present; the Global Satellite Mapping of Precipitation Project [52], the Tropical Rainfall Measuring Mission (TRMM) which has been offering several rainfall products since 1997 with the first spaceborne precipitation radar [50], [53].

Among the main problems of satellite-based rainfall data products is the spatial heterogeneity, given that different satellites are used at different latitudes (i.e. GPCP or CMAP), and their generally coarse resolution (most of them around 2.5 deg – about 280 km at the equator); up to 2014 the TRMM datasets (http://trmm.gsfc.nasa.gov/) had one of the highest resolutions (up to 0.25 deg for the 3B42 and 3B43 products) available when referring to satellite-based rainfall products. TRMM is currently being replaced by the Global Precipitation Measurement (GPM) mission providing satellite precipitation data since 2014 at the resolution of 0.1 deg (about 11 km at the equator), together with a temporal frequency of three hours and a latency of 18 hours [54]. As GPM datasets were not available before 2014, several studies have been done in order to downscale the coarse precipitation data, for instance from TRMM products, using statistical or geostatistical methods and obtain high-resolution rainfall data [46], [55]–[60]. These methods use classic geostatistical analysis (interpolation methods using IDW, kriging, splines, etc.) and may include additional information from covariates, i.e. variables that are available at higher spatial resolution and explaining part of the spatial variability of the precipitation field. Typical covariates are RS geospatial variables like the vegetation indices (e.g., the normalized difference vegetation index, NDVI), the elevation or other parameters extracted from the Digital Elevation Models (DEMs) of the area or *in-situ* weather data. Small-scale precipitation data generated with these techniques can achieve spatial resolutions around 1 km or finer. Modellers have to keep in mind that, for precipitation, traditional statistical downscaling is less successful than for other variables like the temperature and other kinds of interpolation techniques are inadequate. Given the large spatial and temporal variability and high intermittency of precipitation fields, a particularly suited approach relies on stochastic methods instead (e.g., [61]). Stochastic downscaling aims at generating synthetic spatiotemporal precipitation data whose

statistical properties are consistent with the small-scale statistics of observed precipitation (known from e.g., radar measurements), based only on the knowledge of the large-scale precipitation field, either produced by a global or regional model or derived from coarse-scale observations such as satellite measurements. This approach has been proved successful in a climatological framework [62] where precipitation data from a hydrostatic regional climate model have been downscaled with the stochastic rainfall downscaling method called RainFARM [63] and compared to in-situ observations from a network of rain-gauge stations in the Piedmont and Valle d'Aosta regions (north-western Italy). Stochastic precipitation downscaling with possibly an orographic correction implemented can potentially improve the poor representation of the precipitation obtained from coarse resolution datasets and helps end users to assess the likely eco-hydrological/surface impacts of climate change.

Even if the majority of the original or the downscaled TRMM products have been primarily used as input to hydrological models [64], [65], such techniques have been employed also in *in-situ* data derived meteorological modelling [47] and ecological modelling, for example for SDMs [20].

Recent examples in this domain (e.g., [21], [49], [66]) show that RS rainfall data can provide a better insight when modelling the relationship between species and climate, despite the coarser resolution and shorter time period (e.g. 1998 – 2016 for TRMM) than other climatology such as the WorldClim database (1950 – 2000). Indeed, one of the aspects that have favoured the use of RS products and datasets in the past years has been their regular update, which allowed to promptly capture changes in climate. For instance, the WorldClim database provides the monthly climatology averaged over a 30-year long time period in the past (1961-1990) and two 20-year long time periods in the future (2041-2060 and 2061-2080) of a given set of climate variables and bioclimatic indices, but is not regularly updated. Contrary, RS-climate based products take advantage of cloud computing infrastructures being much easier to provide update datasets in a regular base as well as to provide products meaningful for the ecology, physiology and other factors that promote the niche of certain species or biogeochemical cycle. Today, most station-based datasets, such as the Climatic Research Unit (CRU), the Global Precipitation Climatology Centre (GPCC), the E-OBS gridded dataset, and the European Reanalysis and Observations for Monitoring project (EURO4M), have filled this gap with respect to RS data by connecting the weather stations to the servers and automatically obtaining continuous time coverage and regular updates.

When using satellite precipitation products the modellers should be aware of the errors related to these datasets. The recent study of Maggioni et al. [67], for example, analysed systematic and random error components of the TRMM precipitation, highlighting their dependence with the rainfall rates, and suggesting that future satellite bias adjustment procedures should account for this dependence.

2.1.2 Land surface temperature (LST)

LST is an important parameter that is highly responsive to surface energy fluxes and has become valuable to many disciplines, in particular for ecological modelling. Acquisition and monitoring of LST over extensive areas in a repetitive way was a complex challenge until the first EO research programs appeared. Satellite-based EO measurements allowed for a global spatial coverage for LST, but, as a result of the resolution trade-offs involved in using satellite data, the acquisition of satellite LST at high spatial and temporal resolutions is almost unfeasible as of today. This low spatial resolution results in a thermal mixture effect, where the resolution cells are larger than the thermal elements. Several attempts have struggled with the implementation of synergistic downscaling algorithms in order to achieve a high spatial and high temporal resolution [68]–[71]. MODIS and AVHRR are two satellite based LST sources which have been used for several modelling purposes like SDMs [72], [73]. The spatial resolution of LST product from AVHRR is 1.1 km while MODIS has several products from 1 km (MOD11A1 and A2) to 0.05 degree (about 5 km, MOD11C1, C2, and C3) depending on the user's needs for the analysis and modelling. As such, both sensors' data have been used in many case studies for analysis limited to a specific time window [74]–[76]. Additionally, MERRA (Modern-Era Retrospective Analysis for Research and Applications), and AMSRE-E (Advanced Microwave Scanning Radiometer on the Earth Observing System) are other two sources of land surface temperature at a coarser resolution (from 5 km to 56 km) that also are used in species distribution modelling ([21], [66] and references therein). In recent years, several attempts have been done to obtain LST at higher spatial resolutions (e.g., 30 m) maintaining the high temporal resolution of MODIS and AVHRR (4 and 1 times per day,

respectively). This is the so called LST downscaling approach [68], [77], which in this discipline is often viewed as equivalent to other terms such as sharpen [69], [78], [79] or disaggregate ([70], [71] and references therein). Although slight differences in the meanings of these terms may exist, all have the same objective, which is to enhance LST to a higher spatial resolution, while maintaining invariant the thermal radiance. Downscaled LST is a demanding product in terms of computation and accuracy assessment that is widely used in studies in the urban environment ([48] and references therein). However, LST derived directly from sensors like Landsat or ASTER, which are considered having a high spatial resolution, have been sparsely used in SDMs probably due to its low temporal resolution and to the fact that, for many species, air temperature is a predictor having higher correlation than LST with respect to the species presence. An example of SDM using LST is presented by Rödder et al. [80] where LST derived by Landsat is used as predictor in a SDM for sand lizards.

Finally, we would like to stress here that satellite LST measurements may differ by several degrees from near-surface air temperatures measured by surface stations [81]. Databases providing air temperature at the global scale include WorldClim [48], which relies only on *in-situ* data, CRU [82], which generates a combination approach of *in-situ* and RS data, and others. The EUSTACE project (https://www.eustaceproject.eu) is currently developing an approach to estimate near surface air temperature from satellite observations.

2.2 Recent remote sensing methods estimating leaf and canopy properties

Assessing the key parameters describing how soil and vegetation are contributing to surface photosynthesis, evapotranspiration, and net primary production over the domain is of crucial importance for terrestrial process-based models in order to compute energy, water and carbon fluxes, and biogeochemistry of vegetation, and for defining the biophysical predictor variables in SDMs. Most land surface models describe the spatial heterogeneity of the domain by subdividing the grid cells into different categories derived from land cover and land use maps. Then, different soil properties and parameters describing plant functional types are assigned to each category (see e.g. [83]). Another possible approach is to continuously characterize the vegetation based on its radiative response. Several RS products related to vegetation are directly available with a global coverage in many repositories. For example, MODIS provides estimates of LAI and Fraction of Absorbed Photosyntetically Active Radiation (FAPAR) at a resolution of 500 m and frequency of 8 days from 1999 to present. Similarly, thanks to SPOT-VGT (from 1998 to 2015) and PROBA-V (from 2013 to now) missions, also Copernicus Global Land Service computes LAI, FAPAR, fraction of vegetation cover (FCover) and other VIs at resolutions of 1 km (1999-2013) and 300 m (2014-now). Although these products have the clear advantage of passing an external quality control, their resolution might not be suitable to achieve the desired accuracy especially for local applications, thus forcing the modeller to research different alternatives. This section provides a review on recent approaches estimating biophysical and structural properties of vegetation, such as leaf and canopy properties using RS data at high spatial resolution. The reviewed methodologies have been subdivided into empirical, physically-based and semi-empirical approaches. To summarize the collected references, Table 2 provides an overview of the cited approaches. The references have been categorized according to the type of approach and the considered leaf/canopy property. This table gives per cited approach: (a) the sources of remote sensing data, (b) (when available) the performance/ accuracy divided into 0-25%, 25-50%, 50-75%, 75-100% quartiles (i.e. when a method has coefficient of determination 0.67 the performance is assumed to fall within the 50-75% quartile). The metrics usually adopted for estimating a model's accuracy are the Root Mean Square Error (RMSE) and the coefficient of determination (r^2) between the observed biophysical values and those predicted by the model. A symbol is added next to an approach, when auxiliary data, other than RS data, is used as input.

2.2.1 Empirical approaches

Empirical models directly link EO data with the biophysical variables of interest. In specific, the mathematical relationship (linear or non-linear) between the EO data and the biophysical variable is established by applying a function that minimizes the error between the modelled biophysical variable and the in-situ measured data [84].

Various empirical approaches to identify leaf and canopy properties from RS data have been proposed in the literature, including estimations of both biophysical parameters as water content, nitrogen, chlorophyll content and solar-induced chlorophyll fluorescence (SIF) and vegetation indices (VI) as NDVI.

RS derived VIs are some of the oldest tool in remote sensing to provide vegetation parameters. For instance, significant effort on estimating leaf and canopy water from RS data has been spent developing multispectral indices and establishing empirical relationships based on regression analysis with water content [85]–[89]. Among the many variations that exist, the most commonly used indices include NDVI [87], [89], normalized difference water index (NDWI) [87]–[90], and normalized difference infrared index (NDII) [85]–[88], [91]. A related index that quantifies the stress of plants to drought and wetness is the Moisture Stress Index (MSI) [92]. Numerous VIs exploited for monitoring LAI have been compared in [93]–[95]. The results in [93], [95] show that red-edge VIs are among the most efficient indices for estimating LAI. Red-edge bands have been also used to estimate chlorophyll [93], [96], foliar and canopy nitrogen [97]–[99]. Other recent approaches estimate canopy nitrogen using hyperspectral data from leaf or canopy surfaces [100], [101]. Indices estimated from broad bands at visible wavelengths, such as the triangular greenness index (TGI) [102], [103], are also used to estimate chlorophyll content. During the last years, it was proposed that SIF could be estimated by filling-in of near-infrared solar lines [104], [105] using data acquired from GOSAT satellite instrument. However, this instrument provides data in coarse spatial resolution and therefore SIF cannot be estimated yet at local scale.

The main sources of RS data, in the mentioned empirical approaches, are the MODIS [87], [95], Landsat [85], [86], [89], [95], [102], ASTER [85], AWiFS [85], RapidEye [94], [97], and Sentinel-2 [96], [99] satellite imagery and the AISA [93], AVIRIS airborne imagery [102], [103] (see Table 2).

The uncertainty associated with these products is still an unresolved matter. Uncertainty models for quantitative data derived from RS are slowly emerging. The representation of error and uncertainty information in data is essential and there are several approaches (based on parameter estimation, error propagation, etc.) being discussed (see Section 4.3).

Unfortunately, empirical models require extensive field measurements for calibration and the modelling results are site condition, time period and sensor dependent, thus constraining their applicability to other sites specific [106]. However, their reduced computational cost makes them an appreciated asset.

2.2.2 Physically-based approaches

Physically-based models attempt to describe the transfer and interactions of radiation inside the canopy based on physical laws and offer an explicit connection between the vegetation biophysical variables and canopy reflectance [107]. A strong advantage of physically-based models with respect to empirical models is their adaptability to a wide range of land cover situations, time periods and sensor configurations, while at the same time they do not require in-situ data to be acquired simultaneously with the EO data. Throughout the literature, physical models are validated and fine-tuned using field measurements in order to improve their accuracy with respect to real world conditions [108].

Recent efforts focus on the application of model inversion approaches for estimating plants biophysical parameters using remote sensing data. This is the case of [109]–[116], which invert the PROSAIL model [117], a popular leaf and canopy reflectance model combining the PROSPECT [118] and SAIL [119] models. Likewise, the recent REGFLEC model [120], combining PROSPECT, ACRM [121] and 6SV1 [122], has been also inverted in the literature [14], [120], [123]. Besides, three-dimensional models, such as DART [124], can be considered for cases where the canopy is heterogeneous and discontinuous. The DART model is inverted in [125], [126]. Reader could refer to the work in [127] (generated within the framework of the radiation transfer inter-comparison activity), which assesses the reliability of various canopy reflectance models to simulate the radiative properties of testing canopy scenes, to gain an overview on recent models. Most common techniques, for inverting canopy reflectance models using RS data, include numerical inversion procedures; look up tables (LUT) and artificial neural networks (ANN). Traditional inversion approaches iteratively refine physical model parameters, relying on optimization algorithms, such as the quasi-Newton algorithm [128], until the modelled reflectance resembles the measured one. LUT contain pre-

computed canopy biophysical parameter values for a given set of reflectance, and then, for a new data it interpolates among these pre-computed points. The forward mode method is an approach for computing the initial points in LUT [129]. On the other hand, ANN methods, such as the forward back propagation neural network [81], use a training set of data to learn the optimal relationship between canopy biophysical and structural input parameters and the output reflectance.

Leaf and canopy water content can be estimated using numerical inversion procedures [110], LUT [110], [111], and ANN [109], [130], as well as chlorophyll content of the leaf and/or at canopy level which can be estimated using LUT [14], [112], [113], [120], [123], [125], [131] and ANN [115]. Concerning the estimation of LAI, several methods use LUT [14], [112], [114]–[116], [120], [123], [126], [131] and ANN [112], [116].

The aforementioned physical approaches have performed model inversion based on remote sensing data from MODIS [114], Landsat [14], [113], [126], ASTER [114], RapidEye [112], Sentinel-2 [115], MERIS [131], LISS-3 [116], SPOT [123], and CHRIS/PROBA [125], [130] satellite imagery and the HyMap [111], MIVIS [110], and AVIRIS [126] airborne imagery (see Table 2)

2.2.3 Semi-empirical approaches

Semi-empirical models utilize aspects of both physical and empirical models. Specifically, they rely on some theoretical formulations derived from physical models, where several of the parameters are adjusted using empirical data (i.e. EO data).

This is the case of the semi-empirical bidirectional reflectance distribution function (BRDF) models, which have been used in the literature to estimate canopy height and canopy structure. Colgan et al. [132] fused LiDAR and hyperspectral data to estimate the spatial distribution of plant species in savannas and the semi-empirical Ross-Li BRDF model was applied to increase the accuracy of species prediction. Su et al. [133] stated that BRDF model parameters obtained by the inversion of the Rahman-Pinty-Verstraete (RPV) and the RossThin-LiSparseReciprocal (RTnLS) models against MODIS and the Multi-angle Imaging SpectroRadiometer (MISR) data products are useful in increasing the accuracy of estimating canopy structure, especially in semi-arid environments. The study in [134] retrieves forest canopy height through inversion of a simple geometric-optical model with MISR data. However, in [134] prior to inversion, soil understory background contribution is partly isolated using the Li-Ross BRDF model. The semi-empirical CLAIR model was used in [135] to establish the relationship between the Weighted Difference Vegetation Index (WDVI) index and LAI, so as to derive time-series of LAI. The work in [136] estimates the LAI in rice crops from SAR backscattering data using a semi-empirical model based on the the Michigan Microwave Canopy Scattering (MIMICS) model. A semi-empirical method to retrieve understories NDVI for sparse boreal forests from MODIS BRDF data is proposed in [137] and evaluated in [138]. Understory NDVI is useful for improving the estimation of overstory LAI. Since semi-empirical methods rely on empirical data to reduce the complexity of physical models, partial calibration may be required in order to apply these models to different conditions.

The review presented in this section confirms that there is a wide field of approaches dedicated to the estimation of soil, canopy and leaf properties using satellite and airborne imagery. These approaches can be useful for the detection of stress in vegetation and ecosystem degradation. Future satellite missions, providing imagery at higher spatial, spectral, and temporal resolution, are expected to favour the performance of these approaches. For instance, after so many years, the first EO system fully dedicated to monitor and quantify the impact of drought and its side-effects on natural ecosystems, the ECOSTRESS, has delivery date by 2018. The ECOsystem Spaceborne Thermal Radiometer Experiment on Space Station [139] will provide critical insight into plant-water dynamics and in how ecosystems change with climate.

2.3 Remote sensing and spectroscopy of soils

The characterization of soil properties and composition is relevant for both agricultural and hydrological applications. RS data have been useful to provide complementary spatial information to the geostatistical analysis based on in-situ data. Among the products of interest we recall soil moisture, albedo, soil texture [140], and indices related to organic and inorganic matter, as described in the recent review work of Mulder et al. [141].

2.3.1 Soil moisture

Despite its high spatial heterogeneity and the possible disturbance caused by the presence of vegetation, soil moisture up to a depth of 3-5 cm can be estimated over large grid cells from RS data, providing useful information for hydrological models. For example, the Soil Moisture Ocean Salinity (SMOS) mission measures soil moisture since 2010 with a relatively high accuracy (4% standard deviation) but a coarse spatial resolution of about 35-50 km. the Soil Water Index (SWI) provided by the Global Land Service of Copernicus quantifies the soil moisture with a resolution of 0.1 degrees (about 11 km) based on the Advanced SCATterometer (ASCAT) sensor aboard the EUMETSAT MetOp satellite. A slightly higher resolution (9 km) has been achieved thanks to the Soil Moisture Active Passive mission (SMAP) started in 2015 [142]. A complete review on the techniques used to derive soil moisture from RS measurements have been presented by Wang et al. [88]. Al-Yaari et al. [143] compared the global soil moisture products from SMOS and ASCAT in the years 2010-2012 against the results of a land surface model (MERRA-Land), highlighting that the vegetation density plays a key factor in the accuracy of RS soil moisture.

2.3.2 Broadband abiotic soil indices

During the past few decades, it has been shown that soil spectra across the visible (VIS), near infrared (NIR), and short wavelength infrared (SWIR) regions are characterized by significant chromophores (e.g., OH, Fe3+, CO3, and COOH) enabling the quantitative analysis of soil properties [144]–[146]. Consequently, broadband spectral indices have been used to characterize soil minerals and properties. The following are several examples of soil indices.

Several water indices that rely on the sensitivity of the SWIR bands (either 1.2 or 1.6 or 2.1 μm, denoted as SWIR1, SWIR2, and SWIR3, respectively) to water content while assuming the relative stability of the NIR region to this variable help the estimation of water content. The Coloration Index (ColI) is sensitive to ferric oxides [144] is a normalized index of the green and the red bands. The Redness Index (RI) indicates hematite minerals [144] and it is another mathematical manipulation of the same bands. The Clay Minerals Ratio (CMR) highlights hydrothermally altered rocks containing clay and alunite [147] is based on the ration between the SWIR2 and SWIR3 bands. The Ferrous Minerals Ratio (FMR) [147] is based on the ration between the SWIR2 and NIR bands. The Iron Oxide Ratio (IOR) indicates hydrothermally altered rocks that were oxidized due to iron-bearing sulphides [147] and based on the ration between the red and the blue bands.

The Crust Index (CI) aims at distinguishing between cyanobacteria-based crusty surfaces and the exposed substrate (e.g., bare sands) [148]. The CI takes advantage of a unique spectral feature of soil biogenic crust containing cyanobacteria. The special phycobilin pigment in cyanobacteria contributes to producing a relatively higher reflectance in the blue region than does the same type of substrate without biocrusts. Consequently, CI is a normalized index of the blue and the red bands.

2.3.3 Albedo

Broadband albedo is the ratio of the amount of electromagnetic radiation reflected by a surface to the amount of energy incident upon it. This is a unitless variable that is expressed as a fraction or percentage. Albedo may refer to the entire solar spectrum (0.3–4.5 μm) or merely to the visible portion (0.4–0.7 μm). Albedo is an important Earth surface variable for understanding the transfer of energy and mass from the terrestrial ecosystems to the atmosphere [149]. The Brightness Index (BI) quantifies the albedo over the VIS region using the three visible bands (i.e., blue, green, and red). Liang [150] presents regression analysis products for calculating albedo for the different sensors.

2.3.4 Soil organic matter (lignin, cellulose, and protein)

Soil organic matter (SOM) refers to the organic constituents in the soil. It includes undecayed plant and animal residues at various stages of decomposition, cells and tissues of soil organisms, and substances synthesized by soil organisms. It affects the soil quality through both its chemical and physical properties. In contrast to the chemical properties, and thus the spectra, of soils, rocks, and minerals that remain stable over the years, organic matter in

soils varies over time [151]. Therefore, the SOM spectrum should be related to the soil stage, including fresh, dry, or decomposed litter, with respect to the temporal domain [152]. Several studies have suggested diagnostic absorption features for various SOM components, all within the SWIR region [151], [153], [154]. Based on narrow spectral bands, the Cellulose Absorption Index (CAI) was introduced by Daughtry [155] and the Normalized Difference Lignin Index (NDLI) by Serrano et al. [156].

2.4 Remote sensing products for marine applications

Space- and air-borne RS products have been increasingly used for the estimation of marine environment features as time-, labor- and cost-effective alternatives to in situ measurements. There are several available datasets comprising of physical (temperature, salinity, currents, ice, winds, diffuse attenuation, etc.), biochemical (chlorophyll-a, primary productivity, pH, photosynthetically active radiation, etc.), and nutrient (calcite, silicate, nitrate, phosphate, oxygen, etc.) marine products, whose generation requires the exploitation of both RS observations and in situ measurements (Table 3).

2.4.1 International sources

Marine physical products elaborated in the Copernicus project are provided by the GLOBAL Ocean Sea Physical Analysis and Forecasting Product, which contains 3D potential temperature, salinity and currents information from top to bottom global ocean and 2D sea surface level, sea ice thickness, sea ice fraction and sea ice velocities information [157]. These products are available on-line and disseminated through the Copernicus Marine Environment Monitoring Service (CMEMS). Biochemical and nutrient Copernicus products are provided by the Global Ocean Biogeochemistry Analysis as a weekly forecast product, which includes weekly mean files for dissolved iron, nitrate, phosphate, silicate, dissolved oxygen, chlorophyll concentration, phytoplankton concentration and primary production parameters [158]. An additional available dataset, the Bio-ORACLE dataset, which was developed to be a ready-to-use global environmental dataset for modelling the distribution of shallow water marine species [159], contains various global rasters of marine environmental predictors (such as temperature, salinity, photosynthetically available radiation, diffuse attenuation, nutrients, dissolved oxygen), generated either from remotely sensed or in situ measured oceanographic data. Furthermore, the Global Marine Environment Dataset (GMED) combines publicly available climatic, biological and geophysical environmental layers of present (many annual climatologies are available since 1874 to 2000), past (Last Glacial Maximum period) and future (up to 2087) environmental conditions into a uniform dataset having similar extent and spatial resolution [160]. The GMED dataset is ready to be used by species distribution modelling approaches. Although ready-to-use in ecological models, the Bio-ORACLE and GMED datasets are coarse in their spatial resolution (approximately 9 km), and are thus not suitable for studies in the coastal areas. In addition, these datasets do not include data that refer to the past marine climate conditions (Last Glacial Maximum, Mid-Holocene) in the higher spatial resolution versions. The Ocean Climate Layers for Marine Spatial Ecology (MARSPEC) project provides the only available ready-to-use dataset at a spatial resolution of 1 km for the current data and 5 km for the paleoclimate data. Among the mentioned datasets only the CMEMS is currently updated, thus being particularly suitable for real-time applications.

Finally, SAR data are useful for deriving significant wave height (SWH); in particular the SAR wave mode, which is derived by ERS SAR (Hasselmann et al. 2013), Envisat ASAR (Li et al. 2014), and by the recently launched Sentinel-1 (Malenovsky et al. 2012) at a better resolution than ERS and Envisat.

2.4.2 National repositories

The Distributed Active Archive Centre (DAAC) for all Ocean Biology (OB) data, produced or collected under NASA's Earth Observing System Data and Information System, provides data access to sea surface temperature (SST), sea surface salinity (SSS) data marine products generated from MODIS, SeaWiFS, Aquarius and other sensors.

MODIS radiometer instrument, with infrared bands designed to measure SST, has been providing accurate global measurements of SST at 1 km resolution for more than a decade [161]. Furthermore, the infrared channels of

AVHRR instruments, which are carried by the NOAA Polar Operational Environmental Satellites (POES) and the European MetOp Satellites, are also used to measure SST at 1 km resolution [162]. Aquarius [163] and the European SMOS [164] microwave radiometers have been used to estimate SSS with a spatial resolution of about 100-150 km and 30-50 km, respectively (see https://oceandata.sci.gsfc.nasa.gov/ and https://smos-ds-02.eo.esa.int/oads/access/). In future years, two of the main goals set by NASA are to:

1. fine-tune the readings and retrieve data closer to the coasts and the poles
2. combine the Aquarius measurements to those of SMOS to produce more accurate and finer maps of ocean salinity (https://science.nasa.gov/earth-science/oceanography/physical-ocean/salinity).

Phytoplankton distribution in the sea is characterized by measurements of chlorophyll-a concentration, which can be retrieved based on data from satellite ocean colour sensors [165]. MODIS Chlorophyll-a Pigment Concentration product provides two estimates of the concentration of chlorophyll-a at 1km resolution, which are daily uploaded since 2000 for Terra platform [166] and 2002 for Aqua platform [167]. Another sensor that has been used since 2011 to provide chlorophyll-a estimates is the Visible and Infrared Imager/Radiometer Suite (VIIRS), a multi-disciplinary instrument of the Suomi National Polar-orbiting Partnership [168]. Older global chlorophyll-a estimates were measured by SeaWIFS, a satellite-borne sensor with a 1 km resolution and active from 1997 to 2010 [169].

The red or NIR bands of MODIS Aqua satellite have been used to estimate suspended sediment concentration (SSC), which can be detected since the scattering by water molecules becomes insignificant in the red and NIR [170]. Particulate organic and inorganic carbon concentration products are by MODIS.

Finally, Sentinel-3 topography mission, relying on the physical characteristics of the altimeter waveforms received by the SRAL instrument, measures geophysical parameters as sea surface height, significant wave height and wind speed over ocean surface, eddies and tides [171] at a resolution of about 300 m, much higher than the resolution of MODIS and MERIS products (+1 km [172]).

As a recent example of ecological application of climatic RS ocean products, the comparison of near-real-time SST values with a long-term baseline SST at reef location has allowed the estimation of the thermal stress that can lead to coral bleaching and the determination of coral bleaching hotspots [173]. The anomalously warm ocean temperatures have caused an increase in the severity and frequency of mass coral bleaching and mortality events contributing to the deterioration of reef ecosystems [174]. The resulting 5-km Coral Bleaching HotSpots product provides a measure of daily thermal stress.

RS marine features have been assimilated in methods described in [175], [176] to predict potential fishing zones (PFZs). They rely on the synergetic use of SST and chlorophyll-a information. Increased specialization is exhibited by the Indian National Centre for Ocean Information Services to identify PFZs along the Indian coastline.

2.5 Use of remote sensing data in Species Distribution Models (SDMs)

2.5.1 Terrestrial applications

RS data are frequently used to feed SDMs. SDMs are empirical models that try to predict the spatial distribution of a species, a group of species or a community at a global, regional or local scale using spatially explicit predictors. Different environmental variables can be used as predictors in SDMs, but it is clear that RS variables have the advantage of being frequently updated and have proved to have high predictive power. Some of the most common RS-based predictive variables used in models are vegetation indices, in particular NDVI, that are indicators of vegetation cover, photosynthetic activity phenology, and canopy structure and as such can reflect the habitat available for species. It is also possible to use as predictors vegetation maps, that are themselves frequently based on RS data. Since the launch of the Landsat-1 satellite in 1972 it has been possible to use high resolution RS products to produce vegetation maps or to derive vegetation indexes. Although RS data are more and more frequently employed in vegetation mapping they are still only marginally employed in SDMs. This agrees with the claim by Rodríguez et al. [177] that, although there are numerous RS products that are useful for SDMs, there is a great potential that had been underexploited ten years ago, and continues today [178].

Here, we have reviewed a hundred scientific papers that included "Species distribution models" and remote sensing terms to evaluate how RS-based data are used in SDMs and to what extent the spatial resolution of RS products conditions the success of these models. The first thing that should be noticed is that up to three different spatial resolutions may be used in SDMs. These are:

1. resolution of the "model output";
2. resolution of the "response variable" (that is the resolution of species presence or abundance data that are used to feed or validate the model) ;
3. resolution of the "predictor variables" (RS products or other predictors).

We have considered model "resolution output" to classify papers as high resolution (< 30 m), medium resolution (30-250 m) or coarse resolution (> 250 m), references with details on the considered application, sensors used and model resolution are collected in Annex 1. Approximately half of the papers produced high to medium resolution outputs from 2 m [179], [180] to 250 m [181]. Among the remaining papers, a common spatial resolution was 1000 m [22], [73], [182]–[188], probably mainly determined for the great availability of global RS products at that resolution [177] and even coarser resolutions [189], [190]. It is not uncommon that RS products with different resolutions are used and interpolated, fused, or aggregated to make predictions at the resolution defined in the model output. For example, the altitude data, provided for most of the globe by the Shuttle Radar Topography Mission (SRTM) at 30 m or 90 m, is commonly used as a predictor in combination with MODIS EVI or NDVI (250 m), MERIS NDVI (300 m), Spot-Vegetation NDVI (1 km), LST or SST from MODIS (2000-5000 m) [183]–[185], [190]–[193].

Not so common, but also possible, is that Very High Resolution (VHR) RS data are used as predictors in models with a relatively low spatial resolution output. For example, Yabuhara et al. [188] used high resolution ALOS-PRISM (2.5 m) and orthophotos (1 m) combined with 300 m bird census transects to make predictions of changes in distribution of riparian birds along 1 km river segments in Japan. Also Zellweger et al. [23] used LiDAR (1.4 m) and SPOT-5 (10 m) to predict forest bird distribution in 1 km grid cells. LiDAR stands out as a recent source of VHR RS data to build high-resolution terrestrial DEMs [180], coastal bathymetry [194], [195], or provide information on forest structure [23], [196], [197], and has been the object of a recent review considering its use for habitat suitability modelling [198]. Availability of VHR RS products is not the only reason for its relatively low use in species distribution models. In many instances RS data may be available (i.e., Landsat data since the 1970's) but they are computationally costly to be used for regional, continental or global studies, and lower resolution RS products are preferred. This explains that a recent study evaluating high resolution global forest change in the 21st century was considered interesting to be published in Science in 2013 [199] although these RS data have been available for 40 years. In the case of mobile species like birds, coarse resolution products may work better for most species, just because the species depends on resources at a larger scale. Seoane et al. [200] show that coarse vegetation maps like CORINE (250 m) are adequate for species distribution models for many species of birds and that there is little to gain incorporating higher resolution RS maps derived from Landsat (30 m). A similar result was obtained by Rickbeil et al. [201] who showed that incorporating detailed RS data from Landsat to describe the shore areas provides little improvement to coastal bird SDMs using coarser RS products. A common claim is that it is necessary to have species predictions at the scale of local management actions 10-100 m [180], [202], [203]. However, this approach presents a certain limit: when predictors with different spatial resolutions are tested, landscape patterns tend to override local effects and there is little to gain increasing the resolution even for modeling the distribution of plants [180].

2.5.2 Marine applications

Marine RS products are widely used in statistical modelling in order to examine benthos distribution [204]–[206], marine mammals [207]–[210], sharks [211], invertebrates [212], essential fish habitats [213], phytoplankton distribution and blooms [165] as well as invasive species [214]–[217].

The environmental predictors are usually data like SST and its first order products (mean monthly, annually mean, anomalies, etc.), SSS (mean monthly, annually mean, anomalies, etc.) and bathymetry (slope, aspect, curvature, profile, etc.) along with nutrients, sea surface currents and anomalies. Algorithms like GLM, GAM, Random Forest and MaxEnt are among the most commonly used (see [218], [219]). Bio-Oracle and MARSPEC 6 [159], [220] provide

ready-to-use layers for marine SDMs, allowing also non-experts in marine remote sensing to exploit and use the data in SDMs, with several case studies that exploit the distribution of marine algae, fish, invertebrates and invasive species.

2.6 Multi-sensor/multi-platform approaches

The use of multi-sensor approaches is a way to overcome the fixed temporal and spatial resolutions of single data sources and offers advantages for mapping and modelling vegetation parameters (see comparative analyses by Gao et al. [221], Dusseux et al. [222]). By combining radar and optical data, also limitations of vegetation index data derived from optical RS such as saturation effects (e.g., [223]) and dependence of weather conditions can be solved. Data integration is mostly done i) before classification or modelling ("fusion of input data") or ii) after classification or modelling ("fusion of derived information" [224]). More detailed information regarding fusion techniques can be found in [225] and [226].

In the field of land use mapping and monitoring, a wide range of studies, partly based on vegetation indices to estimate (changes) in biomass, employ multi-sensor RS data (reviewed in [224]). The examples reported in this section are collected in Annex 2, describing the application considered in the different references, the satellite sensors used and their resolutions. Most often, Landsat data are combined with ALOS/PALSAR, Radarsat or ERS datasets. However, huge differences exist regarding location of study area, scale and temporal resolution among the studies conducted [224]. For example, Revill et al. [227] evaluated the suitability of optical and radar RS data as input source for a process-based model analysing cropland C dynamics, more precisely for assimilating temporal LAI data in six European agricultural field sites. While RS data substantially improved the model output, the use of radar data alone, being unaffected by cloud cover, was more favourable compared to the combined use.

Mountain and (semi-)arid areas pose some particular challenges for RS applications. Topographically and homogeneously atmospherically corrected data are indispensable in mountain ecosystems, in particular when using multi-sensor approaches. By combining corrected and co-registered Landsat ETM+ and ALOS/PALSAR data, Attarchi and Gloaguen [228] were able to develop a significantly improved statistical model for above ground biomass in a mountain forest site in Iran. In (semi-)arid regions, bright soils and dead vegetation hamper the analysis of optical data, whereas the use of radar data is restricted by e.g. the patchy vegetation structure, different scattering characteristics of various vegetation components and the dominant influence of ground surface [229], [230]. Only a limited number of multi-sensor studies have therefore been conducted in these ecosystems (reviewed in [231]). Synergistic effects of optical and radar data have been used in (semi-)arid regions to model daily evapotranspiration (derivation of biophysical input data for a process-based model [232]), to predict vegetation cover [229] and to estimate aboveground biomass [230], [233]

In estuarine/marine environments, NDVI derived from optical data provides useful information for a variety of ecological applications, e.g. regarding coastal wetland extension [234] or eutrophication [10]. One example of a multi-sensor approach is the study by Chakraborty et al. [235] who analysed MODIS Enhanced Vegetation Index (EVI) and AMSR-E radar signatures to estimate the amount of vegetation biomass that is submerged during monsoon flooding with the aid of a radiative transfer model. Furthermore, Rangoonwala et al. [236] related persistence of marshland flooding (radar data) caused by Hurricane Sandy to changes in vegetation (optical data).

While the use of multi-sensor approaches offers new opportunities with respect to time-series analysis, cross-sensor calibration to make for example NDVI values comparable is a challenging task [237]. The long-term availability of data from the Landsat mission makes this sensor still the most suitable for multi-temporal analysis (e.g., [74]). As Sentinel-2, with the first platform launched in 2015, has a similar spectral coverage but better spatial and temporal resolution, current efforts focus on combining both data sets to provide a near daily global coverage with 30 m resolution (NASA Harmonized Landsat-Sentinel-2 (HLS) project [238]). Although some research have been carried out to develop radiometric correction methodologies that maintain the radiometric homogenization between different sensor time series [239] allowing a direct comparison, there is still a new era to meet for the use of multi-temporal, multi-source RS data in ecology.

2.7 Conclusions and future perspectives

The research directions indicated by Plummer in 2000 with the objective of promoting the use of RS products as drivers of ecosystem models were mainly concerned about the reliability and repeatability of the RS estimates of surface ecological variables. The present review work highlighted that in the past 17 years the diffidence and caution of the ecologist community against RS data have been reduced mainly thanks to the increased availability of global RS products subject to rigorous quality assurance tests. In fact, well-known and tested global datasets are mainly used by ecologists and conservation managers that usually do not have skills and knowledge on the analysis and production of the required RS estimates. A possible drawback of the readily available datasets is that not all the variables are updated in a frequent manner and there is not an available automated process that can provide updated dataset for use in ecological modelling. Moreover, the resolution of the global RS products may not be sufficient for applications at local scales (e.g., [240]). Several examples in literature demonstrated that these limitations have been surpassed thanks to the continuous improvements in empirical and physically based methods to link vegetation properties to RS reflectance signal, by using suitable statistical downscaling techniques for climate products, and by considering different RS signals into multisensor approaches. These possible approaches have not become yet common practices for most of the ecological modellers. Projects such as ECOPOTENTIAL promoting the collaboration between the remote sensing and the ecosystem modeller communities are essential to develop standardize techniques exploiting the full potentiality of RS data for local applications.

Table 2 Overview of recent remote sensing methods for the extraction of leaf and canopy properties. This table gives per method: (a) the abbreviation(s) of remote sensing source(s) of the input data (denoted with red), (b) (when available) the performance divided into quartiles (denoted with green). A symbol ✦ is added next to a method, when auxiliary data other than remote sensing data is used as input (i.e. field campaign data, DEMs). The remote sensing characteristics for a specific source are provided within parentheses next to the complete name of source. All abbreviations are explained in the table under the figure.

	Empirical models	**Semi-empirical models**	**Physically-based models**
Leaf/Canopy Water	[85] LA AS AW P4 [86] LA P3 [87] MO P4		[109] MO P4 [110] MI P3 [111] HY [130] CH P4
Leaf/Canopy Chlorophyll	[93] AI [96] SE P4		[112] RA P4 [113] LA P4 [120] SP P4 ✦ [14] LA P4 [123] SP P4 ✦ [125] CH P4 ✦ [131] ME P3
Leaf Area Index	[94] RA P4 [95] MO LA ME P4	[135] DE P3-P4 [137] RA P3-P4	[112] RA P4 [131] ME P3 [114] MO AS P4 [115] SE P4 ✦ [116] LI P4 [120] SP P4 ✦ [14] LA P4 ✦ [123] SP P3 [126] LA
Canopy Structure (e.g. leaf angle distribution) /Height		[133] MR P2-P4 ✦ [134] MR P2-P3 ✦	
Leaf/Canopy Nitrogen	[97] RA [99] SE P3 [100] AV P4		
Solar Chlorophyll Fluorescence	[104] GO [127] GO		
Understory NDVI		[138] MO	

Remote sensing data sources (satellite/airborne imagery) and their characteristics:

AI: AISA (HS, VHR) **AS**: ASTER (MS, MR) **AV:** AVIRIS (HS, MR) **AW**: AWiFs (MS, CR)
CH: CHRIS/PROBA (HS, MR) **DE**: DEIMOS-1 (MS, MR) **GO:** GOSAT (MS, CR) **HY:** HyMap (HS, HR)
LA: LANDSAT (MS, MR) **LI**: LISS-3 (MS, MR) **ME**: MERIS (HS, CR) **MI**: MIVIS (HS, HR)
MO: MODIS (HS, CR) **MR**: MISR (MS, CR) **RA**: RapidEye (MS, HR) **SE**: Sentinel-2 (MS, HR)
SP: SPOT (MS, HR)

Characteristics of remote sensing data:

MS: Multispectral **HS:** Hyperspectral **VHR**: Very High resolution (≤4m)
HR: High resolution (≤10m) **MR:** Medium resolution (≤30m) **CR**: Coarse resolution (>30m)

Performance subdivisions:

P1 / P2 / P3 / P4: 0-25% / 25-50% / 50-75% / 75-100% quartiles of performance
✦ : Input to the models includes auxiliary data different than remote sensing data

Table 3. Available datasets of marine products.

Dataset	Description	Available products	Website
Bio-ORACLE	Global environmental dataset for marine species distribution modelling	- SST - Ocean salinity - Photosynthetically available radiation - Diffuse attenuation - Nutrients - Dissolved oxygen - pH	http://www.oracle.ugent.be/
CMEMS	Copernicus Marine environment monitoring service products	- SST - ocean salinity - ocean currents - sea ice - sea level - winds - ocean optics - ocean chemistry - ocean biology - ocean chlorophyll	http://marine.copernicus.eu/services-portfolio/access-to-products/
EMIS	Environmental Marine Information System – European Commision	- Biophysical parameters provided by: MODIS-Aqua, SEAWiFS, MERIS, MODIS-Terra, Pathfinder	http://emis.jrc.ec.europa.eu/emis_6_0.php
GMED	Global Marine Datasets for species distribution modelling and environment visualisation	- water depth - ice concentration - salinity - temperature - surface current - chlorophyll-a concentration - wave height - pH - nutrients	http://gmed.auckland.ac.nz/download.html
INCOIS	Indian National Centre for Ocean Information Services – Potential Fishing Zone	- potential fishing zones	http://www.incois.gov.in/MarineFisheries/PfzAdvisory
OB.DAAC	Distributed Active Archive Center for Ocean Biology, NASA's Earth Observing System Data and Information System	- SST - SSS - chlorophyll and calcite concentration - particulate organic and inorganic carbon	https://oceandata.sci.gsfc.nasa.gov
MARSPEC	Ocean Climate layers for Marine Spatial Ecology	- Topography variables - SST parameters - SSS parameters - Paleoclimatic data	http://www.marspec.org/

NOAA	Coral Reef Watch program's satellite data	- bleaching alert area - coral bleaching hotspot - current thermal stress - degree heating week - accumulated thermal stress - sea surface temperature - sea surface temperature anomaly	https://coralreefwatch.noaa.gov/satellite/
Sentinel 3	topography mission products	- SST - sea surface height - significant wave height - wind speed over ocean surface	https://sentinels.copernicus.eu/web/sentinel
SMOS	ESA's Soil Moisture Ocean Salinity Earth Explorer mission providing Near Real Time data	- SSS	https://smos-ds-02.eo.esa.int

3. Validation of ecological models through Earth observations

D. Pasetto[1], R. Casagrandi[2], G. El Serafy[3], L. Mari[2], A. Monteiro[4], A. Ziemba[3]

[1]Laboratory of Ecohydrology, École Polytechnique Fédérale de Lausanne, Switzerland
[2]Dipartimento di Elettronica, Informazione e Bioingegneria, Politecnico di Milano, Italy
[3]Deltares, Delft, The Netherlands
[4]Cibio/InBIO, Research Center in Biodiversity and Genetic Resources, University of Porto, Portugal

The link between ecological models and EOs can help us better understand mechanisms governing our planet in a context of global change. Ecological models as simplified representations of the Earth's living systems can benefit in multiple directions from EO. RS data and products constitute a valuable and increasingly available source of distributed information. RS datasets are currently used not only to feed the inputs of terrestrial and marine ecological models, but also to assess the reliability of model predictions.

Mathematical modelling is a multi-step process. Process-based models are often developed for region-specific applications, with final outputs sometimes resulting from multiple models feeding into one another; the generality of the underlying ecological principles makes them applicable to a wide range of systems, varying in both domain and scale [1]. Ecological processes are often quantified through variables and numerical coefficients (parameters) endowed with acceptable ranges defined through scientific research and documented in the literature [2]. A single model can describe several of such processes; therefore, it is no surprise that the number of active processes can quickly grow to an ungainly number when multiple models are coupled with each others. The exact value to be ascribed to the parameters of ecological models is usually to be determined through proper calibration against direct measurements or RS products. Following the model calibration phase, the validation step consists in the verification of the accuracy and precision of the model results for its intended use [241], which represents a crucial step in the development of ecological models.

Both calibration and validation are based on the computation of error metrics between the model results and the associated ecosystem measurements. Due to the spatially discrete nature of many process-based models, the comparison between ecological model outputs and in-situ data might be inappropriate because of local heterogeneities or unfeasible because of model resolution. RS products provide an economically viable and information-rich datasets, which can be used in efforts to calibrate and validate models, especially when compared to the high cost and low spatial and temporal resolution of operating in-situ monitoring stations. Of course, when ground truthing is problematic, the issue of implementing non-validated RS products would result in the increment of the level of uncertainty on the reference data. Despite these shortcomings, there are several examples of RS data being applied to both automated and manual model calibrations. Kamel et. al. [242] used turbidity images to calibrate model parameters identified through a sensitivity analysis with the objective of reconstructing sedimentation flumes resulting from riverine discharges into the North Sea. In this case, the calibration was performed through comparison between model results and the RS images of suspended sediments, computing the residuals between concentrations, identifying zones of similarities and the error bias. In this same study, a further analysis was executed in regard to in-situ measurements, and the differences in the measurements between monitoring stations and remote sensing came to the realization that the RS products on the whole produced an under-estimation in the water turbidity resulting in a model calibration, which produced improved results when compared with satellite information, but a higher error in respect to monitoring station which are given a higher credibility interval. A similar approach was followed by Chen et al. [243] utilizing the ECOMSED model for a case study off the coast of China, also accounting for the differences between in-situ and RS applications and yielding results consistent with those of Kamel et al.

In this regard, at an early stage, Plummer [6] identified three possible strategies to compare the modelled outputs with RS data:

- *Indirect comparison*, which looks at spatiotemporal correlations between the output of the ecological model, such as LAI, and the associated variables estimated via RS data, for example estimations of LAI using NDVI.

- *Reflectance as an ecological model output*, where modelled outputs are processed to obtain surrogates (e.g. Hybrid Difference Vegetation Index, HDVI) of the RS observation (e.g. NDVI).
- *Coupling ecological and reflectance models*, consisting in feeding a radiative reflectance model (e.g. SAIL) with the outputs of the ecological model (e.g. LAI estimated with a grassland ecological model [244]), and directly compare the measured and modelled radiances.

The last strategy is particularly appealing since it avoids possible discrepancies between the RS products and the model outputs, and the inversion of the radiative transfer model. However, the outputs of the ecological model must be adapted to serve as input of the radiative model, which, on the other side, requires a proper calibration. The coupling between ecological and reflectance models is frequently adopted in hydrological applications. For example, De Lannoy and Reichle [245] estimate surface soil moisture with a land surface model, and use it as input of a radiative transfer model to directly compare the modelled temperature brightness with the observations from SMOS. However, as several RS products are nowadays freely accessible in a number of data repositories (see Table 3), Plummer's indirect comparison is the most adopted strategy for validation, not requiring the coupling with reflectance models.

3.1 Validation metrics

The comparison between the model results and the measurement data passes through the computation of model skill functions and error metrics. This in turn translates into the efficiency of the model to recreate what has been seen to occur in the natural system as compared to the simulation [5]. These measurements are ideally on a similar spatial and temporal resolution as the model, or at least with sufficient resolution to allow for a qualitative comparison. Rykiel [241] lists twelve alternatives used in the literature to validate ecological models, to be selected depending on the available data and the type of model used. These techniques include statistical validation against data, historical and predictive validation, sensitivity analysis and the comparison with other models. The standard way to validate the modelled results is to compare the vector of modelled outputs (of dimension n), here indicated with y^m, with respect to the observed data at the same point in space and time, indicated with y^o. For hindcast, or "in-sample validation", the data used in the calibration and validation period coincide. This could generate an overestimation of the accuracy of the model. For this reason, if enough data are available, it is common practice to adopt "out-of-sample" validation, where different data are used in the calibration and validation periods. The recent review work of Bennett et al. [246] describes several techniques available to characterize the performance of an environmental model, considering numerical, graphical and qualitative methods.

These techniques can be grouped as the following:

- *Direct value comparison,* where the performance of the model is assessed on the ability of its outputs to reproduce some ecologically relevant statistics of the observations, such as the mean $\bar{y} = \sum_{i=1}^{n} y_i/n$, the variance, $\sum_{i=1}^{n}(y_i - \bar{y})^2/n$, or higher-order statistical moments.
- *Element by element comparison*, where the whole dataset is considered under several possible approaches:
  - analysis of scatter plots and the associated linear regression analysis;
  - frequencies of concurrent or missed events, where the interest is to assess if the modelled and the observed data satisfy a property of interest (e.g., given a certain risk tolerance τ, the property $y_i < \tau$ is checked for each element i); in this case the results are typically represented with a contingency table, reporting the occurrences of the model hits, false negatives and positives;
  - residual methods, mainly based on the computation of the residuals, $d_i = y_i^o - y_i^m$, and related metrics like bias, $\sum_{i=1}^{n} d_i/n$, root mean squared error (RMSE), $\sqrt{\sum_{i=1}^{n} {d_i}^2/n}$, or relative errors.
- *Preservation of the data pattern*, where local spatial or temporal cross-correlations are sought. To this goal, the main metrics of interest are the Pearson's correlation coefficient (r)

$$r = \frac{\sum_{i=1}^{n}(y_i^o - \bar{y}^o)(y_i^m - \bar{y}^m)}{\sqrt{\sum_{i=1}^{n}(y_i^o - \bar{y}^o)^2 \sum_{i=1}^{n}(y_i^m - \bar{y}^m)^2}}$$

and the Nash-Sutcliffe efficiency (NSE)

$$NSE = 1 - \frac{\sum_{i=1}^{n}(y_i^o - \bar{y}^m)^2}{\sum_{i=1}^{n}(y_i^o - \bar{y}^o)^2}.$$

Best performances are reached when $r$and NSE are close to 1 (r ranges between -1 and 1, while NSE is less than 1).

- *Indirect metrics,* mainly based on the uncertainty associated with the identification of the model's parameters. As an example, the high covariance in estimated parameters may suggest over-parameterization or other problems in model identification.
- *Data transformation methods*, where the performance of the model is analysed in the frequency domain of the data, for example by means of Fourier transformation, wavelets, or Empirical Orthogonal Functions (EOFs).
- *Qualitative model evaluation,* mostly depending on the assessment of the model results based on the analysis of some of the previously listed metrics and the visual comparison between modelled outputs and data, which is highly relying on the subjective opinion of expert modellers.

The validation strategy to be adopted depends on the particular features of the model, application site, and data availability. As highlighted in [247], [248] the combined use of different metrics is recommended to assess the performance of the model and the possible presence of bias in the outputs. The evaluation of validation metrics in both space and time is essential to establish the reliability of the model, not only in retrieving the global trends of the phenomena under study, but also in describing the local dynamics. To this end, the use of a Taylor diagram [249] can be useful to compare the performances of different models, since it summarizes in a single plot the RMSE, the correlation coefficient and the normalized model standard deviation.

3.2 Validation based on Earth observations

The identification of the best strategy to compare two raster maps is a common problem to several scientific fields, such as image analysis, oceanography, landscape ecology, and remote sensing [250]. For example, in marine ecosystem modelling, computed maps resulting from a biophysical model should reproduce the patterns in the data indicating patches of high phytoplankton concentrations or high nutrient gradients.

When validating the maps produced by a spatially-explicit model against RS products, modellers may possibly face the difficulty of contrasting raster maps with different spatial resolutions and temporal discrepancies. A common strategy for the evaluation of quantitative metrics is to downscale the satellite products to the computational grid of the model, and perform a per-pixel comparison at the temporal resolution of available data. In most cases this procedure does not take into account the measurement errors and the inaccuracies introduced by inappropriate downscaling, factor that might contribute to worsening the model statistics. Smoothing model outputs and data by taking monthly or seasonal averages may help to remove local oscillations. In addition to these resolution issues, *Bennett et al.* [246] underline that it is somehow expected to have some discrepancies in cases where what is modelled (e.g. phytoplankton concentration) is not exactly what is measured (e.g. chlorophyll-a), thus a certain level of model inaccuracy is unavoidable and perfect fits might simply be unrealistic.

Frequently, the model results qualitatively resemble the data map, but with the features of interest slightly shifted, rotated or dilated [250], especially of fields generated by chaotic dynamics and/or processes with a significant stochastic component. In such cases, the direct application of performance metrics based on per-pixel residuals, such the RSME, may not be the best approach, because even small perturbations between two raster maps might cause large error statistics, not reflecting apparent similarity between the maps; on the contrary, modelled results having small errors may catch the average value of the quantity of interest, without reproducing important spatial patterns present in the data (e.g., [251]). For example, in systems subject to turbulence, the chaotic nature of the

solutions and of the spatial-temporal fields forbids a direct comparison between models and experimental data. In such cases, one resorts to comparing low-order and higher-order statistical moments, spectra, correlations, and other measures of spatial structure. When comparing two maps, it is not straightforward to replace the human ability in recognizing similar spatial patterns through objective metrics, which is the main reason why there are still many examples of model outputs validated via qualitative comparison, as highlighted by the review works of Arhonditsis et al. [252] and Stow et al. [250]. There is however the need to adopt rigorous objective criteria in model validation. In a recent paper, Koch et al. [253] assessed the performances of different quantitative metrics in reproducing the qualitative, visual comparison between two maps as performed by humans. They used 12 different types of perturbations to modify the original map and compared the between-maps similarities as perceived by 200 individuals (via a web survey), and as revealed by the most common metrics used in terms of map comparison, i.e.: EOF analysis, Kappa statistics, and Fuzzy theory.

- EOF analysis, largely used in atmospheric sciences [254], is based on the decomposition of a spatiotemporal dataset into a small set of orthogonal spatial functions, similarly to principal component analysis, with the first EOF expressing the maximum variance of the dataset. Each map in the original dataset can be approximated by a linear combination of the spatial functions. The idea is to apply EOF transformation to the data and the model outputs, and then analyse the errors among the first basis functions.
- The Kappa statistic, also called Cohen's Kappa statistics, is based on a per-pixel comparison in which pixels are classified into K alternative categories (or properties of interest); the level of agreement between the model and the data is compared against random pixel categorization. In formulas, indicating with $\mathrm{P(a)}$ the percentage of pixels of the model having the same category of the associated pixels in the data, and $\mathrm{P(e)}$ the percentage of agreement in a random permutation of the pixels among the categories, the Kappa statistics is computed as $(\mathrm{P(a)} - \mathrm{P(e)})/(1 - \mathrm{P(e)})$. In case the model categories are equal to the data categories for each pixel, the Kappa statistic assumes its maximum value, 1. Otherwise, if the level of agreement is lower than a random agreement, the Kappa statistic is negative.
- Fuzzy theory refers to those methods that perform a per-pixel comparison considering also the neighboring cells, thus removing the possible drawbacks caused by shifts between the reference map and the model results. In this category, the most common approaches are the Fuzzy Kappa statistics and moving window techniques. In particular, the former method extends the Kappa statistics by controlling the level of agreement of a pixel with respect to the surrounding pixels of the reference map, weighted by a distance-decay function.

Koch et al. [253] concluded that metrics based on Fuzzy theory have the higher agreement with the results obtained by visual comparison.

Several studies in the literature are proposing new and more elaborated techniques to quantitatively and objectively assess maps similarities (see e.g., [255]). Ecologists willing to compare their results to RS maps should be aware that the proper use of these metrics might help the objective quantification of the model performances.

In the following, we present a non-exhaustive overview of some interesting ecological models (listed in Table 6) whose results have been validated against RS data after the publication of Plummer's paper, with applications focusing on either terrestrial or marine ecosystems. Table 4 summarizes the examples discussed below, subdividing them with respect to the model output and the technique used for validation. For each reference, the satellite sensor generating the products and metrics used in the quantitative validation are specified.

3.3 EO-based validation of terrestrial ecosystem models

Most terrestrial ecological models aim to reproduce the ecosystem dynamics and vegetation patterns through the estimation of processes governing the water, energy and carbon cycles. The main outputs of these models allow ecologists to estimate the dynamics of several variables of interest, such as gross and net primary productivity (GPP/NPP), canopy properties (e.g., LAI), ET, land cover, plant communities and forest succession. The increasing use of RS data to estimate these variables and processes with high accuracy and resolution enhanced considerably

the usage of RS data as an alternative to in-situ data for the model validation. A clear example of the utility of RS data in the assessment of ecological models in locations were in-situ measurements are impractical is presented by Murray-Tortarolo et al. [83]: they compared the ability of eight land surface models in reproducing the LAI derived by MODIS at high latitudes for the period 1986-2005. In this case, several model limitations are highlighted, in particular a general overestimation of the mean LAI computed by the models. Thus, the authors suggested improving the characterization of the phenology by using more accurate plant functional types in all models. However, this study bases the map comparison only on the evaluation of the RMSE, without considering other metrics for the recognition of common correlation and pattern, which would have further improved the model analysis.

In terrestrial system, model validation with RS data occurred from local to global scale studies. Dynamic vegetation and biogeochemical models were the model families most considered, and primary production (GPP/NPP) the product most often validated with RS data. The set of models used included: AquaCrop, CLM, CCSM, ED2, Forest-BGC, LPJ, LPJ-GUESS, LSM**,** ORCHIDEE, SEBS, SDGVM, TRIFFID, ZELIG. The RS products that have been used for the different model comparison have been listed in Table 4.

AquaCrop. This is a crop water productivity model developed to analyse food security and to assess responses of crop production to environment and management. Urban et al. [256] proposed an efficient-low-cost approach to validate FAO's AquaCrop model using RS estimates instead of crop ground measurements. Crop response to water is an important component of decision-making for agricultural water management. The comparison between the AquaCrop simulations and the RS estimates to different crops using NSE coefficient showed a good agreement of above-ground biomass and canopy cover estimations, mainly in non-stressed farm conditions (all NSE>0.80).

CCSM. The Community Climate System Model (CCSM) is a coupled climate model for simulating the Earth's climate system. Randerson et al. [257] analyzed the performance of biogeochemistry models that are integrated within the Community Climate System Model (CCSM), i.e. the Carnegie-Ames-Stanford Approach' (CASA') and the carbon–nitrogen (CN) model, using a systematic framework. LAI observations from MODIS (MOD15A2 collection 4) were considered between 2000 and 2004 and monthly mean MODIS values compared against model estimates. The comparison with MODIS LAI based on scores showed that for both models, the timing of maximum leaf area lagged behind the observations by 1–2 months. The spatial patterns of MODIS NPP [258] were also compared to models estimations. Results evidenced high uncertainty in the comparison. The summary of model evaluation datasets and analysis scored as low to medium the convergence between models and remote sensing estimations for LAI and NPP.

ED2. The Ecosystem Demography Biosphere model version 2 (ED2) [259] couples several processes such as leaf-level physiology, plant allocation, allometry, phenology, dispersal, the effects of fire disturbances, and below-ground soil carbon dynamics and hydrology. Levine et al. [260] tested the effect of ecosystem heterogeneity in the resilience of the Amazon to climate change using ED2 and found a good overall agreement between the seasonal pattern of aboveground biomass (Kg cm^{-2}) and biomass variability (coefficient of variation) estimated by MODIS-GLASLidar and ED2. However, MODIS-GLASLidar net values were always higher than modelled, especially in the end of dry season.

FOREST-BGC is a model of forest ecosystem processes for regional applications. Lopes et al. [261] compared quantitative estimations for NPP in man-made Eucalyptus and Pine forest stands based on FOREST-BGC, MODIS NPP and field measurements estimations. ANOVA and Duncan New Multiple Range tests were performed to identify if average NPP figures were statistically different between all tested methodologies. NPP images were compared using the Kappa test statistic and the proportion of agreement. The overall rate of agreement between FOREST-BGC and field estimations (82.6%) indicated that the model was able to simulate the production of stands with a high degree of accuracy. A strong correlation between the FOREST-BGC NPP and field NPP was found (0.88). The comparison of field NPP with MODIS NPP resulted in a rate of agreement of 54%. Authors conclude that MODIS NPP tended to simplify reality and homogenize the productive potential of the stands and are inefficient for identifying extreme NPP values. FOREST-BGC combined with LAI from remote sensing may provide a suitable tool at a regional and global scale.

LPJ. The Lund-Potsdam-Jena (LPJ) model [262] is a Dynamic Global Vegetation Model (DGVM) developed to study biochemical and biophysical interactions between the atmosphere and terrestrial ecosystem dynamics. This is achieved by modelling the vegetation component through ten functional types regulating processes such as photosynthesis, and plant growth. Coupling the water and carbon cycles, LPJ computes ET, runoff and soil moisture together with vegetation structure. The modelled vegetation structure, GPP and LAI have been compared to RS datasets in many applications, but mostly limiting the comparison to the qualitative identification of common patterns. At global scale, Sitch et al. [262] concluded that LPJ estimations of vegetation structure are in good agreement with land cover data from AVHRR. The comparison of simulated and satellite-derived leaf phenology and leaf type showed also that both variables were modelled reasonably well by LPJ. Hély et al. [263] obtained similar results using LPJ-Guess for the modelization of African Biomes, where simulated annual maximum LAI values quantitatively agreed with the averaged ranges observed by the Global Inventory Modelling and Mapping Studies (GIMMS; 8 km resolution). In both modelled and measured data, the transition zone along precipitation gradients in the tropics and subtropics was well delimited. A recent application of the model in Swiss Alps [264] highlighted qualitative discrepancies between the modelled LAI and MODIS estimation after comparison with Swiss FluxNet sites. Coarse resolution of MODIS and frequent periods of cloud or snow cover were indicated as the potential sources of error. Model performance validation with MODIS data should be careful and alternative data sources should be sought in periods with high cloud or snow cover.

LSM. The Land Surface Model (LSM) examines biogeophysical and biogeochemical land-atmosphere interactions, namely the effects of land surfaces on climate and atmospheric chemistry. Muraoka et al. [265] in a 5-years experiment analyzed the relationship between spectral vegetation indices (NDVI, EVI, Green-Red Vegetation Index, Chlorophyll Index and Canopy Chlorophyll Index) and canopy photosynthetic productivity estimated with LSM 1.0. Results highlighted significant correlations between VIs and canopy photosynthetic capacity over the seasons and years. Regression analysis between modelled maximum GPP and VIs on sunny days showed an overall strong match (r^2>0.88).

ORCHIDEE. The Organizing Carbon and Hydrology in Dynamic Ecosystems (ORCHIDEE) model is a global terrestrial biosphere model [266] estimating carbon, water and energy fluxes between land surfaces and the atmosphere. Traore et al. [267] tested ORCHIDEE for inter-annual variability of the fraction of absorbed active radiation, the GPP, soil moisture, and ET over Africa. Positive spatial correlation (r > 0.8) between patterns of modelled fAPAR and fAPAR3g from AVHRR was found. Nonetheless, despite capturing the patterns of fAPAR within each subregion, the model was not able to reproduce the magnitude of the observed spatial fAPAR gradients well. Comparison between model and observation was quantified by their spatial correlation, root-mean-square difference, and magnitude of their variations in terms of spatial gradients represented by the ratios of modelled to observed standard deviation across the grid cells of each subregion. Correlation between the modelled soil moisture versus Soil Moisture from MicroWave satellite product (SM-MW) indicated also poor agreement between modelled and satellite measured spatial patterns (r < 0.5).

RHESSy. The Regional Hydro-Ecological Simulation System (RHESSY) [268] is a hydroecological model developed to quantify carbon, water and nutrient fluxes at the catchment scale. Hwang et al. [269] applied RHESSy to a small catchment in Korea where the model was calibrated and validated against field measurements. The validated model was then extended to the regional scale in order to evaluate the trustworthy of MODIS-derived LAI (MOD15A2) and GPP (MOD17A2) products. This interesting example of using a distributed model to assess the quality of RS products highlighted a consistent overestimation of MODIS LAI and GPP during the summer season. Comparison between MODIS GPP products and in-situ data obtained from flux towers and LAI measurements for deciduous broadleaf and evergreen needleleaf forests indicated that MODIS GPP potentially overestimates carbon uptake during drought conditions by the lack of a soil water stress term in MODIS GPP algorithm. In order to address this gap, recent efforts to estimate soil water potential from the shortwave infrared and near infrared bands of MODIS and integrate them into the GPP calculation have been performed

SEBS. The Surface Energy Balance System (SEBS) [270] is a model for the estimation of turbulent heat fluxes and ET. Tian et al. [271] attempted to simulate forest ET using SEBS forced with MODIS products (NDVI and land LST), Global Land Surface Satellite (GLASS) Albedo and LAI products. A two-year (2010–2011) comparison amongst the

SEBS outputs, eddy-covariance data (ground reference) and MODIS MOD16 ET product shown poor agreement and significant underestimation of ET with respect to MOD16 ET (r^2=0.35).

ZELIG model [256] is an individual tree model that simulates the establishment, annual diameter growth, and mortality of each tree on an array of model plots. Song et al. [272] combined the forest succession gap model ZELIG and a canopy reflectance model (geometric optical radiative transfer model, GORT) to produce spectral trajectories of forest succession from young to old-growth stages. Simulated trajectories were compared with those constructed from Landsat Thematic Mapper (TM) imagery. That allowed understanding the potential of mapping forest successional stages with remote sensing. Multiple linear regression analysis revealed a synergistic value of using multitemporal Landsat imagery to predict distributions of forest succession from young to old-growth stages, despite the relatively low overall adjusted Pearson correlation coefficient (r^2=0.54).

In addition to single-model studies, also semi-empirical works or studies based on model ensembles have found a suitable source of validation in RS data. Martinez-Lopez et a. [273] developed an open-source empirical spatio-dynamic wetland plant community model. Wetland plant community maps obtained by means of remote sensing from 1992 to 2008 and with overall accuracies between 74% and 89% were used as independent validation data. Multiple-resolution-goodness-of-fit metrics were adopted for each validation year, comparing the modelled plant community maps and the ones obtained by RS classification. This validation effort identified a good agreement between data and model in both in time and space.

Overall, as denoted by Ito's historical meta-analysis (1862-2011) [274], RS data is a non-negligible source of knowledge on terrestrial ecosystem dynamics, patterns and processes. For instance, it contributed to the convergence of estimations on global terrestrial NPP estimations obtained from different sources over time, despite the considerable remaining uncertainty. The decrease of the range of variability between RS and dynamic global vegetation models estimations seems to be one prominent challenge for present and future terrestrial ecology research.

3.4 EO-based validation of marine models

Validation of ecological models based on RS is a frequent practice in marine systems. For example, the MOHID model outputs for the operational forecasting of the west Iberian coast were validated against the SST product of Improving the Description of the Suspended Particulate Matter Concentrations in the Southern North Sea through Assimilating Remotely Sensed Data, MyOcean ([275], which, thanks to a combination of infrared and microwave sensors, is available also in case of cloud cover.

The marine ecological models that have profited the most from validation are those describing biogeochemical processes and cycles. Such models typically describe local interactions between abiotic and biotic agents (with varying degrees of complexity), while at the same time accounting for transport provided by the underlining ocean circulation fields. The products that are most often subject to validation by means of RS observations are related to measures of primary (most notably chlorophyll) production, but there are also examples referring to phytoplankton community composition (PCC)). Some available models that have recently been discussed in the literature are BFM, ECOHAM, ERSEM and PISCES.

BFM. The Biogeochemical Flux Model (BFM) [276] is a numerical model describing the dynamics of the major biogeochemical processes occurring in marine systems, including nitrogen, phosphorus, silica, carbon and dissolved oxygen cycles, as well as plankton, detritus and benthic biological compartments. A specific feature of the model is the subdivision of the planktonic community into functional groups, so as to create a planktonic food web. The biogeochemical model can be coupled to standard hydrodynamic codes and applied to different spatial scales. Some of the outputs of the model (chlorophyll concentration and primary production) have been validated (either qualitatively or by means of quantitative indicators, such as the NSE coefficient, Pearson's correlation coefficient and Spearman's rank correlation coefficient) against satellite observations (see [277]–[280] for global-scale applications, and [281]–[283] for the Mediterranean Sea). Vichi et al. [278], in particular, performed an extensive skill assessment of BFM at the global scale over a 20-year long period using a wide array of quantitative indicators (model bias, average absolute error, root mean square differences, Nash-Sutcliffe coefficient, reliability index,

Pearson's correlation coefficient). The authors concluded that, in spite of non-negligible biases, during summer the model is at least as good a predictor of global chlorophyll concentration as the mean of the data (NSE > 0), and that it provides good estimates of the spatial distribution of the maxima of global primary production.

ECOHAM. The ECOlogical model, HAMburg (ECOHAM) [284], [285] is a regional coupled hydrodynamic-biogeochemical model that describes carbon, nitrogen and oxygen cycles, and that includes the concentrations of phytoplankton, zooplankton, bacteria, detritus and dissolved organic matter in the water column as prognostic variables. The model has been mainly applied over the northwest European continental shelf area. Its chlorophyll concentrations outputs have been validated with MODIS observations through the computation of per-pixel errors and the evaluation of Pearson's correlation coefficient [286].

ERSEM. The European Regional Seas Ecosystem Model (ERSEM) was born as an already complex ecosystem model [287] originally developed using "fifty or so state variables types" [288] aimed to describe the biogeochemical seasonal cycles in the North Sea. Starting from the description of standard organisms of three different functional types (primary producers, consumers and decomposers), the biological part of the model has been progressively enriched [289]–[291] by better qualifying compartments (i.e. including size-based categories and describing microbial dynamics). The model has been applied to marine regions around the globe, from the North Sea to the Mediterranean and tropical seas. The modelling accuracy of its physical component has also been improved, from the 1D simulations within a model column to the coupling with the NEMO ocean engine, and used in a variety of contexts [292]. ERSEM proved to be quite reliable in reproducing the biogeochemistry in marine ecosystems after assimilation of chlorophyll data [248], [293] and remotely-sensed optical data, as the weekly diffuse light attenuation [294]. In particular, Edwards et al. [248] presented a quantitative validation exercise of POLCOMS-ERSEM and NEMO-ERSEM, two coupled hydrodynamic-ecosystem models used for operational shelf-sea modelling in the UK, against satellite-based daily measurements of chlorophyll. Several performance indicators (mean error, root mean square error, model bias, normalized standard deviation, Pearson's correlation coefficient – the last two of which also combined in a Taylor diagram) were used in this study. As an example, the authors found Pearson's r = 0.29 and r = 0.26 for POLCOMS-ERSEM and NEMO-ERSEM, respectively, in a 2-year-long hindcast exercise concerning surface chlorophyll in the North Sea.

PISCES. The Pelagic Interactions Scheme for Carbon and Ecosystem Studies (PISCES) [295], is a biogeochemical model of intermediate complexity derived from the Hamburg Model of Carbon Cycle (HAMOCC5) [296]. PISCES simulates the cycles of oxygen, carbon and the main nutrients controlling the lower trophic levels of marine ecosystems (phytoplankton, microzooplankton and mesozooplankton). The model is intended to represent ocean productivity and biogeochemical cycles across major biogeographic ocean provinces at different spatiotemporal resolutions; some of its output variables (such as chlorophyll concentration) have been contrasted with satellite data [297]. In particular, Schneider et al. [298] compared global marine productivity estimates from this model with multi-year satellite measurements of ocean colour normalized standard deviation and Pearson's correlation coefficient combined in a Taylor diagram). Values of Pearson's r close to 1 were found for model estimates of both primary production and chlorophyll concentration at the global scale.

3.5 Conclusions and future perspectives

The validation of ecological models outputs through EO is a reality in terrestrial and marine science. The set of variables and models considered for such purpose is increasing with the increasing availability of RS data and standardized datasets favouring comparison. Although non-exhaustive, our review points to considerable variability in the spatial and temporal congruence between modelled and RS variables according to different validation approaches, ranging from qualitative visual comparisons to quantitative rigorous metrics. Also, model outputs and RS data frequently differed in their spatial and temporal resolution, and the consequent use of downscaling and interpolation techniques generate errors and uncertainties that are rarely considered. Time- and space-aggregated variables tended to increase consistency between model outputs and validation data. Discrepancies in punctual validation exercises, such as those based on per-pixel metrics, should encourage the scientific community to further pursue the setup of standards for the comparison of ecological model and RS data, and the identification of sets of comparable variables.

Table 4 5 Essential variables (first column) that have been described in some key terrestrial/biogeochemical marine models and which have been subject to either a qualitative (second column) or a quantitative (third column) validation against RS images. For each reference, the model, the RS data source and the validation metrics (quantitative validation only) are reported

Terrestrial models		
Variable used in validation	**Qualitative validation**	**Quantitative validation**
Gross Primary Productivity	[260] ED2; MODIS-GLASLidar [264] LPJ, MODIS [264] Space-LPJ, MODIS [269] RHESSys, MODIS (MOD17A2)	[265] LSM, Canopy VIs (Pearson's r^2) [299] AquaCrop, Landsat NDVI (NSE)
Net Primary Productivity		[257] CCSM (CASA, CN), MODIS NPP (Pearson's r^2) [261] FOREST-BGC , MODIS NPP (Kappa statistic) [274] DGVM , NOAA-AVHRR, MODIS (direct value comparison)
Leaf Area Index	[264] LPJ and space-LPJ, MODIS [269] RHESSys, MODIS	[257] CCSM (CASA, CN), MODIS (normalized RMSE) [263] LPJ-GUESS, GIMMS (direct value comparison)
Evapotranspiration	[271] SEBS, MODIS	
Land Cover	[263] LPJ, AVHRR	
Wetland plant community	[273] wetland plant communities model; Landsat land cover	
Forest succession		[272] ZELIG-GORT; LandsatTM forest cover (Pearson's r^2)

Biogeochemical marine models		
Variable used in validation	**Qualitative validation**	**Quantitative validation**
Chlorophyll concentration	[277] BFM, SeaWiFS, CZCS [283] BFM, SeaWiFS [295], PISCES, SeaWiFS [296] HAMOOC5, SeaWiFS	[248] ERSEM, SeaWiFS (Taylor diagram, model bias) [278] BFM, SeaWiFS (NSE) [279] BFM, SeaWiFS (Analysis of similarities) [280] BFM, SeaWiFS (NSE) [281] BFM, MODIS (Pearson's *r*, RMSE, model bias) [282] BFM, SeaWiFS (NSE) [286] ECOHAM, MODIS (residuals, Pearson's *r*) [293] ERSEM, MODIS (RMSE, model bias, Pearson's *r*, NSE) [297] PISCES, GlobColour (Taylor diagrams) [298] PISCES, SeaWiFS (Taylor diagrams) [300] ERSEM and BFM, MERIS and MODIS (Taylor diagrams)
Net Primary Productivity	[278] BFM, SeaWiFS	[282] BFM, SeaWiFS (Taylor diagrams) [298] PISCES, SeaWiFS (direct value comparison)
Phytoplankton Community Composition, Phytoplankton Functional Types	[277] BFM, SeaWiFS [294] ERSEM, SeaWiFS	

Table 6 Lists of the terrestrial and marine ecosystem models considered and the associated web page

Terrestrial ecosystem models		
Abbreviation	**Name**	**Link for additional info**
AcquaCrop	AcquaCrop	http://www.fao.org/land-water/databases-and-software/aquacrop/en/
CCSM	Community Climate System Model	http://www.cesm.ucar.edu/models/ccsm4.0/
FOREST-BGC	FOREST-BGC	http://www.ntsg.umt.edu/node/434
ED2	Ecosystem Demography Biosphere	https://github.com/EDmodel/ED2
LPJ	Lund-Potsdam-Jena Model	https://www.pik-potsdam.de/research/projects/activities/biosphere-water-modelling/lpjml
LPJ-GUESS	LPJ-GUESS Ecosystem Model	http://iis4.nateko.lu.se/lpj-guess/
LSM	Land Surface Model	https://daac.ornl.gov/MODELS/guides/LSM_guide.html
ORCHIDEE	ORCHIDEE	http://forge.ipsl.jussieu.fr/orchidee
RHESSy	Regional Hydro-Ecological Simulation System	http://fiesta.bren.ucsb.edu/~rhessys/
SDGM	Sheffield Dynamic Global Vegetation Model	http://www.biogeo.org/ASJ/SDGVM.html
SEBS	Surface Energy Balance System	http://pcraster.geo.uu.nl/projects/applications/sebs/
TRIFFID	Top-down Representation of Interactive Foliage and Flora Including Dynamics	http://climate.uvic.ca/model/common/HCTN_24.pdf
ZELIG	ZELIG Tree Simulator Model	http://ecobas.org/www-server/rem/mdb/zelig.html
Biogeochemical marine models		
Abbreviation	**Name**	**Link for additional info**
BFM	Biochemical Flux Model	http://bfm-community.eu/model-description-1/model-description
ECOHAM	ECOlogical model, HAMburg	http://www.meece.eu/library/ECOHAM4.html
ERSEM	European Regional Seas Ecosystem Model	http://www.pml.ac.uk/Modelling/Models/ERSEM

GETM	General Estuarine Transport Model	http://www.getm.eu/
NEMO	Nucleus for European Modelling of the Ocean	http://www.nemo-ocean.eu/
PISCES	Pelagic Interactions Scheme for Carbon and Ecosystem Studies	http://www.nemo-ocean.eu/

4. Integrating ecosystem models and Earth observations via data assimilation

A. Ziemba[1], G. El Serafy[1], D. Pasetto[2]

[1]Deltares, Delft, The Netherlands
[2]Laboratory of Ecohydrology, École Polytechnique Fédérale de Lausanne, Switzerland

One of the main goals of ecological modelling is the numerical reproduction of the dynamics of an ecosystem, allowing scientists to better understand past events and generate forecasts of probable future scenarios [301]. This is typically achieved by way of statistical models that correlate the ecosystem variables of interest with its covariates, or process-based models that are ground on a mathematical description of the physical processes governing the system [302]. These mathematical and statistical constructs typically consists of a series of interactions among various model components, i.e. input parameters, forcing, and state variables, which should yield acceptable reproductions of the real ecological process under analysis. However, the ecological systems being reproduced are intricate and complex; high levels of interdependencies exist between the components, thereby requiring simplifications and assumption to be used to construct models [303]. Moreover, ecological models suffer from the presence of many sources of errors, as initial conditions, atmospheric forcings, model parameters, and model structure [301], [304], [305]. These errors may propagate in time amplifying the uncertainty on the model outputs.

As presented in Section 2, RS data have been extensively used in ecology for the spatial description of the model inputs, for example by the characterization of the land cover and the atmospheric forcing (precipitation, temperature), helping reducing the uncertainties associated to these variables. In this section we describe how RS data have been used in ecological applications to improve the model results with the help of Data Assimilation (DA) techniques.

While the calibration and validation of models is a pre-requisite for initial deployment, both the operationalization and forecasting ability of models can take advantage of state-updating. This allows improving the model projections in operational applications, where short-term forecasts of the system dynamics are regularly computed. In this framework, for the correct interpretation of the model predictions, it is essential to quantify the errors and discrepancies within the model outputs. Then, the information provided by RS imagery can be combined into the model space to perform an update of the model state variables [9]. This correction of the model outputs with RS data allows a reduction of the errors resulting by the mathematical simplification of the real system. Figure 2 depicts the different sources of errors occurring in both the RS-based observations (in this case chlorophyll estimates) and the results of a marine biophysical model, errors that must be taken into account when performing the state-update procedure.

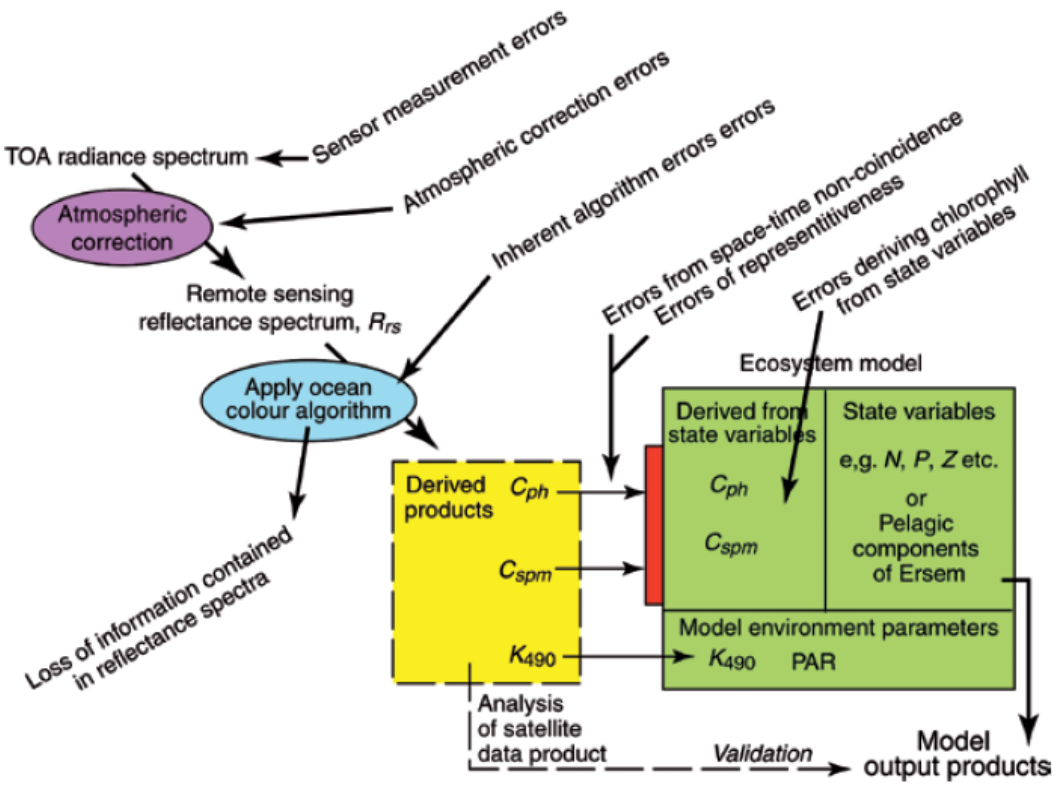

Figure 2 Sources of errors, and potential loss of data in conventional assimilation of satellite-derived chlorophyll data [306].

4.1 Data assimilation techniques

DA techniques have been developed to correct the model predictions and reduce the model output uncertainty by incorporating new observations of the system into the model. The main idea is to better track the dynamics of systems subject to stochastic forcing by sequentially updating the system state variables with respect to the observations, thus having an initial condition more reliable for the subsequent forecast. This approach can be extended to the estimation of model parameters, overcoming problems of over-fitting and equifinality which are common to many standard calibration techniques [303].

Since the beginning of the 90's, due to an increase of the computational power and the availability of RS data, the applicability of DA methods have been explored in several environmental fields such as meteorology, oceanography, and hydrology [307]–[309], with applications including the estimation of the soil moisture content to the river basin hydrology.

4.1.1 State space model

Assuming we want to estimate the dynamic of an ecological system which is described by the variables $\mathrm{x_t}$, the key ingredients common to all DA schemes (see e.g., [201]) are

1. The dynamical model $\mathcal{M}$ that, given the forcing data q_t and a set of parameters θ, approximates the transition (or the forecast) of the state variables of the system, from the estimate at time $t-1$, indicated with x_{t-1}^{a}, to the new state, called forecast or background, and indicated with x_t^f. In formulas:

$$\mathrm{x_t^f} = \mathcal{M}(\mathrm{x_{t-1}^a}, \mathrm{q_t}, \theta) + \eta_t \qquad (1)$$

   where η_t accounts for the model error.

2. The observation model $\mathcal{H}$, that links the model forecast to the real observations y_t taking into account the observation error v_t:

$$y_t^f = \mathcal{H}(x_t^f, \phi) + v_t \quad (2)$$

where ϕ represents the parameters involved in the computation. Note that in most cases the observations are indirect or partial measurements of the state variables.

3. The update step, also called analysis or filtering step, is the core of the DA scheme, and corrects the model state variables toward the observations, from the forecast x_t^f to the analysis x_t^a, reducing the model uncertainty.

Equations (1) and (2) constitute the state-space model. Various DA methods can be used in step 3 in order to adjust the predictions and, if necessary, refine the model parameter θ. As highlighted by Plummer [6] and Bach and Mauser [310], at the beginning of the century DA was already seen as a fundamental tool to merge satellite measurements into environmental models. As an example, Houser et al. [309] assimilated the surface soil moisture obtained with the NASA L band push broom microwave radiometer into the Land Atmosphere Transfer Scheme (TOPLATS) following different approaches:

- Statistical correction: a simple statistical assimilation method that adjusts the modelled surface soil moisture mean and standard deviation in order to match the observed statistics
- Newtonian nudging: a forcing term is added to the model equations to force the model toward the observations
- Optimal (or Statistical) interpolation: similarly to kriging, the soil water content computed with the model (background) is linearly corrected with respect to the misfit between the observations and model results.

The main difficulty in the application of optimal interpolation is the computation of the model covariance matrices, which requires advanced knowledge of the system. Methods such as auto-regressive moving-average can be used in order to compensate for these properties and correlations in space and time [308], [309].

4.1.2 Data assimilation: the Bayesian approach and the ensemble Kalman filter

Modern DA approaches are based on a Bayesian description of the update step. The update step aims in computing the probability density function (PDF) of the state variable x_t conditioned to the available information, i.e. the set of previous observations $y_{1:t} = \{y_1, \dots, y_t\}$, probability that is indicated with $p(x_t \mid y_{1:t})$. Of particular interest is the computation of the state mean and covariance, $\bar{x}_t$ and P_t, respectively. Bayes law rewrites the filtering PDF as

$$p(x_t \mid y_{1:t}) = C\, p(y_t \mid x_t) p(x_t \mid y_{1:t-1}) \quad (3)$$

where C is a normalization constant, $p(x_t \mid y_{1:t-1})$ is the forecast PDF, representing the temporal evolution of the state PDF through the dynamical model, and $p(y_t \mid x_t)$ is the likelihood of the newly acquired observation with respect the model results. The sequential computation of forecast and filtering PDFs (Eq. 3) has an analytical solution only for few particular cases, the most important being the linear state space model having Gaussian errors η_t and ε_t. In this case the forecast and filtering PDFs are Gaussian, and the well-known Kalman Filter (KF) [311] describes the mean and covariance matrix of the state variables. Solutions to Eq. (3) for nonlinear models can be subdivided in three categories:

1. Variational methods, such as 3DVAR and 4DVAR, which compute the updates state variables by minimizing a cost function associated to Eq. (3). These methods are largely applied to atmospheric models for meteorological forecasts, such as the European Centre for Medium-Range Weather Forecasts (ECMWF) [312], [313]. The implementation of variational methods is not straightforward, since the solution of the minimization problem requires the computation of the Jacobian matrix and the adjoint model associated to Eq. (1).
2. Kalman-based methods, such as the Extended Kalman Filter (EKF) and the Ensemble Kalman Filter (EnKF) [314], [315], which approximate the matrices required in the Kalman updated respectively through linearizing the model (EKF) and computing an ensemble of model trajectories (EnKF)
3. Particle filter (PF) methods, as the Sequential Importance Resampling (SIR) [316], which apply Monte Carlo

sampling directly to Eq. (3), without the Gaussian assumption that is implicit in Kalman-based approaches. De Bernardis et al. [317] recently applied PF for the assimilation of NDVI measurements in a crop phonological model.

The large number and varied implementations of EnKF present in literature demonstrates the adaptability and robustness of this DA technique to increase model accuracy through state vector updating [318]. This methodology combines the uncertainty within state vectors concerning the initial state, model estimate, and confidence in data being assimilated and develops a covariance matrix to weight these three components' importance unto the analysis. However, one of the main limitations of the KF-based techniques is the underline assumption of the Gaussian distribution of model state variables and observations. This requirement holds only in the presence of linear model functions, assumption that is rarely representative of environmental processes, and that in some cases can lead to unphysical distribution of model state variables. Modellers are frequently faced with highly non-linear systems, which, as a consequence, demand non-Gaussian assimilation techniques. Alternative approaches include the combination of various DA methods [319]–[321] or interaction of various Gaussian processes [322]. Bocquet et al. [322] explore the use of gradient cost functions in non-linear applications such as pollution dispersion models. In highly non-linear models, alternative approaches as variational methods and PF have proved to be increasingly beneficial in ranges of applications, from hydrology to morphodynamics and terrestrial system dynamics [319], [320], [323]–[325].

4.2 Data assimilation repositories

Given the spread of methodologies through which DA can be implemented, the task of coupling the ecological model with multiple DA methods can be a daunting task. There are several research groups that have been developing open access repositories having various assimilation methodologies and the interfaces for the coupling DA algorithms and an end-user's models. This section presents an overview of Open Data Assimilation (http://www.openda.org), Parallel Data Assimilation Framework (http://pdaf.awi.de), and the Data Assimilation Research Testbed (DART) (http://www.image.ucar.edu/DAReS/DART).

4.2.1 Open Data Assimilation

Open Data Assimilation (OpenDA) is a repository of algorithms coded in mostly Java with C utilized for computationally heavy components. Currently available assimilation methods within OpenDA include KF, EnKF, PF, 3DVar and the Ensemble Square Root Kalman filter (EnSR), which is a deterministic implementation of the EnKF update step. OpenDA provides also methods for the calibration of model parameters, such as simplex, conjugate gradients, Does not Use Derivatives (DUD), Powell, and others. Many of these algorithms can be easily implemented 'off-the-shelf' via the interface provided by OpenDA with minimal coding required, exemplifying the modular concept of the platform. This straightforward approach is based on the writing and reading of the exchange files for the interface, and might result computationally expensive for large applications. OpenDA has also the possibility to couple the model and the DA methods on-line, which minimizes the but requires rewriting the source code of the model as libraries. Van Velzen et al. [326] explored the fundamental components of the implementation of OpenDA and coupled EnKF with the NEMO ocean wave model. In this experiment, a synthetic scenario is created utilizing real data from Jason-1 and ENVISAT to assimilate Sea Surface Height of the ocean. Potentialities for localization and parallel computing are addressed as well as the assimilation set-up.

The interaction between OpenDA and the model space can be realized at run-time also through the Open Model Interface (OpenMI) (http://www.openmi.org/). The OpenMI standard is a software component which allows models to interact and exchange data during computation, allowing the sharing of data at each time-step interval, and has already been applied by a range of common model suppliers including hydrological, hydrodynamic, water quality, and sediment models from suppliers such as Deltares, DHI, and Innovyze. Because OpenMI allows for information exchange at each time-step, it easily interfaces with the assimilation techniques present within OpenDA. Ridler et al. [327] looked intensively at the utility of implementing OpenMI with OpenDA, illustrating work-flow diagrams, and implementation suggestions.

OpenDA has been successfully applied for the assimilation of RS measurements, especially in marine applications. For example, Kurniawan et al. [328] improved the simulation of flow vectors and tidal forcings of the Singapore Regional Waters by assimilating TOPEX/POSEIDON data, satellite altimetry data from the RADs database, and level-2 altimetry data products. Serpoushan et al. [329] used the EnKF of the OpenDA toolbox in order to assimilate significant wave height and wind data into the wave model SWAN for the Persian Gulf.

Garcia et al. [330] applies OpenDA for the automated calibration of a costal model (Delft-3D-FLOW) in order to determine the chemical properties within the San Quintin Bay (Baja California, Mexico). The water quality is critical for the growth and survival of the Japanese oyster *Crassotrea gigas*, which lives in the bay. The study provided a proof of concept that OpenDA is a valuable tool for the automated calibration of coastal models on the sub-meso scale.

4.2.2 Parallel Data Assimilation Framework

The Parallel Data Assimilation Framework (PDAF) [331] is an open library written in FORTRAN90 supporting a parallel implementation of DA schemes. Due to a standard interface, PDAF can be easily coupled to models written in different languages [332]. The library includes several variants of the EnKF method, such as the Ensemble Transform Kalman Filter (ETKF) and its local version (LETKF). The integration of PDAF algorithms with models requires minimal changes within the model source code, leaving the heavy computing numerical components free of change, but requiring a small set of routines which are specific for each model and observations (see http://pdaf.awi.de).

Kurtz et al. [333] integrated PDAF with a land-surface-subsurface model. A synthetic study is proposed to exemplify the processing power and scalability due to the parallelization of this framework, utilizing a model with 0.8 million unknowns. Losa et al. [334] coupled PDAF to the German Federal Maritime and Hydrographic Agency's (BSH) for the operational forecasting of the North and Baltic Seas. In this case a Kalman-based filter assimilates NOAA's SST. This study involves an in-depth investigation into the implementation of the framework and a quality comparison of the results.

4.2.3 Data Assimilation Research Testbed

DART is a combination of models, DA algorithms, as well as both real and synthetic observations in a FORTRAN 90 format that allows for investigation and development of DA. The DART platform is operated and maintained by the Data Assimilation Research Section (DAReS) (see http://www.image.ucar.edu/DAReS), and allows for community development and integration of algorithms and models into the framework. DART has a number of models ranging from land surface models to ocean and atmospheric models, among which are: NOAH Land Surface Model, Model for Prediction Across Scales (MPAS) Ocean, Atmosphere components, and Coupled Ocean/Atmosphere Mesoscale Prediction (COAMPS). DART includes the most popular DA techniques: Ensemble Adjusted Kalman Filter (EAKF), EnKF, and PF. DART provides multiple pre-scripted options for creating synthetic observations (i.e. observations obtained from a true run of the model) and also for the localization of both real and synthetic data sets for model integration.

There have been multiple applications of DART to various data sources ranging from high quality in-situ data to a wide selection of RS products. Hacker and Angevine [335] assimilated high quality in-situ data from Atmospheric Radiation Measurement (ARM) Facility into a single column version of the Weather Research and Forecasting Model (WRF). This project's aim was to determine if the implementation and heavy weighting of the in-situ measurement would be able to accurately predict the fluxes occurring at the land air boundary and subsequently determine the land surface state. Detailed findings and methods of introducing bias and covariance into the system are explored throughout the paper. Mizzi et al. [336] improved the gas retrievals of the Weather Research and Forecasting Model with chemistry (WRF-Chem) through the DART assimilation of sparse RS data of carbon monoxide and particulate matter, obtained by the Terra/Measurement of Pollution in the Troposphere (MOPITT) and the Infrared Atmospheric Sounding Interferometer (IASI) instruments. In this case the spatial detail within each of the RS images remains limited and the model is used to provide an estimate in the missing locations. This is a clear example

showing that DA techniques are useful tools to improve the monitoring of a system by using ecological model to fill the gap among sparse observations.

DART has been coupled to the Community Land Model (CLM) for the assimilation of snow cover data products from MODIS [337], and for the integration of the environmental variables compiled by the National Ecological Observatory Network (NEON) , which have different spatial and temporal resolutions ranging from continental satellite imagery to individual organism surveys.

4.3 Determination of the observation uncertainty

Earth Observations are typically affected by a certain degree of error, which plays a crucial role in the correction of the model outputs [304], [308]. Waller et al. [338] identified four main sources of errors that typically afflict RS observations: instrument errors, errors in the observational model (e.g., in radiative transfer models), errors of representativity (due to upscaling or downscaling processes between measurement and model meshes, with possible loss of information), pre-processing errors introduced when cleaning the data (e.g. removing the effect of clouds for radiance). Lahoz and Lannoy [339] discuss the origin of these errors and the method through which they spread and propagate from level 0 (raw satellite data) to the higher level data products.

The importance of the characterization of the measurement uncertainty is shown in [340] for the estimation of soil moisture and contaminant concentrations. As an idea, the analysis step of a DA scheme should strongly correct the model outputs toward the observations with low uncertainty, while highly uncertain measurements should generate small changes in the model results.

The Bayesian analysis step that is at the bases of the described DA procedures (VAR, KF, EnKF, PF) requires the quantification of the PDF associated to the measurement error v_t (Eq. 2). The error v_t is typically characterized as an additive Gaussian noise, with zero mean and covariance matrix R, possibly time-dependent [316]: $v_k \sim N(0, R_t)$. The entries of the covariance matrix R represent the variance of the single observations and the cross-covariances, and completely describe the measurement error for the DA purposes. When dealing with in-situ data, errors of measurements collected at different locations are assumed to be independent, thus R results in a diagonal matrix with elements corresponding to the sensor variances. The computation of R is more difficult for the assimilation of RS data, since the cross-covariances should be computed at the pixel level. The components of R should take into account the cumulative effect of all the sources of error identified by [338]. Crosetto et al. [341] proposed a procedure to characterized the uncertainty associated to high-level RS products, which is based on:

1. identification of all sources of uncertainty involved in the computation of the RS products,
2. probabilistic modelling of these uncertainties,
3. uncertainty propagation with a Monte Carlo scheme,
4. sensitivity analysis to assess the impact on the output of the different sources of uncertainties

and applied the procedure for the detection of burned area based on the Pathfinder AVHRR data. Other applications of this uncertainty analysis include the EQeau model estimating the snow water equivalent from satellite C-band SAR data [342], and the uncertainty on the estimation of urban land-use and changes with SPOT data [343]. Even if such examples are present in literature, most RS models used to obtain high-level products neglect the uncertainty propagation of the instrument and parameter errors, and the product accuracy is only assessed a posteriori, by means of costly validations with respect to in-situ measurements or other RS data. The comparison with the output of calibrated process-based models may also help in the evaluation of the observation errors: Wanders et al. [324] use the hydrological model SWAP to assess the average standard error on surface soil moisture retrievals from different microwave sensors: ASCAT, AMSR-E (Advanced Microwave Scanning Radiometer - Earth Observing System) and SMOS. The average standard deviations of the errors (0.049, 0.057 and 0.051 m3m−3 for AMSR-E, SMOS, and ASCAT, respectively) are then used in the EnFK assimilation applied to the LISFLOOD hydrological model of the Upper Danube Basin [344].

Today, a large effort is devoted in evaluating the a posteriori error, with the goal of improving the algorithms processing the RS data by providing a per-pixel quantification of the errors. For example, HYDROPT algorithm [345] processes MERIS data to estimate the suspended particulate matter in the sea water, computing the associated confidence intervals in terms of per-pixel standard deviation obtained from MERIS Level 2 Product Confidence Data flag [346]. El Serafy et al. [9] assimilated these RS measurement into the computational water quality and sediment transport model of the Northern Sea (Delft3D-WAQ) with the EnKF procedure.

The computation of the cross-covariances of the observation error at a pixel level presents an even greater challenge. A possibility to circumvent this lack of information in the application of DA techniques is to estimate the entries of R using the statistics associated to the observations-minus-forecast, and observation-minus-analyses residuals. Such an approach aims in computing the error statistics before every update using the difference between the model simulations and the observation. Desroziers et al. [347] initially proposed this procedure as a diagnostic of the background and observation error variances. Recent studies explored the validity of Desroziers' approach [348], [349], its possible improvement with an ensemble of model runs [350], the combination with EnKF [338], [348], and the application for computing the interchannel observation-error correlation for Infrared Atmospheric Sounding Interferometer (IASI) [351].

A different and more sophisticated approach described by Plummer [6] and Bach and Mauser [310] consists in coupling the ecological model with a radiative transfer model, in such a way to directly compare the model predictions with the RS measurements (e.g., level 1 products). The main advantage of this approach is to avoid inconsistencies (in the methodology, parameterization, and computational grid) between the ecological products obtained inverting the RS measurements and those computed from the process-based model outputs. Moreover this approach entails a better description of the observation error, which relays only on the on the standard deviation of the instrument error. This coupled approach has been largely employed for hydrological applications with both Kalman-based [352]–[354] and variational-based [355]–[357] assimilation of RS radiometer data. De Lannoy and Reichle [245] have recently assimilated SMOS observations of temperature brightness in the Goddard Earth Observing System model with the scope of improving the estimation of soil moisture at a global scale with the EnKF technique. The coupled approach introduces an additional source of uncertainty in the radiative transfer model, due to parameters, structure or soil/vegetation information. De Lannoy and Reichle [245] increase the error standard deviation of the measured temperature brightness from 4K to 6K because of this uncertainty. In this case the spatial error correlation is assumed isotropic with exponential correlation function, and correlation length estimated following Desroziers' technique [347].

4.4 Determination of model uncertainty

The forecast step of DA schemes requires the quantification of the model uncertainty in order to perform an effective analysis. However, many ecosystem models do not yet integrate uncertainty analysis into their predictions [358]. Refsgaard [301] proposes a general framework and guidelines to be addressed when evaluating uncertainty in environmental modelling processes. Within this framework a diligent explanation of the terminology, classification, and taxonomy of uncertainty is also presented in order to conform to popular semantics within the topic. The general approaches of sensitivity analyses, multi-dimensional uncertainty assessment, inverse and multiple model simulations are addressed among others. In details, the main sources of uncertainty to take into account when computing the forecast (Eq. 1) are [301]:

1. Input uncertainty, i.e. the quantification of the errors on the initial condition of the system, x_0, and the external forcing q_t, e.g. precipitation [359], surface temperature, land cover/land use [360], etc.
2. Parameter uncertainty, defined in terms of the probabilistic characterization of the parameters, θ, which control the ecological process.
3. Structural uncertainty, generated by the inadequacy of the model and eventual output bias, which are due to approximations and simplifications of the ecological processes occurring in the real system. The probabilistic distribution of the error term η_t (Eq. 3) should take into account this source of uncertainty.
4. Numerical uncertainty, due to the numerical algorithms and the spatial-temporal discretization used in the solution of the model equations. This source of error is frequently ignored in environmental modelling, and, thus, implicitly considered in the error term η_t.

These uncertainties may have either an epistemic nature, i.e. due to lack of knowledge (e.g. on the parameter distribution), either a stochastic nature, which is intrinsic of the phenomena under study (e.g. when dealing with

climate data). MC-based DA schemes, such as EnKF and particle filters, obtain the forecast step by running the model with an ensemble of realizations, each associated to different samples of the inputs, forcing term, and model error. The definition of these PDFs is typically straightforward for the input and the forcing, based on direct error statistics. For example, a common choice in sampling from rainfall is to consider a multiplicative lognormal noise with an assigned temporal and spatial correlation (see, e.g. [245]). More difficult and computational expensive is the assessment of the parameter uncertainty. Sensitivity analysis and Bayesian parameter calibration techniques help in reducing these epistemic uncertainties, resulting in a more accurate characterization of the parameter PDF.

The characterization of the structural uncertainty η_t is nontrivial and constitutes one of the main issues in model forecasting [308], at the point that many applications neglect this source of uncertainty, thus clearly underestimating the model output variances. The simplest approach considers the model error as a Gaussian distribution, $\eta_t \sim N(m_t, Q_t)$, where m_t is the error mean (in general equal to zero if the model does not present systematic bias) and Q_t the covariance matrix. As happening for the observation error, the structural uncertainty is determined by the error covariance matrix Q_t and its correlation scale, which are not known in high-dimensional ecological models. Reichle [361] clearly states that the specification of the covariance matrix is largely subjective, meaning that a ad-hoc error estimations have been developed for different models and applications. Recent technique to tackle this problem try to estimates the model error forcing from DA diagnostics, i.e. from the differences between model and observations, similarly to what is done for the observation error. Piccolo and Cullen [362] showed that this approach is successful if there are sufficient observations.

The correct estimation of the model error is fundamental when assimilating RS data into ecological models, since it should allow the measurement to follow into the confidence interval of the model outputs. Modelling the terrestrial soil moisture at a global scale, De Lannoy and Reichle [245] assign static perturbation statistics for the error of the land surface model GEOS-5 CLSM. In this case two model state variables are perturbed with an additive noise characterized by fix temporal and spatial correlations. The spatial correlation of the input errors improves the smoothness of the state variables and of the consequent DA update.

El Serafy et al. [9] proposed an iterative procedure to compute the variance and the correlation scale associated to the error covariance matrix Q_k. The procedure, applied for the uncertainty quantification of the suspended particulate matter concentration in the Delft3D-WAQ model, permitted to recognize the dominant spatial correlations of the system error during the chosen temporal window of forecast (e.g., one month).

As the materials presented here within aim to characterize the potential improvements possible through the assimilation of RS data into models, it is also paramount to address the potentiality of over-estimating the resulting certainty of results from such applications. Reichstein and Richardson [304] proposes a code of best practices in order to best analyze the results from a DA application. They investigate an array of data sources from within the environmental sciences as explored by other researches and determine that on many occasions uncertainties in the data can be of the same order of magnitude as the resulting application of a model-DA.

4.5 Assimilation of Earth observations in ecosystem models

DA has been more and more applied in several fields of ecology. As reported for example in [7], DA has been used for modelling the spread of infectious diseases, fire, fisheries, and carbon cycle. Lahoz and Lannoy [339] have completed an extensive review of DA applications on hydrological models for the terrestrial water cycle, with emphasis on the assimilation of RS measurements. The main state variables of LSM include water content and temperature of soil moisture, snow, and vegetation. The main RS measurements that have been assimilated for the estimation of these variables and for improving streamflow forecasts (e.g. [363]) are surface soil moisture, snow cover or albedo, snow water equivalent, backscatter, brightness temperature, surface soil temperature, evapotranspiration, and LAI [339]. Despite the recent advances in coupling RS data to hydrological models, Vereecken et al. [364] addresses the limitations of assimilating RS soil moisture, as its dependency from vegetation and soil roughness which may cause bias in the measurements. The coarse spatial resolution, typically in the order of several or more kilometres, and the low penetration depth of the sensors is not enough to make a marked improvement when correcting the results of hydrological models. Recent applications of EnKF to hydrological models are focusing on assimilation procedures of soil moisture products (mainly derived from SMOS) capable of

removing possible measurement and model biases (e.g. [321], [365]–[367] or directly assimilating brightness temperature [245].

Carbon cycle models, i.e. those models that aim to quantify the carbon exchanges between the terrestrial Earth surface, the vegetation and the atmosphere, often together with water and energy fluxes, have been increasingly exploiting DA techniques [7], [368]. Main output of interest of these models are GPP and NPP, which estimation has been improved assimilating both in situ-measurements (e.g. eddy covariance fluxes), and RS measurements such as NDVI [369], [370] and surface temperature measurements [371].

RS data have been largely employed in the realm of agroecosystem modelling since LANDSAT-1 was launched in 1972, which enabled the first RS measurements of several vegetation indices. Dorigo et al. [372] presented an encompassing blend of state and driver biophysical parameters as indicators for various ecological functions and processes, highlighting that RS measurements of LAI, fractional cover (fCOVER), fraction of photosynthetically active radiation absorbed by the canopy (fAPAR), and plant chlorophyll concentration are among the most important canopy state variables and therefore frequently assimilated in agroecosystem models. As an example, [310] refined the biomass, canopy height, and yield obtained from a land surface model through assimilation of multiple RS products including land classification from LANDSAT/TM, and ERS-derived soil moisture content.

KF-based techniques have been largely applied for the assimilation of RS measurements in ocean models. As an example, Belyaev et al. [373] used KF to improve the results of the large scale oceanic model NOAA-GFDL applied to a tropical area of the Atlantic Ocean. In this case the result of the assimilating ocean temperatures collected through the PIRATA project is a small but clear improvement in the outputs [373]. EnKF technique has been successfully used in a number of modelling applications in conjunction with MERIS satellite data in order to reduce modelling errors and achieve a better fit of the output with respect to in-situ observations [8], [374]–[376]. EnKF has been used to combine MERIS SPM data from ESA's ENVISAT satellite into the Delft-3D Water Quality model [377], in order to update the modelled SPM over the North Sea and Dutch coastal waters [8]. One of the key results of this study is that the uncertainty and errors within the model space and both the raw and gridded RS data must be carefully calculated in order to properly weight the two against one another and achieve proper updates at each time step [8].

4.6 Conclusions and future perspectives

DA techniques are computationally solid approaches for the sequential update of the model state variables (and possibly model parameters) towards the newly acquired observations, keeping into account the distribution of the model and observation errors. DA techniques represent ideal tools to incorporate into ecosystem models the large amount of information that is continuously received from space. The increased number of ecological applications adopting DA strategies, in particular ensemble-based methods such as EnKF, to improve the system predictions demonstrates the general interest of the community and the advantages of these approaches. Two main recommendations emerge from the proposed review. First, to fully explore the variety of DA techniques available in literature, the development of ecosystem models should move in the direction of structure the codes in a way that they can be easily connected to the available platforms containing DA and calibration algorithms, such as the described DART, OpenDA, and PDAF. In fact, the small investment required in terms of updating the model codes is greatly compensate by the accessibility to a number of state of the art, well tested algorithms useful for the assimilation of RS data and the assessment of model uncertainty. We also remark that, except for the presence of few examples in hydrological applications, the strategy suggested by Plummer [6] of directly coupling ecosystem models with reflectance transfer models is rarely adopted in ecological applications. Although the direct coupling would required the calibration of a larger number of model parameters, the possibility of comparing the simulated reflectance with the RS measurements would allow a better description of the observation uncertainties, as well as decreasing the errors associated with mismatches and interpolations of model and RS grids. The limited use of this approach is probably due to the large availability of free global RS images, in conjunction with the difficulties associated with the calibration of physically-based reflectance transfer models. Collaborations between the remote sensing and the ecosystem modellers communities should help to overcome these difficulties.

5. References

[1] K. A. Rose, J. I. Allen, Y. Artioli, M. Barange, J. Blackford, F. Carlotti, R. Cropp, U. Daewel, K. Edwards, K. Flynn, S. L. Hill, R. HilleRisLambers, G. Huse, S. Mackinson, B. Megrey, A. Moll, R. Rivkin, B. Salihoglu, C. Schrum, L. Shannon, Y.-J. Shin, S. L. Smith, C. Smith, C. Solidoro, M. St. John, and M. Zhou, "End-To-End Models for the Analysis of Marine Ecosystems: Challenges, Issues, and Next Steps," *Mar Coast Fish*, vol. 2, no. 1, pp. 115–130, 2010.

[2] B. J. Robson, "When do aquatic systems models provide useful predictions, what is changing, and what is next?," *Environ Model Softw*, vol. 61, pp. 287–296, 2014.

[3] K. Hyder, A. G. Rossberg, J. I. Allen, M. C. Austen, R. M. Barciela, H. J. Bannister, P. G. Blackwell, J. L. Blanchard, M. T. Burrows, E. Defriez, T. Dorrington, K. P. Edwards, B. Garcia-Carreras, M. R. Heath, D. J. Hembury, J. J. Heymans, J. Holt, J. E. Houle, S. Jennings, S. Mackinson, S. J. Malcolm, R. McPike, L. Mee, D. K. Mills, C. Montgomery, D. Pearson, J. K. Pinnegar, M. Pollicino, E. E. Popova, L. Rae, S. I. Rogers, D. Speirs, M. A. Spence, R. Thorpe, R. K. Turner, J. van der Molen, A. Yool, and D. M. Paterson, "Making modelling count - increasing the contribution of shelf-seas community and ecosystem models to policy development and management," *Mar Policy*, vol. 61, pp. 291–302, 2015.

[4] L. Polimene, C. Brunet, M. Butenschon, V. Martinez-Vicente, C. Widdicombe, R. Torres, and J. I. Allen, "Modelling a light-driven phytoplankton succession," *J Plankton Res*, vol. 36, no. 1, pp. 214–229, 2014.

[5] N. K. Ganju, M. J. Brush, B. Rashleigh, A. L. Aretxabaleta, P. del Barrio, J. S. Grear, L. A. Harris, S. J. Lake, G. McCardell, J. O'Donnell, D. K. Ralston, R. P. Signell, J. M. Testa, and J. M. P. Vaudrey, "Progress and Challenges in Coupled Hydrodynamic-Ecological Estuarine Modeling," *Estuaries and Coasts*, vol. 39, no. 2, pp. 311–332, 2016.

[6] S. E. Plummer, "Perspectives on combining ecological process models and remotely sensed data," *Ecol Modell*, vol. 129, no. 2, pp. 169–186, 2000.

[7] S. Niu, Y. Luo, M. C. Dietze, T. F. Keenan, Z. Shi, J. Li, and F. S. C. Iii, "The role of data assimilation in predictive ecology," *Ecosphere*, vol. 5, no. 5, p. art65, 2014.

[8] G. Y. El Serafy, M. Blaas, M. A. Eleveld, H. J. Van Der Woerd, N. Sea, G. Y. El Serafy, M. Blaas, M. A. Eleveld, and H. J. van der Woerd, "Data Assimilation of Satellite Data of Suspended Particulate Matter in Delft3D-WAQ for the North Sea," in *Proceedings of the Joint EUMETSAT/AMS Conference*, 2007, pp. 1–8.

[9] G. Y. El Serafy, M. A. Eleveld, M. Blaas, T. Van Kessel, S. G. Aguilar, and H. J. Van Der Woerd, "Improving the Description of the Suspended Particulate Matter Concentrations in the Southern North Sea through Assimilating Remotely Sensed Data," *Ocean Sci*, vol. 46, no. 3, pp. 179–204, 2011.

[10] N. Pettorelli, *The normalized difference vegetation index*. Oxford University Press, 2013.

[11] B. Smith, W. Knorr, J.-L. Widlowski, B. Pinty, and N. Gobron, "Combining remote sensing data with process modelling to monitor boreal conifer forest carbon balances," *For Ecol Manage*, vol. 255, no. 12, pp. 3985–3994, 2008.

[12] X. Feng, G. Liu, J. M. Chen, M. Chen, J. Liu, W. M. Ju, R. Sun, and W. Zhou, "Net primary productivity of China's terrestrial ecosystems from a process model driven by remote sensing," *J Environ Manage*, vol. 85, no. 3, pp. 563–573, 2007.

[13] W. Ju, P. Gao, Y. Zhou, J. M. Chen, S. Chen, and X. Li, "Prediction of summer grain crop yield with a process-based ecosystem model and remote sensing data for the northern area of the Jiangsu Province, China," *Int J Remote Sens*, vol. 31, no. 6, pp. 1573–1587, 2010.

[14] R. Houborg, M. McCabe, A. Cescatti, F. Gao, M. Schull, and A. Gitelson, "Joint leaf chlorophyll content and leaf area index retrieval from Landsat data using a regularized model inversion system (REGFLEC)," *Remote Sens Environ*, vol. 159, pp. 203–221, 2015.

[15] W. Qi, C. Zhang, G. Fu, C. Sweetapple, and H. Zhou, "Evaluation of global fine-resolution precipitation products and their uncertainty quantification in ensemble discharge simulations," *Hydrol Earth Syst Sci*, vol. 20, no. 2, pp. 903–920, 2016.

[16] W. Wang, H. Lu, D. Yang, K. Sothea, Y. Jiao, B. Gao, X. Peng, and Z. Pang, "Modelling Hydrologic Processes in the Mekong River Basin Using a Distributed Model Driven by Satellite Precipitation and Rain Gauge Observations," *PLoS One*, vol. 11, no. 3, p. e0152229, 2016.

[17] D. J. Leroux, T. Pellarin, T. Vischel, J.-M. Cohard, T. Gascon, F. Gibon, A. Mialon, S. Galle, C. Peugeot, and L. Seguis, "Assimilation of SMOS soil moisture into a distributed hydrological model and impacts on the water cycle variables over the Ouémé catchment in Benin," *Hydrol Earth Syst Sci*, vol. 20, no. 7, pp. 2827–2840, 2016.

[18] N. P. Molotch, M. T. Durand, B. Guan, S. A. Margulis, and R. E. Davis, "Snow Cover Depletion Curves and Snow Water Equivalent Reconstruction," V. Lakshmi, D. Alsdorf, M. Anderson, S. Biancamaria, M. Cosh, J. Entin, G. Huffman, W. Kustas, P. van Oevelen, T. Painter, J. Parajka, M. Rodell, and C. Rüdiger, Eds. John Wiley & Sons, Inc, Hoboken, NJ, 2014, pp. 157–173.

[19] D. Amitrano, G. Di Martino, A. Iodice, D. Riccio, G. Ruello, F. Ciervo, M. N. Papa, and Y. Koussoubé, "Effectiveness of high-resolution SAR for water resource management in low-income semi-arid countries," *Int J Remote Sens*, vol. 35, no. 1, pp. 70–88, 2014.

[20] S. Saatchi, W. Buermann, H. ter Steege, S. Mori, and T. B. Smith, "Modeling distribution of Amazonian tree species and diversity using remote sensing measurements," *Remote Sens Environ*, vol. 112, no. 5, pp. 2000–2017, 2008.

[21] V. Deblauwe, V. Droissart, R. Bose, B. Sonké, A. Blach-Overgaard, J.-C. Svenning, J. J. Wieringa, B. R. Ramesh, T. Stévart, and T. L. P. Couvreur, "Remotely sensed temperature and precipitation data improve species distribution modelling in the tropics," *Glob Ecol Biogeogr*, vol. 25, no. 4, pp. 443–454, 2016.

[22] A. F. Cord, D. Klein, D. S. Gernandt, J. A. P. de la Rosa, and S. Dech, "Remote sensing data can improve predictions of species richness by stacked species distribution models: a case study for Mexican pines," *J Biogeogr*, vol. 41, no. 4, pp. 736–748, 2014.

[23] F. Zellweger, V. Braunisch, A. Baltensweiler, and K. Bollmann, "Remotely sensed forest structural complexity predicts multi species occurrence at the landscape scale," *For Ecol Manage*, vol. 307, pp. 303–312, 2013.

[24] M. Deshayes, D. Guyon, H. Jeanjean, N. Stach, A. Jolly, and O. Hagolle, "The contribution of remote sensing to the assessment of drought effects in forest ecosystems," *Ann For Sci*, vol. 63, pp. 579–595, 2006.

[25] J. F. Brown, B. D. Wardlow, T. Tadesse, M. J. Hayes, and B. C. Reed, "The Vegetation Drought Response Index (VegDRI): A New Integrated Approach for Monitoring Drought Stress in Vegetation," *GIScience Remote Sens*, vol. 45, no. 1, pp. 16–46, 2008.

[26] T. Tadesse, B. D. Wardlow, M. J. Hayes, M. D. Svoboda, and J. F. Brown, "The Vegetation Outlook (VegOut): A New Method for Predicting Vegetation Seasonal Greenness," *GIScience Remote Sens*, vol. 47, no. 1, pp. 25–52, 2010.

[27] A. Omstedt, *Guide to Process Based Modeling of Lakes and Coastal Seas*. Berlin, Heidelberg: Springer Berlin Heidelberg, 2011.

[28] M. R. Dhanak and N. I. Xiros, Eds., *Springer Handbook of Ocean Engineering*, 1st ed. Springer International Publishing, 2016.

[29] D. Roelvink and A. Reniers, *A Guide to Modeling Coastal Morphology*, vol. 12. WORLD SCIENTIFIC, 2011.

[30] V. Klemas, "Remote Sensing Techniques for Studying Coastal Ecosystems: An Overview," *J Coast Res*, vol. 27, pp. 2–17, 2011.

[31] H. Li, M. Arias, A. Blauw, H. Los, A. E. Mynett, and S. Peters, "Enhancing generic ecological model for short-term prediction of Southern North Sea algal dynamics with remote sensing images," *Ecol Modell*, vol. 221, no. 20, pp. 2435–2446, 2010.

[32] H. Lenhart, D. K. Mills, H. Baretta-bekker, S. M. Van Leeuwen, J. Van Der Molen, J. W. Baretta, M. Blaas, X. Desmit, W. Kühn, G. Lacroix, H. J. Los, A. Ménesguen, R. Neves, R. Proctor, P. Ruardij, M. D. Skogen, A. Vanhoutte-brunier, M. T. Villars, and S. L. Wakelin, "Predicting the consequences of nutrient reduction on the eutrophication status of the North Sea," *J Mar Syst*, vol. 81, no. 1–2, pp. 148–170, 2010.

[33] H. Ashouri, K.-L. Hsu, S. Sorooshian, D. K. Braithwaite, K. R. Knapp, L. D. Cecil, B. R. Nelson, O. P. Prat, H. Ashouri, K.-L. Hsu, S. Sorooshian, D. K. Braithwaite, K. R. Knapp, L. D. Cecil, B. R. Nelson, and O. P. Prat, "PERSIANN-CDR: Daily Precipitation Climate Data Record from Multisatellite Observations for Hydrological and Climate Studies," *Bull Am Meteorol Soc*, vol. 96, no. 1, pp. 69–83, 2015.

[34] R. Müller, U. Pfeifroth, C. Träger-Chatterjee, R. Cremer, J. Trentmann, and R. Hollmann, "Surface Solar Radiation Data Set - Heliosat (SARAH) - Edition 1," 2015.

[35] I. Eberhardt, B. Schultz, R. Rizzi, I. Sanches, A. Formaggio, C. Atzberger, M. Mello, M. Immitzer, K. Trabaquini, W. Foschiera, and A. José Barreto Luiz, "Cloud Cover Assessment for Operational Crop Monitoring Systems in Tropical Areas," *Remote Sens*, vol. 8, no. 3, p. 219, 2016.

[36] A. M. Wilson and W. Jetz, "Remotely Sensed High-Resolution Global Cloud Dynamics for Predicting Ecosystem and Biodiversity Distributions," *PLOS Biol*, vol. 14, no. 3, p. e1002415, 2016.

[37] Y. Wang, L. Liu, Y. Hu, D. Li, and Z. Li, "Development and validation of the Landsat-8 surface reflectance products using a MODIS-based per-pixel atmospheric correction method," *Int J Remote Sens*, vol. 37, no. 6, pp. 1291–1314, 2016.

[38] G. Huang, M. Ma, H. Li, and C. Huang, "High resolution surface radiation products for studies of regional energy, hydrologic and ecological processes over Heihe river basin, northwest China," *Agric For Meteorol*, vol. 230, pp. 67–78, 2016.

[39] G. Huang, M. Ma, S. Liang, S. Liu, and X. Li, "A LUT-based approach to estimate surface solar irradiance by combining MODIS and MTSAT data," *J Geophys Res Atmos*, vol. 116, no. D22, p. n/a-n/a, 2011.

[40] G. Peng, J. Li, Y. Chen, A. P. Norizan, and L. Tay, "High-resolution surface relative humidity computation using MODIS image in Peninsular Malaysia," *Chinese Geogr Sci*, no. 3, pp. 260–264, 2006.

[41] C. Recondo, J. J. Peón, E. Zapico, and E. Pendás, "Empirical models for estimating daily surface water vapour pressure, air temperature, and humidity using MODIS and spatiotemporal variables. Applications to peninsular Spain," *Int J Remote Sens*, vol. 34, no. 22, pp. 8051–8080, 2013.

[42] K. Wang, P. Wang, Z. Li, M. Cribb, and M. Sparrow, "A simple method to estimate actual evapotranspiration from a combination of net radiation, vegetation index, and temperature," *J Geophys Res*, vol. 112, no. D15, p. D15107, 2007.

[43] T. Luo, A. Jutla, and S. Islam, "Evapotranspiration estimation over agricultural plains using MODIS data for all sky conditions," *Int J Remote Sens*, vol. 36, no. 5, pp. 1235–1252, 2015.

[44] Y. Ke, J. Im, S. Park, and H. Gong, "Spatiotemporal downscaling approaches for monitoring 8-day 30m actual evapotranspiration," *ISPRS J Photogramm Remote Sens*, vol. 126, pp. 79–93, 2017.

[45] S. Michaelides, V. Levizzani, E. Anagnostou, P. Bauer, T. Kasparis, and J. E. Lane, "Precipitation: Measurement, remote sensing, climatology and modeling," *Atmos Res*, vol. 94, no. 4, pp. 512–533, 2009.

[46] Y. Shi and L. Song, "Spatial downscaling of monthly TRMM precipitation based on EVI and other geospatial variables over the Tibetan plateau from 2001 to 2012," *Mt Res Dev*, vol. 35, no. 2, pp. 180–194, 2015.

[47] M. Ninyerola, X. Pons, and J. M. Roure, "Monthly precipitation mapping of the Iberian Peninsula using spatial interpolation tools implemented in a Geographic Information System," *Theor Appl Climatol*, vol. 89,

no. 3–4, pp. 195–209, 2007.

[48] R. J. Hijmans, S. E. Cameron, J. L. Parra, P. G. Jones, and A. Jarvis, “Very high resolution interpolated climate surfaces for global land areas,” *Int J Climatol*, vol. 25, no. 15, pp. 1965–1978, 2005.

[49] D. N. Karger, O. Conrad, J. Böhner, T. Kawohl, H. Kreft, R. W. Soria-Auza, N. E. Zimmermann, H. P. Linder, and M. Kessler, “CHELSA climatologies at high resolution for the earth’s land surface areas (Version 1.1),” *World Data Cent Clim DKRZ*, Jan. 2016.

[50] G. J. Huffman, R. F. Adler, P. Arkin, A. Chang, R. Ferraro, A. Gruber, J. Janowiak, A. McNab, B. Rudolf, U. Schneider, G. J. Huffman, R. F. Adler, P. Arkin, A. Chang, R. Ferraro, A. Gruber, J. Janowiak, A. McNab, B. Rudolf, and U. Schneider, “The Global Precipitation Climatology Project (GPCP) Combined Precipitation Dataset,” *Bull Am Meteorol Soc*, vol. 78, no. 1, pp. 5–20, 1997.

[51] P. Xie, P. A. Arkin, P. Xie, and P. A. Arkin, “Global Precipitation: A 17-Year Monthly Analysis Based on Gauge Observations, Satellite Estimates, and Numerical Model Outputs,” *Bull Am Meteorol Soc*, vol. 78, no. 11, pp. 2539–2558, 1997.

[52] K. Aonashi, J. Awaka, M. Hirose, T. Kozu, T. Kubota, G. Liu, S. Shige, S. Kida, S. Seto, N. Takahashi, and Y. N. Takayabu, “GSMaP Passive Microwave Precipitation Retrieval Algorithm : Algorithm Description and Validation,” *J Meteorol Soc Japan*, vol. 87, no. 87, pp. 119–136, 2009.

[53] T. Kubota, S. Shige, H. Hashizume, K. Aonashi, N. Takahashi, S. Seto, M. Hirose, Y. N. Takayabu, T. Ushio, K. Nakagawa, K. Iwanami, M. Kachi, and K. Okamoto, “Global Precipitation Map Using Satellite-Borne Microwave Radiometers by the GSMaP Project: Production and Validation,” *IEEE Trans Geosci Remote Sens*, vol. 45, no. 7, pp. 2259–2275, 2007.

[54] A. Y. Hou, R. K. Kakar, S. Neeck, A. A. Azarbarzin, C. D. Kummerow, M. Kojima, R. Oki, K. Nakamura, T. Iguchi, A. Y. Hou, R. K. Kakar, S. Neeck, A. A. Azarbarzin, C. D. Kummerow, M. Kojima, R. Oki, K. Nakamura, and T. Iguchi, “The Global Precipitation Measurement Mission,” *Bull Am Meteorol Soc*, vol. 95, no. 5, pp. 701–722, 2014.

[55] W. W. Immerzeel, M. M. Rutten, and P. Droogers, “Spatial downscaling of TRMM precipitation using vegetative response on the Iberian Peninsula,” *Remote Sens Environ*, vol. 113, no. 2, pp. 362–370, 2009.

[56] R. Quiroz, C. Yarlequé, A. Posadas, V. Mares, and W. W. Immerzeel, “Improving daily rainfall estimation from NDVI using a wavelet transform,” *Environ Model Softw*, vol. 26, no. 2, pp. 201–209, 2011.

[57] N.-W. Park and N.-W. Park, “Spatial downscaling of TRMM precipitation using geostatistics and fine dcale environmental variables,” *Adv Meteorol*, vol. 2013, pp. 1–9, 2013.

[58] J. E. Hunink, W. W. Immerzeel, and P. Droogers, “A High-resolution Precipitation 2-step mapping Procedure (HiP2P): Development and application to a tropical mountainous area,” *Remote Sens Environ*, vol. 140, pp. 179–188, 2014.

[59] G. Xu, X. Xu, M. Liu, A. Sun, and K. Wang, “Spatial downscaling of TRMM precipitation product using a combined multifractal and regression approach: demonstration for South China,” *Water*, vol. 7, no. 6, pp. 3083–3102, 2015.

[60] X. Zheng and J. Zhu, “A methodological approach for spatial downscaling of TRMM precipitation data in North China,” *Int J Remote Sens*, vol. 36, no. 1, pp. 144–169, 2015.

[61] L. Ferraris, S. Gabellani, N. Rebora, and A. Provenzale, “A comparison of stochastic models for spatial rainfall downscaling,” *Water Resour Res*, vol. 39, no. 12, 2003.

[62] D. D’Onofrio, E. Palazzi, J. von Hardenberg, A. Provenzale, S. Calmanti, D. D’Onofrio, E. Palazzi, J. von Hardenberg, A. Provenzale, and S. Calmanti, “Stochastic Rainfall Downscaling of Climate Models,” *J Hydrometeorol*, vol. 15, no. 2, pp. 830–843, 2014.

[63] N. Rebora, L. Ferraris, J. von Hardenberg, and A. Provenzale, “RainFARM: Rainfall Downscaling by a Filtered

Autoregressive Model," *J Hydrometeorol*, vol. 7, no. 4, pp. 724–738, 2006.

[64] A. Bodian, A. Dezetter, A. Deme, and L. Diop, "Hydrological Evaluation of TRMM Rainfall over the Upper Senegal River Basin," *Hydrology*, vol. 3, no. 2, p. 15, 2016.

[65] B. Collischonn, W. Collischonn, and C. E. M. Tucci, "Daily hydrological modeling in the Amazon basin using TRMM rainfall estimates," *J Hydrol*, vol. 360, no. 1, pp. 207–216, 2008.

[66] E. Waltari, R. Schroeder, K. McDonald, R. P. Anderson, and A. Carnaval, "Bioclimatic variables derived from remote sensing: assessment and application for species distribution modelling," *Methods Ecol Evol*, vol. 5, no. 10, pp. 1033–1042, 2014.

[67] V. Maggioni, M. R. P. Sapiano, and R. F. Adler, "Estimating Uncertainties in High-Resolution Satellite Precipitation Products: Systematic or Random Error?," *J Hydrometeorol*, vol. 17, no. 4, pp. 1119–1129, 2016.

[68] D. Liu and R. Pu, "Downscaling Thermal Infrared Radiance for Subpixel Land Surface Temperature Retrieval," *Sensors*, vol. 8, no. 4, pp. 2695–2706, 2008.

[69] W. Zhan, Y. Chen, J. Zhou, J. Li, and W. Liu, "Sharpening Thermal Imageries: A Generalized Theoretical Framework From an Assimilation Perspective," *IEEE Trans Geosci Remote Sens*, vol. 49, no. 2, pp. 773–789, Feb. 2011.

[70] W. Zhan, Y. Chen, J. Zhou, J. Wang, W. Liu, J. Voogt, X. Zhu, J. Quan, and J. Li, "Disaggregation of remotely sensed land surface temperature: Literature survey, taxonomy, issues, and caveats," *Remote Sens Environ*, vol. 131, pp. 119–139, 2013.

[71] O. Merlin, B. Duchemin, O. Hagolle, F. Jacob, B. Coudert, G. Chehbouni, G. Dedieu, J. Garatuza, and Y. Kerr, "Disaggregation of MODIS surface temperature over an agricultural area using a time series of Formosat-2 images," *Remote Sens Environ*, vol. 114, no. 11, pp. 2500–2512, 2010.

[72] A. Cord and D. Rödder, "Inclusion of habitat availability in species distribution models through multi-temporal remote-sensing data?," *Ecol Appl*, vol. 21, no. 8, pp. 3285–3298, 2011.

[73] A. F. Cord, D. Klein, F. Mora, and S. Dech, "Comparing the suitability of classified land cover data and remote sensing variables for modeling distribution patterns of plants," *Ecol Modell*, vol. 272, pp. 129–140, 2014.

[74] Y. Fan, P. J. Weisberg, and R. S. Nowak, "Spatio-temporal analysis of remotely-sensed forest mortality associated with road de-icing salts.," *Sci Total Environ*, vol. 472, pp. 929–38, 2014.

[75] C. M. Frey, C. Kuenzer, and S. Dech, "Quantitative comparison of the operational NOAA-AVHRR LST product of DLR and the MODIS LST product V005," *Int J Remote Sens*, vol. 33, no. 22, pp. 7165–7183, 2012.

[76] M. Neteler and Markus, "Estimating Daily Land Surface Temperatures in Mountainous Environments by Reconstructed MODIS LST Data," *Remote Sens*, vol. 2, no. 1, pp. 333–351, 2010.

[77] E. Pardo-Igúzquiza, M. Chica-Olmo, and P. M. Atkinson, "Downscaling cokriging for image sharpening," *Remote Sens Environ*, vol. 102, no. 1, pp. 86–98, 2006.

[78] C. J. Tomlinson, L. Chapman, J. E. Thornes, and C. Baker, "Remote sensing land surface temperature for meteorology and climatology: a review," *Meteorol Appl*, vol. 18, no. 3, pp. 296–306, 2011.

[79] N. Agam, W. P. Kustas, M. C. Anderson, F. Li, and C. M. U. Neale, "A vegetation index based technique for spatial sharpening of thermal imagery," *Remote Sens Environ*, vol. 107, no. 4, pp. 545–558, 2007.

[80] D. Rödder, S. Nekum, A. F. Cord, and J. O. Engler, "Coupling Satellite Data with Species Distribution and Connectivity Models as a Tool for Environmental Management and Planning in Matrix-Sensitive Species," *Environ Manage*, vol. 58, no. 1, pp. 130–143, 2016.

[81] E. J. Good, "An in situ-based analysis of the relationship between land surface 'skin' and screen-level air

temperatures," *J Geophys Res Atmos*, vol. 121, no. 15, pp. 8801–8819, 2016.

[82] M. New, D. Lister, M. Hulme, and I. Makin, "A high-resolution data set of surface climate over global land areas," *Clim Res*, vol. 21, no. 1, pp. 1–25, 2002.

[83] G. Murray-Tortarolo, A. Anav, P. Friedlingstein, S. Sitch, S. Piao, Z. Zhu, B. Poulter, S. Zaehle, A. Ahlström, M. Lomas, S. Levis, N. Viovy, and N. Zeng, "Evaluation of Land Surface Models in Reproducing Satellite-Derived LAI over the High-Latitude Northern Hemisphere. Part I: Uncoupled DGVMs," *Remote Sens*, vol. 5, no. 10, pp. 4819–4838, 2013.

[84] E. Chuvieco, *Fundamentals of satellite remote sensing : an environmental approach*. .

[85] M. T. Yilmaz, E. R. Hunt, and T. J. Jackson, "Remote sensing of vegetation water content from equivalent water thickness using satellite imagery," *Remote Sens Environ*, vol. 112, no. 5, pp. 2514–2522, 2008.

[86] M. T. Yilmaz, E. R. Hunt, L. D. Goins, S. L. Ustin, and V. C. Vanderbilt, "Vegetation water content during SMEX04 from ground data and Landsat 5 Thematic Mapper imagery," *Remote Sens Environ*, vol. 112, no. 2, pp. 350–362, 2008.

[87] Y.-B. Cheng, S. L. Ustin, D. Riaño, and V. C. Vanderbilt, "Water content estimation from hyperspectral images and MODIS indexes in Southeastern Arizona," *Remote Sens Environ*, vol. 112, no. 2, pp. 363–374, 2008.

[88] L. Wang, E. R. Hunt, J. J. Qu, X. Hao, and C. S. T. Daughtry, "Remote sensing of fuel moisture content from ratios of narrow-band vegetation water and dry-matter indices," *Remote Sens Environ*, vol. 129, pp. 103–110, 2013.

[89] R. Colombo, L. Busetto, M. Meroni, M. Rossini, and C. Panigada, "Optical remote sensing of vegetation water content," in *Hyperspectral Remote Sensing of Vegetation*, CRC Press, Taylor and Francis group, 2011, pp. 227–244.

[90] B. Gao, "NDWI—A normalized difference water index for remote sensing of vegetation liquid water from space," *Remote Sens Environ*, vol. 58, no. 3, pp. 257–266, 1996.

[91] M. A. Hardisky, V. Klemas, and R. M. Smart, "The influence of soil salinity, growth form, and leaf moisture on the spectral radiance of Spartina alterniflora canopies," *Photogramm Eng Remote Sensing*, vol. 49, no. 1, pp. 77–83, 1983.

[92] E. Hunt JR and B. Rock, "Detection of changes in leaf water content using Near- and Middle-Infrared reflectances☆," *Remote Sens Environ*, vol. 30, no. 1, pp. 43–54, 1989.

[93] A. Viña, A. A. Gitelson, A. L. Nguy-Robertson, and Y. Peng, "Comparison of different vegetation indices for the remote assessment of green leaf area index of crops," *Remote Sens Environ*, vol. 115, no. 12, pp. 3468–3478, 2011.

[94] A. Kross, H. McNairn, D. Lapen, M. Sunohara, and C. Champagne, "Assessment of RapidEye vegetation indices for estimation of leaf area index and biomass in corn and soybean crops," *Int J Appl Earth Obs Geoinf*, vol. 34, pp. 235–248, 2015.

[95] A. L. Nguy-Robertson, Y. Peng, A. A. Gitelson, T. J. Arkebauer, A. Pimstein, I. Herrmann, A. Karnieli, D. C. Rundquist, and D. J. Bonfil, "Estimating green LAI in four crops: Potential of determining optimal spectral bands for a universal algorithm," *Agric For Meteorol*, vol. 192, pp. 140–148, 2014.

[96] J. Delegido, J. Verrelst, L. Alonso, and J. Moreno, "Evaluation of Sentinel-2 Red-Edge Bands for Empirical Estimation of Green LAI and Chlorophyll Content," *Sensors*, vol. 11, no. 12, pp. 7063–7081, 2011.

[97] A. Ramoelo, A. K. Skidmore, M. A. Cho, M. Schlerf, R. Mathieu, and I. M. A. Heitkönig, "Regional estimation of savanna grass nitrogen using the red-edge band of the spaceborne RapidEye sensor," *Int J Appl Earth Obs Geoinf*, vol. 19, pp. 151–162, 2012.

[98] P. Miphokasap, K. Honda, C. Vaiphasa, M. Souris, and M. Nagai, "Estimating Canopy Nitrogen

Concentration in Sugarcane Using Field Imaging Spectroscopy," *Remote Sens*, vol. 4, no. 12, pp. 1651–1670, 2012.

[99] M. Schlemmer, A. Gitelson, J. Schepers, R. Ferguson, Y. Peng, J. Shanahan, and D. Rundquist, "Remote estimation of nitrogen and chlorophyll contents in maize at leaf and canopy levels," *Int J Appl Earth Obs Geoinf*, vol. 25, pp. 47–54, 2013.

[100] Y. Knyazikhin, M. A. Schull, P. Stenberg, M. Mottus, M. Rautiainen, Y. Yang, A. Marshak, P. Latorre Carmona, R. K. Kaufmann, P. Lewis, M. I. Disney, V. Vanderbilt, A. B. Davis, F. Baret, S. Jacquemoud, A. Lyapustin, and R. B. Myneni, "Hyperspectral remote sensing of foliar nitrogen content," *Proc Natl Acad Sci*, vol. 110, no. 3, pp. E185–E192, 2013.

[101] C. Zhang, J. Kovacs, M. Wachowiak, and F. Flores-Verdugo, "Relationship between Hyperspectral Measurements and Mangrove Leaf Nitrogen Concentrations," *Remote Sens*, vol. 5, no. 2, pp. 891–908, 2013.

[102] E. R. Hunt, C. S. T. Daughtry, J. U. H. Eitel, and D. S. Long, "Remote Sensing Leaf Chlorophyll Content Using a Visible Band Index," *Agron J*, vol. 103, no. 4, p. 1090, 2011.

[103] E. R. Hunt, P. C. Doraiswamy, J. E. McMurtrey, C. S. T. Daughtry, E. M. Perry, and B. Akhmedov, "A visible band index for remote sensing leaf chlorophyll content at the canopy scale," *Int J Appl Earth Obs Geoinf*, vol. 21, pp. 103–112, 2013.

[104] C. Frankenberg, A. Butz, and G. C. Toon, "Disentangling chlorophyll fluorescence from atmospheric scattering effects in O 2 A-band spectra of reflected sun-light," *Geophys Res Lett*, vol. 38, no. 3, 2011.

[105] C. Frankenberg, J. B. Fisher, J. Worden, G. Badgley, S. S. Saatchi, J.-E. Lee, G. C. Toon, A. Butz, M. Jung, A. Kuze, and T. Yokota, "New global observations of the terrestrial carbon cycle from GOSAT: Patterns of plant fluorescence with gross primary productivity," *Geophys Res Lett*, vol. 38, no. 17, 2011.

[106] H. Croft, J. M. Chen, and Y. Zhang, "The applicability of empirical vegetation indices for determining leaf chlorophyll content over different leaf and canopy structures," *Ecol Complex*, vol. 17, pp. 119–130, 2014.

[107] R. Houborg, H. Soegaard, and E. Boegh, "Combining vegetation index and model inversion methods for the extraction of key vegetation biophysical parameters using Terra and Aqua MODIS reflectance data," *Remote Sens Environ*, vol. 106, no. 1, pp. 39–58, 2007.

[108] E. Chuvieco and A. Huete, *Fundamentals of satellite remote sensing*. CRC Press, 2009.

[109] M. Trombetti, D. Riaño, M. A. Rubio, Y. B. Cheng, and S. L. Ustin, "Multi-temporal vegetation canopy water content retrieval and interpretation using artificial neural networks for the continental USA," *Remote Sens Environ*, vol. 112, no. 1, pp. 203–215, 2008.

[110] R. Colombo, M. Meroni, A. Marchesi, L. Busetto, M. Rossini, C. Giardino, and C. Panigada, "Estimation of leaf and canopy water content in poplar plantations by means of hyperspectral indices and inverse modeling," *Remote Sens Environ*, vol. 112, no. 4, pp. 1820–1834, 2008.

[111] W. Dorigo, R. Richter, F. Baret, R. Bamler, and W. Wagner, "Enhanced Automated Canopy Characterization from Hyperspectral Data by a Novel Two Step Radiative Transfer Model Inversion Approach," *Remote Sens*, vol. 1, no. 4, pp. 1139–1170, 2009.

[112] F. Vuolo, C. Atzberger, K. Richter, G. D'Urso, and J. Dash, "Retrieval of biophysical vegetation products from RapidEye imagery," in *ISPRS TC VII Symposium - 100 Years ISPRS*, 2010, pp. 281–286.

[113] C. Yin, B. He, X. Quan, and Z. Liao, "Chlorophyll content estimation in arid grasslands from Landsat-8 OLI data," *Int J Remote Sens*, vol. 37, no. 3, pp. 615–632, 2016.

[114] Y. Qu, W. Han, and M. Ma, "Retrieval of a Temporal High-Resolution Leaf Area Index (LAI) by Combining MODIS LAI and ASTER Reflectance Data," *Remote Sens*, vol. 7, no. 1, pp. 195–210, 2014.

[115] K. Richter, T. B. Hank, F. Vuolo, W. Mauser, and G. D'Urso, "Optimal Exploitation of the Sentinel-2 Spectral

Capabilities for Crop Leaf Area Index Mapping," *Remote Sens*, vol. 4, no. 12, pp. 561–582, 2012.

[116] V. K. Sehgal, D. Chakraborty, and R. N. Sahoo, "Inversion of radiative transfer model for retrieval of wheat biophysical parameters from broadband reflectance measurements," *Inf Process Agric*, vol. 3, no. 2, pp. 107–118, 2016.

[117] S. Jacquemoud, W. Verhoef, F. Baret, C. Bacour, P. J. Zarco-Tejada, G. P. Asner, and C. François, "PROSPECT+SAIL models: A review of use for vegetation characterization," *Remote Sens Environ*, vol. 113, pp. S56–S66, 2009.

[118] S. Jacquemoud and F. Baret, "PROSPECT: A model of leaf optical properties spectra," *Remote Sens Environ*, vol. 34, no. 2, pp. 75–91, 1990.

[119] W. Verhoef, "Light scattering by leaf layers with application to canopy reflectance modeling: The SAIL model," *Remote Sens Environ*, vol. 16, no. 2, pp. 125–141, 1984.

[120] R. Houborg and M. C. Anderson, "Utility of an image-based canopy reflectance modeling tool for remote estimation of LAI and leaf chlorophyll content at regional scales," *J Appl Remote Sens*, vol. 3, no. 1, p. 33529, 2009.

[121] A. Kuusk, "A two-layer canopy reflectance model," *J Quant Spectrosc Radiat Transf*, vol. 71, no. 1, pp. 1–9, 2001.

[122] S. Y. Kotchenova and E. F. Vermote, "Validation of a vector version of the 6S radiative transfer code for atmospheric correction of satellite data Part II Homogeneous Lambertian and anisotropic surfaces," *Appl Opt*, vol. 46, no. 20, p. 4455, 2007.

[123] E. Boegh, R. Houborg, J. Bienkowski, C. F. Braban, T. Dalgaard, N. van Dijk, U. Dragosits, E. Holmes, V. Magliulo, K. Schelde, P. Di Tommasi, L. Vitale, M. R. Theobald, P. Cellier, and M. A. Sutton, "Remote sensing of LAI, chlorophyll and leaf nitrogen pools of crop- and grasslands in five European landscapes," *Biogeosciences*, vol. 10, no. 10, pp. 6279–6307, 2013.

[124] V. Demarez and J. P. Gastellu-Etchegorry, "A Modeling Approach for Studying Forest Chlorophyll Content," *Remote Sens Environ*, vol. 71, no. 2, pp. 226–238, 2000.

[125] L. Yanez-Rausell, Z. Malenovsky, M. Rautiainen, J. G. P. W. Clevers, P. Lukes, J. Hanus, and M. E. Schaepman, "Estimation of Spruce Needle-Leaf Chlorophyll Content Based on DART and PARAS Canopy Reflectance Models," *IEEE J Sel Top Appl Earth Obs Remote Sens*, vol. 8, no. 4, pp. 1534–1544, 2015.

[126] A. Banskota, S. P. Serbin, R. H. Wynne, V. A. Thomas, M. J. Falkowski, N. Kayastha, J.-P. Gastellu-Etchegorry, and P. A. Townsend, "An LUT-Based Inversion of DART Model to Estimate Forest LAI from Hyperspectral Data," *IEEE J Sel Top Appl Earth Obs Remote Sens*, vol. 8, no. 6, pp. 3147–3160, 2015.

[127] J.-L. Widlowski, C. Mio, M. Disney, J. Adams, I. Andredakis, C. Atzberger, J. Brennan, L. Busetto, M. Chelle, G. Ceccherini, R. Colombo, J.-F. Côté, A. Eenmäe, R. Essery, J.-P. Gastellu-Etchegorry, N. Gobron, E. Grau, V. Haverd, L. Homolová, H. Huang, L. Hunt, H. Kobayashi, B. Koetz, A. Kuusk, J. Kuusk, M. Lang, P. E. Lewis, J. L. Lovell, Z. Malenovský, M. Meroni, F. Morsdorf, M. Mõttus, W. Ni-Meister, B. Pinty, M. Rautiainen, M. Schlerf, B. Somers, J. Stuckens, M. M. Verstraete, W. Yang, F. Zhao, and T. Zenone, "The fourth phase of the radiative transfer model intercomparison (RAMI) exercise: Actual canopy scenarios and conformity testing," *Remote Sens Environ*, vol. 169, pp. 418–437, 2015.

[128] B. Combal, F. Baret, M. Weiss, A. Trubuil, D. Macé, A. Pragnère, R. Myneni, Y. Knyazikhin, and L. Wang, "Retrieval of canopy biophysical variables from bidirectional reflectance: Using prior information to solve the ill-posed inverse problem," *Remote Sens Environ*, vol. 84, no. 1, pp. 1–15, 2003.

[129] S. A. Soenen, D. R. Peddle, C. A. Coburn, R. J. Hall, and F. G. Hall, "Canopy reflectance model inversion in multiple forward mode: forest structural information retrieval from solution set distributions.," *Photogramm Eng Remote Sensing*, vol. 75, no. 4, pp. 361–374, 2009.

[130] J. Cernicharo, A. Verger, and F. Camacho, "Empirical and Physical Estimation of Canopy Water Content

from CHRIS/PROBA Data," *Remote Sens*, vol. 5, no. 10, pp. 5265–5284, 2013.

[131] Y. Si, M. Schlerf, R. Zurita-Milla, A. Skidmore, and T. Wang, "Mapping spatio-temporal variation of grassland quantity and quality using MERIS data and the PROSAIL model," *Remote Sens Environ*, vol. 121, pp. 415–425, 2012.

[132] M. Colgan, C. Baldeck, J.-B. Féret, and G. Asner, "Mapping Savanna Tree Species at Ecosystem Scales Using Support Vector Machine Classification and BRDF Correction on Airborne Hyperspectral and LiDAR Data," *Remote Sens*, vol. 4, no. 12, pp. 3462–3480, 2012.

[133] L. Su, Y. Huang, M. J. Chopping, A. Rango, and J. V. Martonchik, "An empirical study on the utility of BRDF model parameters and topographic parameters for mapping vegetation in a semi-arid region with MISR imagery," *Int J Remote Sens*, vol. 30, no. 13, pp. 3463–3483, 2009.

[134] M. Chopping, A. Nolin, G. G. Moisen, J. V. Martonchik, and M. Bull, "Forest canopy height from the Multiangle Imaging SpectroRadiometer (MISR) assessed with high resolution discrete return lidar," *Remote Sens Environ*, vol. 113, no. 10, pp. 2172–2185, 2009.

[135] F. Vuolo, N. Neugebauer, S. Bolognesi, C. Atzberger, and G. D'Urso, "Estimation of Leaf Area Index Using DEIMOS-1 Data: Application and Transferability of a Semi-Empirical Relationship between two Agricultural Areas," *Remote Sens*, vol. 5, no. 3, pp. 1274–1291, 2013.

[136] V. Kumar, M. Kumari, and S. K. Saha, "Leaf area index estimation of lowland rice using semi-empirical backscattering model," *J Appl Remote Sens*, vol. 7, no. 1, p. 73474, 2013.

[137] W. Yang, H. Kobayashi, R. Suzuki, and K. Nasahara, "A Simple Method for Retrieving Understory NDVI in Sparse Needleleaf Forests in Alaska Using MODIS BRDF Data," *Remote Sens*, vol. 6, no. 12, pp. 11936–11955, 2014.

[138] J. Pisek, M. Rautiainen, M. Nikopensius, and K. Raabe, "Estimation of seasonal dynamics of understory NDVI in northern forests using MODIS BRDF data: Semi-empirical versus physically-based approach," *Remote Sens Environ*, vol. 163, pp. 42–47, 2015.

[139] S. P. Neeck, "The NASA Earth Science Flight Program: an update," 2015, p. 963907.

[140] K. Liao, S. Xu, J. Wu, and Q. Zhu, "Spatial estimation of surface soil texture using remote sensing data," *Soil Sci Plant Nutr*, vol. 59, no. 4, pp. 488–500, 2013.

[141] V. L. Mulder, S. de Bruin, M. E. Schaepman, and T. R. Mayr, "The use of remote sensing in soil and terrain mapping — A review," *Geoderma*, vol. 162, no. 1, pp. 1–19, 2011.

[142] D. Entekhabi, E. G. Njoku, P. E. O'Neill, K. H. Kellogg, W. T. Crow, W. N. Edelstein, J. K. Entin, S. D. Goodman, T. J. Jackson, J. Johnson, J. Kimball, J. R. Piepmeier, R. D. Koster, N. Martin, K. C. McDonald, M. Moghaddam, S. Moran, R. Reichle, J. C. Shi, M. W. Spencer, S. W. Thurman, L. Tsang, and J. Van Zyl, "The Soil Moisture Active Passive (SMAP) Mission," *Proc IEEE*, vol. 98, no. 5, pp. 704–716, 2010.

[143] A. Al-Yaari, J.-P. Wigneron, A. Ducharne, Y. H. Kerr, W. Wagner, G. De Lannoy, R. Reichle, A. Al Bitar, W. Dorigo, P. Richaume, and A. Mialon, "Global-scale comparison of passive (SMOS) and active (ASCAT) satellite based microwave soil moisture retrievals with soil moisture simulations (MERRA-Land)," *Remote Sens Environ*, vol. 152, pp. 614–626, 2014.

[144] E. Ben-Dor, N. Levin, A. Singer, A. Karnieli, O. Braun, and G. J. Kidron, "Quantitative mapping of the soil rubification process on sand dunes using an airborne hyperspectral sensor," *Geoderma*, vol. 131, no. 1, pp. 1–21, 2006.

[145] E. Ben-Dor, "Quantitative remote sensing of soil properties," 2002, pp. 173–243.

[146] R. Mathieu, M. Pouget, B. Cervelle, and R. Escadafal, "Relationships between Satellite-Based Radiometric Indices Simulated Using Laboratory Reflectance Data and Typic Soil Color of an Arid Environment," *Remote Sens Environ*, vol. 66, no. 1, pp. 17–28, 1998.

[147] S. A. Drury, *Image interpretation in geology*. London: Allen and Unwin, 1987.

[148] A. Karnieli, "Development and implementation of spectral crust index over dune sands," *Int J Remote Sens*, vol. 18, no. 6, pp. 1207–1220, 1997.

[149] D. A. Roberts, K. L. Roth, and R. L. Perroy, "Hyperspectral Vegetation Indices," in *Hyperspectral Remote Sensing of Vegetation*, P. S. Thenkabail, J. G. Lyon, and A. Huete, Eds. Boca Raton, FL: CRC Press, 2012, pp. 309–328.

[150] S. Liang, *Quantitative Remote Sensing of Land Surfaces*. Hoboken, NJ: John Wiley & Sons, 2004.

[151] E. Ben-Dor, Y. Inbar, and Y. Chen, "The reflectance spectra of organic matter in the visible near-infrared and short wave infrared region (400–2500 nm) during a controlled decomposition process," *Remote Sens Environ*, vol. 61, no. 1, pp. 1–15, 1997.

[152] T. Ilani, I. Herrmann, A. Karnieli, and G. Arye, "Characterization of the biosolids composting process by hyperspectral analysis," *Waste Manag*, vol. 48, pp. 106–114, 2016.

[153] P. J. Curran, J. L. Dungan, B. A. Macler, S. E. Plummer, and D. L. Peterson, "Reflectance spectroscopy of fresh whole leaves for the estimation of chemical concentration," *Remote Sens Environ*, vol. 39, no. 2, pp. 153–166, 1992.

[154] C. D. Eldvidge, "Visible and near infrared reflectance characteristics of dry plant materials," *Int J Remote Sens*, vol. 11, no. 10, pp. 1775–1795, 1990.

[155] C. S. T. Daughtry, "Discriminating crop residues from soil by shortwave infrared reflectance," *Agron J*, vol. 93, no. 1, p. 125, 2001.

[156] L. Serrano, J. Peñuelas, and S. L. Ustin, "Remote sensing of nitrogen and lignin in Mediterranean vegetation from AVIRIS data: Decomposing biochemical from structural signals," *Remote Sens Environ*, vol. 81, no. 2, pp. 355–364, 2002.

[157] J.-M. Lellouche, O. Legalloudec, C. Regnier, B. Levier, E. Greiner, and M. Drevillon, "Quality Information Document For Global Sea Physical Analysis and Forecasting Product GLOBAL_ANALYSIS_FORECAST_PHY_001_024," 2016.

[158] C. Perruche, P. Rivière, G. Lapeyre, X. Carton, and P. Pondaven, "Effects of surface quasi-geostrophic turbulence on phytoplankton competition and coexistence," no. 1961, pp. 105–135, 2011.

[159] L. Tyberghein, H. Verbruggen, K. Pauly, C. Troupin, F. Mineur, and O. De Clerck, "Bio-ORACLE: a global environmental dataset for marine species distribution modelling," *Glob Ecol Biogeogr*, vol. 21, no. 2, pp. 272–281, 2012.

[160] Z. Basher, D. A. Bowden, and M. J. Costello, "Global Marine Environment Datasets (GMED)," *World Wide Web electronic publication. Version 1.0*, 2014. .

[161] K. A. Kilpatrick, G. Podestá, S. Walsh, E. Williams, V. Halliwell, M. Szczodrak, O. B. Brown, P. J. Minnett, and R. Evans, "A decade of sea surface temperature from MODIS," *Remote Sens Environ*, vol. 165, pp. 27–41, 2015.

[162] A. G. O'Carroll, T. August, P. Le Borgne, and A. Marsouin, "The accuracy of SST retrievals from Metop-A IASI and AVHRR using the EUMETSAT OSI-SAF matchup dataset," *Remote Sens Environ*, vol. 126, pp. 184–194, 2012.

[163] D. M. Le Vine, G. S. E. Lagerloef, and S. E. Torrusio, "Aquarius and Remote Sensing of Sea Surface Salinity from Space," *Proc IEEE*, vol. 98, no. 5, pp. 688–703, 2010.

[164] Y. H. Kerr, P. Waldteufel, J.-P. Wigneron, S. Delwart, F. Cabot, J. Boutin, M.-J. Escorihuela, J. Font, N. Reul, C. Gruhier, S. E. Juglea, M. R. Drinkwater, A. Hahne, M. Martín-Neira, and S. Mecklenburg, "The SMOS Mission: New Tool for Monitoring Key Elements ofthe Global Water Cycle," *Proc IEEE*, vol. 98, no. 5, pp. 666–687, 2010.

[165] D. Blondeau-Patissier, J. F. R. Gower, A. G. Dekker, S. R. Phinn, and V. E. Brando, “A review of ocean color remote sensing methods and statistical techniques for the detection, mapping and analysis of phytoplankton blooms in coastal and open oceans,” *Prog Oceanogr*, vol. 123, pp. 123–144, 2014.

[166] K. L. Carder, F. R. Chen, J. P. Cannizzaro, J. W. Campbell, and B. G. Mitchell, “Performance of the MODIS semi-analytical ocean color algorithm for chlorophyll-a,” *Adv Sp Res*, vol. 33, no. 7, pp. 1152–1159, 2004.

[167] F. E. Paparazzo, G. N. Williams, J. P. Pisoni, M. Solís, J. L. Esteves, and D. E. Varela, “Linking phytoplankton nitrogen uptake, macronutrients and chlorophyll-a in SW Atlantic waters: The case of the Gulf of San Jorge, Argentina,” *J Mar Syst*, vol. 172, pp. 43–50, 2017.

[168] M. Wang and S. Son, “VIIRS-derived chlorophyll-a using the ocean color index method,” *Remote Sens Environ*, vol. 182, pp. 141–149, 2016.

[169] K. J. W. Hyde, J. E. O’Reilly, and C. A. Oviatt, “Validation of SeaWiFS chlorophyll a in Massachusetts Bay,” *Cont Shelf Res*, vol. 27, no. 12, pp. 1677–1691, 2007.

[170] P. Dorji, P. Fearns, and M. Broomhall, “A Semi-Analytic Model for Estimating Total Suspended Sediment Concentration in Turbid Coastal Waters of Northern Western Australia Using MODIS-Aqua 250 m Data,” *Remote Sens*, vol. 8, no. 7, p. 556, 2016.

[171] V. Rosmorduc, J. Benveniste, E. Bronner, S. Dinardo, O. Lauret, C. Maheu, M. Milagro, N. Picot, A. Ambrozio, R. Escolà, A. Garcia-Mondejar, M. Restano, E. Schrama, and M. Terra-Homem, “Radar Altimetry Tutorial and Toolbox,” 2016. [Online]. Available: http://www.altimetry.info/radar-altimetry-tutorial/. [Accessed: 02-May-2017].

[172] H. Woerd and M. Wernand, “True Colour Classification of Natural Waters with Medium-Spectral Resolution Satellites: SeaWiFS, MODIS, MERIS and OLCI,” *Sensors*, vol. 15, no. 10, pp. 25663–25680, 2015.

[173] G. Liu, S. Heron, C. Eakin, F. Muller-Karger, M. Vega-Rodriguez, L. Guild, J. De La Cour, E. Geiger, W. Skirving, T. Burgess, A. Strong, A. Harris, E. Maturi, A. Ignatov, J. Sapper, J. Li, and S. Lynds, “Reef-Scale Thermal Stress Monitoring of Coral Ecosystems: New 5-km Global Products from NOAA Coral Reef Watch,” *Remote Sens*, vol. 6, no. 11, pp. 11579–11606, 2014.

[174] C. M. Eakin, J. A. Morgan, S. F. Heron, T. B. Smith, G. Liu, L. Alvarez-Filip, B. Baca, E. Bartels, C. Bastidas, C. Bouchon, M. Brandt, A. W. Bruckner, L. Bunkley-Williams, A. Cameron, B. D. Causey, M. Chiappone, T. R. L. Christensen, M. J. C. Crabbe, O. Day, E. de la Guardia, G. Díaz-Pulido, D. DiResta, D. L. Gil-Agudelo, D. S. Gilliam, R. N. Ginsburg, S. Gore, H. M. Guzmán, J. C. Hendee, E. A. Hernández-Delgado, E. Husain, C. F. G. Jeffrey, R. J. Jones, E. Jordán-Dahlgren, L. S. Kaufman, D. I. Kline, P. A. Kramer, J. C. Lang, D. Lirman, J. Mallela, C. Manfrino, J.-P. Maréchal, K. Marks, J. Mihaly, W. J. Miller, E. M. Mueller, E. M. Muller, C. A. Orozco Toro, H. A. Oxenford, D. Ponce-Taylor, N. Quinn, K. B. Ritchie, S. Rodríguez, A. R. Ramírez, S. Romano, J. F. Samhouri, J. A. Sánchez, G. P. Schmahl, B. V. Shank, W. J. Skirving, S. C. C. Steiner, E. Villamizar, S. M. Walsh, C. Walter, E. Weil, E. H. Williams, K. W. Roberson, and Y. Yusuf, “Caribbean Corals in Crisis: Record Thermal Stress, Bleaching, and Mortality in 2005,” *PLoS One*, vol. 5, no. 11, p. e13969, 2010.

[175] S. B. Choudhury, B. Jena, M. V. Rao, K. H. Rao, V. S. Somvanshi, D. K. Gulati, and S. K. Sahu, “Validation of integrated potential fishing zone (IPFZ) forecast using satellite based chlorophyll and sea surface temperature along the east coast of India,” *Int J Remote Sens*, vol. 28, no. 12, pp. 2683–2693, 2007.

[176] S. Maity, T. S. Kumar, S. Dutta, A. Akhand, and S. Hazra, “Satellite Based Integrated Potential Fishing Zone Advisories: A Feasibility Analysis in the Coastal Water of West Bengal,” *Proc Zool Soc*, vol. 68, no. 1, pp. 14–19, 2015.

[177] J. P. Rodríguez, L. Brotons, J. Bustamante, and J. Seoane, “The application of predictive modelling of species distribution to biodiversity conservation,” *Divers Distrib*, vol. 13, no. 3, pp. 243–251, 2007.

[178] K. S. He, B. A. Bradley, A. F. Cord, D. Rocchini, M.-N. Tuanmu, S. Schmidtlein, W. Turner, M. Wegmann, and N. Pettorelli, “Will remote sensing shape the next generation of species distribution models?,” *Remote*

Sens Ecol Conserv, vol. 1, no. 1, pp. 4–18, 2015.

[179] A. M. Howard, N. Nibbelink, S. Bernardes, D. M. Fragaszy, and M. Madden, “Remote sensing and habitat mapping for bearded capuchin monkeys (Sapajus libidinosus): landscapes for the use of stone tools,” *J Appl Remote Sens*, vol. 9, no. 1, p. 96020, 2015.

[180] J.-N. Pradervand, A. Dubuis, L. Pellissier, A. Guisan, and C. Randin, “Very high resolution environmental predictors in species distribution models: Moving beyond topography?,” *Prog Phys Geogr*, vol. 38, no. 1, pp. 79–96, 2014.

[181] J. Seoane, J. Bustamante, and R. Diaz-Delgado, “Effect of Expert Opinion on the Predictive Ability of Environmental Models of Bird Distribution,” *Conserv Biol*, vol. 19, no. 2, pp. 512–522, 2005.

[182] E. M. De Clercq, S. Leta, A. Estrada-Peña, M. Madder, S. Adehan, and S. O. Vanwambeke, “Species distribution modelling for Rhipicephalus microplus (Acari: Ixodidae) in Benin, West Africa: comparing datasets and modelling algorithms.,” *Prev Vet Med*, vol. 118, no. 1, pp. 8–21, 2015.

[183] J. Pedrana, J. Bbustamante, A. Rodríguez, and A. Travani, “Primary productivity and anthropogenic disturbance as determinants of Upland Goose Chloephaga picta distribution in southern Patagonia,” *Ibis (Lond 1859)*, vol. 153, no. 3, pp. 517–530, 2011.

[184] J. Pedrana, J. Bustamante, A. Travaini, and A. Rodríguez, “Factors influencing guanaco distribution in southern Argentine Patagonia and implications for its sustainable use,” *Biodivers Conserv*, vol. 19, no. 12, pp. 3499–3512, 2010.

[185] J. Pedrana, J. Bustamante, A. Travaini, and A. Rodríguez, “Environmental factors influencing the distribution of the Lesser Rhea (Rhea pennata pennata) in southern Patagonia,” *Emu*, vol. 111, no. 4, p. 350, 2011.

[186] A. Travaini, J. Bustamante, A. Rodríguez, S. Zapata, D. Procopio, J. Pedrana, and R. Martínez Peck, “An integrated framework to map animal distributions in large and remote regions,” *Divers Distrib*, vol. 13, no. 3, pp. 289–298, 2007.

[187] G. Vacchiano and R. Motta, “An improved species distribution model for Scots pine and downy oak under future climate change in the NW Italian Alps,” *Ann For Sci*, vol. 72, no. 3, pp. 321–334, 2015.

[188] Y. Yabuhara, Y. Yamaura, T. Akasaka, and F. Nakamura, “Predicting Long-Term Changes in Riparian Bird Communities in Floodplain Landscapes,” *River Res Appl*, vol. 31, no. 1, pp. 109–119, 2015.

[189] J. Seoane, J. Viñuela, R. Díaz-Delgado, and J. Bustamante, “The effects of land use and climate on red kite distribution in the Iberian peninsula,” *Biol Conserv*, vol. 111, no. 3, pp. 401–414, 2003.

[190] E. Becker, K. Forney, P. Fiedler, J. Barlow, S. Chivers, C. Edwards, A. Moore, and J. Redfern, “Moving Towards Dynamic Ocean Management: How Well Do Modeled Ocean Products Predict Species Distributions?,” *Remote Sens*, vol. 8, no. 2, p. 149, 2016.

[191] E. S. Acheson, A. A. Plowright, and J. T. Kerr, “Where have all the mosquito nets gone? Spatial modelling reveals mosquito net distributions across Tanzania do not target optimal Anopheles mosquito habitats.,” *Malar J*, vol. 14, p. 322, 2015.

[192] M. Zucchetta, C. Venier, M. A. Taji, A. Mangin, and R. Pastres, “Modelling the spatial distribution of the seagrass Posidonia oceanica along the North African coast: Implications for the assessment of Good Environmental Status,” *Ecol Indic*, vol. 61, pp. 1011–1023, 2016.

[193] A. K. Conley, D. O. Fuller, N. Haddad, A. N. Hassan, A. M. Gad, and J. C. Beier, “Modeling the distribution of the West Nile and Rift Valley Fever vector Culex pipiens in arid and semi-arid regions of the Middle East and North Africa.,” *Parasit Vectors*, vol. 7, p. 289, 2014.

[194] A. M. Rengstorf, C. Mohn, C. Brown, M. S. Wisz, and A. J. Grehan, “Predicting the distribution of deep-sea vulnerable marine ecosystems using high-resolution data: Considerations and novel approaches,” *Deep*

Sea Res Part I Oceanogr Res Pap, vol. 93, pp. 72–82, 2014.

[195] M. Young, D. Ierodiaconou, and T. Womersley, "Forests of the sea: Predictive habitat modelling to assess the abundance of canopy forming kelp forests on temperate reefs," *Remote Sens Environ*, vol. 170, pp. 178–187, 2015.

[196] J. W. Wilson, J. O. Sexton, R. Todd Jobe, and N. M. Haddad, "The relative contribution of terrain, land cover, and vegetation structure indices to species distribution models," *Biol Conserv*, vol. 164, pp. 170–176, 2013.

[197] G. F. Ficetola, A. Bonardi, C. A. Mücher, N. L. M. Gilissen, and E. Padoa-Schioppa, "How many predictors in species distribution models at the landscape scale? Land use versus LiDAR-derived canopy height," *Int J Geogr Inf Sci*, vol. 28, no. 8, pp. 1723–1739, 2014.

[198] J. C. Vogeler and W. B. Cohen, "A review of the role of active remote sensing and data fusion for characterizing forest in wildlife habitat models," *Rev Teledetección*, vol. 0, no. 45, p. 1, 2016.

[199] M. C. Hansen, P. V Potapov, R. Moore, M. Hancher, S. A. Turubanova, A. Tyukavina, D. Thau, S. V Stehman, S. J. Goetz, T. R. Loveland, A. Kommareddy, A. Egorov, L. Chini, C. O. Justice, and J. R. G. Townshend, "High-resolution global maps of 21st-century forest cover change.," *Science (80-)*, vol. 342, no. 6160, pp. 850–3, 2013.

[200] J. Seoane, J. Bustamante, and R. Díaz-Delgado, "Are existing vegetation maps adequate to predict bird distributions?," *Ecol Modell*, vol. 175, no. 2, pp. 137–149, 2004.

[201] G. J. M. Rickbeil, N. C. Coops, M. C. Drever, and T. A. Nelson, "Assessing coastal species distribution models through the integration of terrestrial, oceanic and atmospheric data," *J Biogeogr*, vol. 41, no. 8, pp. 1614–1625, 2014.

[202] D. M. Samson, R. S. Archer, T. O. Alimi, K. L. Arheart, D. E. Impoinvil, R. Oscar, D. O. Fuller, and W. A. Qualls, "New baseline environmental assessment of mosquito ecology in northern Haiti during increased urbanization.," *J Vector Ecol*, vol. 40, no. 1, pp. 46–58, 2015.

[203] W. Thanapongtharm, C. Linard, W. Wiriyarat, P. Chinsorn, B. Kanchanasaka, X. Xiao, C. Biradar, R. G. Wallace, and M. Gilbert, "Spatial characterization of colonies of the flying fox bat, a carrier of Nipah virus in Thailand.," *BMC Vet Res*, vol. 11, p. 81, 2015.

[204] H. Reiss, S. Cunze, K. König, H. Neumann, and I. Kröncke, "Species distribution modelling of marine benthos: a North Sea case study," *Mar Ecol Prog Ser*, vol. 442, pp. 71–86, 2011.

[205] C. Moritz, M. Lévesque, D. Gravel, S. Vaz, D. Archambault, and P. Archambault, "Modelling spatial distribution of epibenthic communities in the Gulf of St. Lawrence (Canada)," *J Sea Res*, vol. 78, pp. 75–84, 2013.

[206] H. Reiss, S. Birchenough, A. Borja, L. Buhl-Mortensen, J. Craeymeersch, J. Dannheim, A. Darr, I. Galparsoro, M. Gogina, H. Neumann, J. Populus, A. M. Rengstorf, M. Valle, G. Van Hoey, M. L. Zettler, and S. Degraer, "Benthos distribution modelling and its relevance for marine ecosystem management," *ICES J Mar Sci*, vol. 72, no. 2, pp. 297–315, 2015.

[207] C. D. MacLeod, C. R. Weir, C. Pierpoint, and E. Harland, "The habitat preferences of marine mammals west of Scotland (UK)," *J Mar Biol Assoc United Kingdom*, vol. 87, no. 1, pp. 157–164, 2017.

[208] E. Praca, A. Gannier, K. Das, and S. Laran, "Modelling the habitat suitability of cetaceans: Example of the sperm whale in the northwestern Mediterranean Sea," *Deep Sea Res (Part I, Oceanogr Res Pap*, vol. 56, no. 4, pp. 648–657, 2009.

[209] A. Bombosch, D. P. Zitterbart, I. Van Opzeeland, S. Frickenhaus, E. Burkhardt, M. S. Wisz, and O. Boebel, "Predictive habitat modelling of humpback (Megaptera novaeangliae) and Antarctic minke (Balaenoptera bonaerensis) whales in the Southern Ocean as a planning tool for seismic surveys," *Deep Sea Res Part I Oceanogr Res Pap*, vol. 91, pp. 101–114, 2014.

[210] M. Tobeña, R. Prieto, M. Machete, and M. A. Silva, "Modeling the Potential Distribution and Richness of Cetaceans in the Azores from Fisheries Observer Program Data," *Front Mar Sci*, vol. 3, p. 202, 2016.

[211] J. Dambach and D. Rödder, "Applications and future challenges in marine species distribution modeling," *Aquat Conserv Mar Freshw Ecosyst*, vol. 21, no. 1, pp. 92–100, 2011.

[212] L. M. Krigsman, M. M. Yoklavich, E. J. Dick, and G. R. Cochrane, "Models and maps: predicting the distribution of corals and other benthic macro-invertebrates in shelf habitats," *Ecosphere*, vol. 3, no. 1, p. art3, 2012.

[213] V. D. Valavanis, G. J. Pierce, A. F. Zuur, A. Palialexis, A. Saveliev, I. Katara, and J. Wang, "Modelling of essential fish habitat based on remote sensing, spatial analysis and GIS," *Hydrobiologia*, vol. 612, no. 1, pp. 5–20, 2008.

[214] H. Verbruggen, L. Tyberghein, G. S. Belton, F. Mineur, A. Jueterbock, G. Hoarau, C. F. D. Gurgel, and O. De Clerck, "Improving Transferability of Introduced Species' Distribution Models: New Tools to Forecast the Spread of a Highly Invasive Seaweed," *PLoS One*, vol. 8, no. 6, p. e68337, 2013.

[215] S. Leidenberger, M. Obst, R. Kulawik, K. Stelzer, K. Heyer, A. Hardisty, and S. J. Bourlat, "Evaluating the potential of ecological niche modelling as a component in marine non-indigenous species risk assessments," *Mar Pollut Bull*, vol. 97, no. 1, pp. 470–487, 2015.

[216] Poursanidis D, "Ecological Niche Modeling of the the invasive lionfish Pterois miles (Bennett, 1828) in the Mediterranean Sea," in *Panhellenic Symposium on Oceanography and Fisheries 11*, 2015, pp. 621–624.

[217] P. Evangelista, N. Young, P. Schofield, and C. Jarnevich, "Modeling suitable habitat of invasive red lionfish Pterois volitans (Linnaeus, 1758) in North and South America's coastal waters," *Aquat Invasions*, vol. 11, no. 3, pp. 313–326, 2016.

[218] J. Franklin, *Mapping Species Distributions: Spatial Inference and Prediction*. Cambridge, UK: Cambridge University Press, 2010.

[219] A. T. Peterson, J. Soberón, R. G. Pearson, R. P. Anderson, E. Martínez-Meyer, M. Nakamura, and M. B. Araújo, *Ecological Niches and Geographic Distributions*. Princeton, New Jersey: Princeton University Press, 2011.

[220] E. J. Sbrocco and P. H. Barber, "MARSPEC: ocean climate layers for marine spatial ecology," *Ecology*, vol. 94, no. 4, pp. 979–979, 2013.

[221] S. Gao, Z. Niu, N. Huang, and X. Hou, "Estimating the Leaf Area Index, height and biomass of maize using HJ-1 and RADARSAT-2," *Int J Appl Earth Obs Geoinf*, vol. 24, pp. 1–8, 2013.

[222] P. Dusseux, T. Corpetti, L. Hubert-Moy, and S. Corgne, "Combined Use of Multi-Temporal Optical and Radar Satellite Images for Grassland Monitoring," *Remote Sens*, vol. 6, no. 7, pp. 6163–6182, 2014.

[223] W. Koppe, M. L. Gnyp, S. D. Hennig, F. Li, Y. Miao, X. Chen, L. Jia, and G. Bareth, "Multi-Temporal Hyperspectral and Radar Remote Sensing for Estimating Winter Wheat Biomass in the North China Plain," *Photogramm - Fernerkundung - Geoinf*, vol. 2012, no. 3, pp. 281–298, 2012.

[224] N. Joshi, M. Baumann, A. Ehammer, R. Fensholt, K. Grogan, P. Hostert, M. Jepsen, T. Kuemmerle, P. Meyfroidt, E. Mitchard, J. Reiche, C. Ryan, and B. Waske, "A Review of the Application of Optical and Radar Remote Sensing Data Fusion to Land Use Mapping and Monitoring," *Remote Sens*, vol. 8, no. 1, p. 70, 2016.

[225] C. Pohl and J. L. Van Genderen, "Multisensor image fusion in remote sensing: Concepts, methods and applications," *Int J Remote Sens*, vol. 19, no. 5, pp. 823–854, 1998.

[226] J. A. Richards, "Analysis of remotely sensed data: the formative decades and the future," *IEEE Trans Geosci Remote Sens*, vol. 43, no. 3, pp. 422–432, 2005.

[227] A. Revill, O. Sus, B. Barrett, and M. Williams, "Carbon cycling of European croplands: A framework for the

assimilation of optical and microwave Earth observation data," *Remote Sens Environ*, vol. 137, pp. 84–93, 2013.

[228] S. Attarchi and R. Gloaguen, "Improving the Estimation of Above Ground Biomass Using Dual Polarimetric PALSAR and ETM+ Data in the Hyrcanian Mountain Forest (Iran)," *Remote Sens*, vol. 6, no. 5, pp. 3693–3715, 2014.

[229] S. Huang, C. Potter, R. L. Crabtree, S. Hager, and P. Gross, "Fusing optical and radar data to estimate sagebrush, herbaceous, and bare ground cover in Yellowstone," *Remote Sens Environ*, vol. 114, no. 2, pp. 251–264, 2010.

[230] M. Xing, X. Quan, X. Li, and B. He, "An Extended Approach for Biomass Estimation in a Mixed Vegetation Area Using ASAR and TM Data," *Photogramm Eng Remote Sens*, vol. 80, no. 5, pp. 429–438, 2014.

[231] C. Eisfelder, C. Kuenzer, and S. Dech, "Derivation of biomass information for semi-arid areas using remote-sensing data," *Int J Remote Sens*, vol. 33, no. 9, pp. 2937–2984, 2012.

[232] G. Hu and L. Jia, "Monitoring of Evapotranspiration in a Semi-Arid Inland River Basin by Combining Microwave and Optical Remote Sensing Observations," *Remote Sens*, vol. 7, no. 3, pp. 3056–3087, 2015.

[233] T. Svoray and M. Shoshany, "SAR-based estimation of areal aboveground biomass (AAB) of herbaceous vegetation in the semi-arid zone: a modi cation of the water-cloud model," *Int J Remote Sens int j Remote Sens*, vol. 2319, no. 19, pp. 4089–4100, 2002.

[234] J. C. Rodgers, A. W. Murrah, and W. H. Cooke, "The Impact of Hurricane Katrina on the Coastal Vegetation of the Weeks Bay Reserve, Alabama from NDVI Data," *Estuaries and Coasts*, vol. 32, no. 3, pp. 496–507, 2009.

[235] R. Chakraborty, P. Ferrazzoli, and R. Rahmoune, "Application of passive microwave and optical signatures to monitor submerging of vegetation due to floods," *Int J Remote Sens*, vol. 35, no. 16, pp. 6310–6328, 2014.

[236] A. Rangoonwala, N. M. Enwright, E. Ramsey III, and J. P. Spruce, "Radar and optical mapping of surge persistence and marsh dieback along the New Jersey Mid-Atlantic coast after Hurricane Sandy," *Int J Remote Sens*, vol. 37, no. 7, pp. 1692–1713, 2016.

[237] P. D'Odorico, A. Gonsamo, A. Damm, and M. E. Schaepman, "Experimental Evaluation of Sentinel-2 Spectral Response Functions for NDVI Time-Series Continuity," *IEEE Trans Geosci Remote Sens*, vol. 51, no. 3, pp. 1336–1348, 2013.

[238] M. Drusch, U. Del Bello, S. Carlier, O. Colin, V. Fernandez, F. Gascon, B. Hoersch, C. Isola, P. Laberinti, P. Martimort, A. Meygret, F. Spoto, O. Sy, F. Marchese, and P. Bargellini, "Sentinel-2: ESA's Optical High-Resolution Mission for GMES Operational Services," *Remote Sens Environ*, vol. 120, pp. 25–36, 2012.

[239] X. Pons, L. Pesquer, J. Cristóbal, and O. González-Guerrero, "Automatic and improved radiometric correction of Landsat imagery using reference values from MODIS surface reflectance images," *Int J Appl Earth Obs Geoinf*, vol. 33, pp. 243–254, 2014.

[240] P. Mairota, B. Cafarelli, R. Labadessa, F. Lovergine, C. Tarantino, R. M. Lucas, H. Nagendra, and R. K. Didham, "Very high resolution Earth observation features for monitoring plant and animal community structure across multiple spatial scales in protected areas," *Int J Appl Earth Obs Geoinf*, vol. 37, pp. 100–105, 2015.

[241] E. J. Rykiel, "Testing ecological models: the meaning of validation," *Ecol Modell*, vol. 90, no. 3, pp. 229–244, 1996.

[242] A. M. Y. Kamel, G. Y. El Serafy, B. Bhattacharya, T. van Kessel, and D. P. Solomatine, "Using remote sensing to enhance modelling of fine sediment dynamics in the Dutch coastal zone," *J Hydroinformatics*, vol. 16, no. 2, pp. 458–476, 2014.

[243] X. Chen, J. Lu, T. Cui, W. Jiang, L. Tian, L. Chen, and W. Zhao, "Coupling remote sensing retrieval with numerical simulation for SPM study—Taking Bohai Sea in China as a case," *Int J Appl Earth Obs Geoinf*, vol. 12, pp. S203–S211, 2010.

[244] D. Lo Seen, E. Mougin, S. Rambal, A. Gaston, and P. Hiernaux, "A regional Sahelian grassland model to be coupled with multispectral satellite data. II: Toward the control of its simulations by remotely sensed indices," *Remote Sens Environ*, vol. 52, no. 3, pp. 194–206, 1995.

[245] G. J. M. De Lannoy and R. H. Reichle, "Global Assimilation of Multiangle and Multipolarization SMOS Brightness Temperature Observations into the GEOS-5 Catchment Land Surface Model for Soil Moisture Estimation," *J Hydrometeorol*, vol. 17, no. 2, pp. 669–691, 2016.

[246] N. D. Bennett, B. F. W. Croke, G. Guariso, J. H. A. Guillaume, S. H. Hamilton, A. J. Jakeman, S. Marsili-Libelli, L. T. H. Newham, J. P. Norton, C. Perrin, S. A. Pierce, B. Robson, R. Seppelt, A. A. Voinov, B. D. Fath, and V. Andreassian, "Characterising performance of environmental models," *Environ Model Softw*, vol. 40, pp. 1–20, 2013.

[247] J. I. Allen, J. T. Holt, J. Blackford, and R. Proctor, "Error quantification of a high-resolution coupled hydrodynamic-ecosystem coastal-ocean model: Part 2. Chlorophyll-a, nutrients and SPM," *J Mar Syst*, vol. 68, no. 3, pp. 381–404, 2007.

[248] K. P. Edwards, R. Barciela, and M. Butenschön, "Validation of the NEMO-ERSEM operational ecosystem model for the North West European Continental Shelf," *Ocean Sci*, vol. 8, pp. 983–1000, 2012.

[249] K. E. Taylor, "Summarizing multiple aspects of model performance in a single diagram," *J Geophys Res Atmos*, vol. 106, no. D7, pp. 7183–7192, 2001.

[250] C. A. Stow, J. Jolliff, S. C. Doney, J. I. Allen, M. A. M. Friedrichs, K. A. Rose, and P. Wallhead, "Skill assessment for coupled biological/physical models of marine systems," *J Mar Syst*, vol. 76, no. 1, pp. 4–15, 2009.

[251] J. K. Jolliff, J. C. Kindle, I. Shulman, B. Penta, M. A. M. Friedrichs, R. Helber, and R. A. Arnone, "Summary diagrams for coupled hydrodynamic-ecosystem model skill assessment," *J Mar Syst*, vol. 76, no. 1, pp. 64–82, 2009.

[252] G. B. Arhonditsis, B. A. Adams-VanHarn, L. Nielsen, C. A. Stow, and K. H. Reckhow, "Evaluation of the Current State of Mechanistic Aquatic Biogeochemical Modeling: Citation Analysis and Future Perspectives," *Environ Sci Technol*, vol. 40, no. 21, pp. 6547–6554, 2006.

[253] J. Koch, K. H. Jensen, and S. Stisen, "Toward a true spatial model evaluation in distributed hydrological modeling: Kappa statistics, Fuzzy theory, and EOF-analysis benchmarked by the human perception and evaluated against a modeling case study," *Water Resour Res*, vol. 51, no. 2, pp. 1225–1246, 2015.

[254] A. Hannachi, I. T. Jolliffe, and D. B. Stephenson, "Empirical orthogonal functions and related techniques in atmospheric science: A review," *Int J Climatol*, vol. 27, no. 9, pp. 1119–1152, 2007.

[255] K. A. Rose, B. M. Roth, and E. P. Smith, "Skill assessment of spatial maps for oceanographic modeling," *J Mar Syst*, vol. 76, no. 1, pp. 34–48, 2009.

[256] D. L. Urban, G. B. Bonan, T. M. Smith, and H. H. Shugart, "Spatial applications of gap models," *For Ecol Manage*, vol. 42, no. 1–2, pp. 95–110, 1991.

[257] J. T. Randerson, F. M. Hoffman, P. E. Thornton, N. M. Mahowald, K. Lindsay, Y.-H. Lee, C. D. Nevison, S. C. Doney, G. Bonan, R. Stockli, C. Covey, S. W. Running, and I. Y. Fung, "Systematic assessment of terrestrial biogeochemistry in coupled climate-carbon models," *Glob Chang Biol*, vol. 15, no. 10, pp. 2462–2484, Oct. 2009.

[258] M. Zhao, F. A. Heinsch, R. R. Nemani, and S. W. Running, "Improvements of the MODIS terrestrial gross and net primary production global data set," *Remote Sens Environ*, vol. 95, no. 2, pp. 164–176, 2005.

[259] D. Medvigy, S. C. Wofsy, J. W. Munger, D. Y. Hollinger, and P. R. Moorcroft, "Mechanistic scaling of ecosystem function and dynamics in space and time: Ecosystem Demography model version 2 scaling of ecosystem function and dynamics in space and time: Ecosystem Demography model version," *J Geophys Res*, vol. 114, no. 2, 2009.

[260] N. M. Levine, K. Zhang, M. Longo, A. Baccini, O. L. Phillips, S. L. Lewis, E. Alvarez-Dávila, A. C. Segalin de Andrade, R. J. W. Brienen, T. L. Erwin, T. R. Feldpausch, A. L. Monteagudo Mendoza, P. Nuñez Vargas, A. Prieto, J. E. Silva-Espejo, Y. Malhi, and P. R. Moorcroft, "Ecosystem heterogeneity determines the ecological resilience of the Amazon to climate change.," *Proc Natl Acad Sci U S A*, vol. 113, no. 3, pp. 793–7, 2016.

[261] D. M. Lopes, J. T. Aranha, N. Walford, J. O'Brien, and N. Lucas, "Accuracy of remote sensing data versus other sources of information for estimating net primary production in *Eucalyptus globulus* Labill. and *Pinus pinaster* Ait. ecosystems in Portugal," *Can J Remote Sens*, vol. 35, no. 1, pp. 37–53, Jan. 2009.

[262] S. Sitch, B. Smith, I. C. Prentice, A. Arneth, A. Bondeau, W. Cramer, J. O. Kaplan, S. Levis, W. Lucht, M. T. Sykes, K. Thonicke, and S. Venevsky, "Evaluation of ecosystem dynamics, plant geography and terrestrial carbon cycling in the LPJ dynamic global vegetation model," *Glob Chang Biol*, vol. 9, no. 2, pp. 161–185, 2003.

[263] C. Hély, L. Bremond, S. Alleaume, B. Smith, M. T. Sykes, and J. Guiot, "Sensitivity of African biomes to changes in the precipitation regime," *Glob Ecol Biogeogr*, vol. 15, no. 3, pp. 258–270, 2006.

[264] C. Pappas, S. Fatichi, S. Rimkus, P. Burlando, and M. O. Huber, "The role of local-scale heterogeneities in terrestrial ecosystem modeling," *J Geophys Res Biogeosciences*, vol. 120, no. 2, pp. 341–360, 2015.

[265] H. Muraoka, H. M. Noda, S. Nagai, T. Motohka, T. M. Saitoh, K. N. Nasahara, and N. Saigusa, "Spectral vegetation indices as the indicator of canopy photosynthetic productivity in a deciduous broadleaf forest," *J Plant Ecol*, vol. 6, no. 5, pp. 393–407, 2013.

[266] G. Krinner, N. Viovy, N. de Noblet-Ducoudré, J. Ogée, J. Polcher, P. Friedlingstein, P. Ciais, S. Sitch, and I. C. Prentice, "A dynamic global vegetation model for studies of the coupled atmosphere-biosphere system," *Global Biogeochem Cycles*, vol. 19, no. 1, 2005.

[267] A. K. Traore, P. Ciais, N. Vuichard, B. Poulter, N. Viovy, M. Guimberteau, M. Jung, R. Myneni, and J. B. Fisher, "Evaluation of the ORCHIDEE ecosystem model over Africa against 25 years of satellite-based water and carbon measurements," *J Geophys Res Biogeosciences*, vol. 119, no. 8, pp. 1554–1575, 2014.

[268] C. L. Tague, L. E. Band, C. L. Tague, and L. E. Band, "RHESSys: Regional Hydro-Ecologic Simulation System—An Object-Oriented Approach to Spatially Distributed Modeling of Carbon, Water, and Nutrient Cycling," *Earth Interact*, vol. 8, no. 19, pp. 1–42, 2004.

[269] T. Hwang, S. Kang, J. Kim, Y. Kim, D. Lee, and L. Bend, "Evaluating drought effect on MODIS Gross Primary Production (GPP) with an eco-hydrological model in the mountainous forest, East Asia," *Glob Chang Biol*, vol. 14, no. 5, pp. 1037–1056, 2008.

[270] Z. Su, "The Surface Energy Balance System (SEBS) for estimation of turbulent heat fluxes," *Hydrol Earth Syst Sci*, vol. 6, no. 1, pp. 85–99, 2002.

[271] X. Tian, C. van der Tol, Z. Su, Z. Li, E. Chen, X. Li, M. Yan, X. Chen, X. Wang, X. Pan, F. Ling, C. Li, W. Fan, and L. Li, "Simulation of Forest Evapotranspiration Using Time-Series Parameterization of the Surface Energy Balance System (SEBS) over the Qilian Mountains," *Remote Sens*, vol. 7, no. 12, pp. 15822–15843, 2015.

[272] C. Song, T. A. Schroeder, and W. B. Cohen, "Predicting temperate conifer forest successional stage distributions with multitemporal Landsat Thematic Mapper imagery," *Remote Sens Environ*, vol. 106, no. 2, pp. 228–237, 2007.

[273] J. Martínez-López, J. Martínez-Fernández, B. Naimi, M. F. Carreño, and M. A. Esteve, "An open-source spatio-dynamic wetland model of plant community responses to hydrological pressures," *Ecol Modell*, vol.

306, pp. 326–333, 2015.

[274] A. Ito, "A historical meta-analysis of global terrestrial net primary productivity: are estimates converging?," *Glob Chang Biol*, vol. 17, no. 10, pp. 3161–3175, 2011.

[275] M. Mateus, G. Riflet, P. Chambel, L. Fernandes, R. Fernandes, M. Juliano, F. Campuzano, H. de Pablo, and R. Neves, "An operational model for the West Iberian coast: products and services," *Ocean Sci*, vol. 8, no. 4, pp. 713–732, 2012.

[276] M. Vichi, N. Pinardi, and S. Masina, "A generalized model of pelagic biogeochemistry for the global ocean ecosystem. Part I: Theory," *J Mar Syst*, vol. 64, no. 1, pp. 89–109, 2007.

[277] M. Vichi, S. Masina, and A. Navarra, "A generalized model of pelagic biogeochemistry for the global ocean ecosystem. Part II: Numerical simulations," *J Mar Syst*, vol. 64, no. 1, pp. 110–134, 2007.

[278] M. Vichi and S. Masina, "Skill assessment of the PELAGOS global ocean biogeochemistry model over the period 1980-2000," *Biogeosciences*, vol. 6, no. 11, pp. 2333–2353, 2009.

[279] M. Vichi, J. I. Allen, S. Masina, and N. J. Hardman-Mountford, "The emergence of ocean biogeochemical provinces: A quantitative assessment and a diagnostic for model evaluation," *Global Biogeochem Cycles*, vol. 25, no. 2, p. n/a-n/a, 2011.

[280] W. J. McKiver, M. Vichi, T. Lovato, A. Storto, and S. Masina, "Impact of increased grid resolution on global marine biogeochemistry," *J Mar Syst*, vol. 147, pp. 153–168, 2015.

[281] P. Lazzari, A. Teruzzi, S. Salon, S. Campagna, C. Calonaci, S. Colella, M. Tonani, and A. Crise, "Pre-operational short-term forecasts for Mediterranean Sea biogeochemistry," *Ocean Sci*, vol. 6, pp. 25–39, 2010.

[282] P. Lazzari, C. Solidoro, V. Ibello, S. Salon, A. Teruzzi, K. Béranger, S. Colella, and A. Crise, "Seasonal and inter-annual variability of plankton chlorophyll and primary production in the Mediterranean Sea: a modelling approach," *Biogeosciences*, vol. 9, no. 1, pp. 217–233, 2012.

[283] G. Mattia, M. Zavatarelli, M. Vichi, and P. Oddo, "The Eastern Mediterranean Sea biogeochemical dynamics in the 1990s: A numerical study," *J Geophys Res Ocean*, vol. 118, no. 4, pp. 2231–2248, 2013.

[284] J. Pätsch and W. Kühn, "Nitrogen and carbon cycling in the North Sea and exchange with the North Atlantic—A model study. Part I. Nitrogen budget and fluxes," *Cont Shelf Res*, vol. 28, no. 6, pp. 767–787, 2008.

[285] W. Kühn, J. Pätsch, H. Thomas, A. V. Borges, L.-S. Schiettecatte, Y. Bozec, and A. E. F. Prowe, "Nitrogen and carbon cycling in the North Sea and exchange with the North Atlantic—A model study, Part II: Carbon budget and fluxes," *Cont Shelf Res*, vol. 30, no. 16, pp. 1701–1716, 2010.

[286] B. Tiedje, A. Moll, and L. Kaleschke, "Comparison of temporal and spatial structures of chlorophyll derived from MODIS satellite data and ECOHAM3 model data in the North Sea," *J Sea Res*, vol. 64, no. 3, pp. 250–259, 2010.

[287] J. W. Baretta, W. Ebenhöh, and P. Ruardij, "The European regional seas ecosystem model, a complex marine ecosystem model," *Netherlands J Sea Res*, vol. 33, no. 3–4, pp. 233–246, 1995.

[288] J. C. Blackford and P. J. Radford, "A structure and methodology for marine ecosystem modelling," *Netherlands J Sea Res*, vol. 33, no. 3, pp. 247–260, 1995.

[289] J. G. Baretta-Bekker, J. W. Baretta, and W. Ebenhöh, "Microbial dynamics in the marine ecosystem model ERSEM II with decoupled carbon assimilation and nutrient uptake," *J Sea Res*, vol. 38, no. 3, pp. 195–211, 1997.

[290] J. C. Blackford, J. I. Allen, and F. J. Gilbert, "Ecosystem dynamics at six contrasting sites: a generic modelling study," *J Mar Syst*, vol. 52, no. 1, pp. 191–215, 2004.

[291] J. C. Blackford and F. J. Gilbert, “pH variability and CO2 induced acidification in the North Sea,” *J Mar Syst*, vol. 64, no. 1, pp. 229–241, 2007.

[292] M. Butenschön, J. Clark, J. N. Aldridge, J. I. Allen, Y. Artioli, J. Blackford, J. Bruggeman, P. Cazenave, S. Ciavatta, S. Kay, G. Lessin, S. van Leeuwen, J. van der Molen, L. de Mora, L. Polimene, S. Sailley, N. Stephens, and R. Torres, “ERSEM 15.06: a generic model for marine biogeochemistry and the ecosystem dynamics of the lower trophic levels,” *Geosci Model Dev*, vol. 9, no. 4, pp. 1293–1339, 2016.

[293] S. Ciavatta, R. Torres, S. Saux-Picart, and J. I. Allen, “Can ocean color assimilation improve biogeochemical hindcasts in shelf seas?,” *J Geophys Res*, vol. 116, no. C12, p. C12043, 2011.

[294] S. Ciavatta, R. Torres, V. Martinez-Vicente, T. Smyth, G. Dall’Olmo, L. Polimene, and J. I. Allen, “Assimilation of remotely-sensed optical properties to improve marine biogeochemistry modelling,” *Prog Oceanogr*, vol. 127, pp. 74–95, 2014.

[295] O. Aumont and L. Bopp, “Globalizing results from ocean in situ iron fertilization studies,” *Global Biogeochem Cycles*, vol. 20, no. 2, Jun. 2006.

[296] O. Aumont, E. Maier-Reimer, S. Blain, and P. Monfray, “An ecosystem model of the global ocean including Fe, Si, P colimitations,” *Global Biogeochem Cycles*, vol. 17, no. 2, 2003.

[297] O. Aumont, C. Ethé, A. Tagliabue, L. Bopp, and M. Gehlen, “PISCES-v2: an ocean biogeochemical model for carbon and ecosystem studies,” *Geosci Model Dev*, vol. 8, pp. 2465–2513, 2015.

[298] B. Schneider, L. Bopp, M. Gehlen, J. Segschneider, T. L. Frölicher, P. Cadule, P. Friedlingstein, S. C. Doney, M. J. Behrenfeld, and F. Joos, “Climate-induced interannual variability of marine primary and export production in three global coupled climate carbon cycle models,” *Biogeosciences*, vol. 5, no. 2, pp. 597–614, 2008.

[299] D. Kim and J. Kaluarachchi, “Validating FAO AquaCrop using Landsat images and regional crop information,” *Agric Water Manag*, vol. 149, pp. 143–155, 2015.

[300] D. A. Ford, J. van der Molen, K. Hyder, J. Bacon, R. Barciela, V. Creach, R. McEwan, P. Ruardij, and R. Forster, “Observing and modelling phytoplankton community structure in the North Sea: can ERSEM-type models simulate biodiversity?,” *Biogeosciences Discuss*, pp. 1–39, 2016.

[301] J. C. Refsgaard, J. P. van der Sluijs, A. L. Højberg, P. A. Vanrolleghem, J. P. Van Der Sluijs, A. L. Hojberg, P. A. Vanrolleghem, J. Christian, J. P. Van Der Sluijs, A. Lajer, P. A. Vanrolleghem, J. P. van der Sluijs, A. L. Højberg, and P. A. Vanrolleghem, “Uncertainty in the environmental modelling process e A framework and guidance,” *Environ Model Softw*, vol. 22, no. 11, pp. 1543–1556, 2007.

[302] K. Cuddington, M.-J. Fortin, L. R. Gerber, A. Hastings, A. Liebhold, M. O’Connor, and C. Ray, “Process-based models are required to manage ecological systems in a changing world,” *Ecosphere*, vol. 4, no. 2, pp. 1–12, 2013.

[303] K. Beven and J. Freer, “Equifinality, data assimilation, and uncertainty estimation in mechanistic modelling of complex environmental systems using the GLUE methodology,” *J Hydrol*, vol. 249, pp. 11–29, 2001.

[304] T. F. Keenan, M. S. Carbone, M. Reichstein, and A. D. Richardson, “The model–data fusion pitfall: assuming certainty in an uncertain world,” *Oecologia*, vol. 167, pp. 587–597, 2011.

[305] M. C. Kennedy and A. O’Hagan, “Bayesian calibration of computer models,” *J R Stat Soc Ser B (Statistical Methodol*, vol. 63, no. 3, pp. 425–464, 2001.

[306] I. S. Robinson, *Remote Sensing of Shelf Sea Ecosystems*. European Science Foundation, Marine Board, 2008.

[307] D. McLaughlin, “Recent developments in hydrologic data assimilation,” *Rev Geophys*, vol. 33, no. S2, p. 977, 1995.

[308] D. McLaughlin, “An integrated approach to hydrologic data assimilation: interpolation, smoothing, and

filtering," *Adv Water Resour*, vol. 25, no. 8, pp. 1275–1286, 2002.

[309] P. R. Houser, J. W. Shuttleworth, J. S. Famiglietti, H. V Gupta, K. H. Syed, and D. C. Goodrich, "Integration of soil moisture remote sensing and hydrologic modeling using data assimilation," *Water Resour Res*, vol. 34, no. 12, pp. 3405–3420, 1998.

[310] H. Bach and W. Mauser, "Methods and examples for remote sensing data assimilation in land surface process modeling," *IEEE Trans Geosci Remote Sens*, vol. 41, no. 7, pp. 1629–1637, 2003.

[311] R. E. Kalman, "A New Approach to Linear Filtering and Prediction Problems," *J Basic Eng*, vol. 82, no. 1, p. 35, 1960.

[312] A. Benedetti, M. Janisková, A. Benedetti, and M. Janisková, "Assimilation of MODIS Cloud Optical Depths in the ECMWF Model," *Mon Weather Rev*, vol. 136, no. 5, pp. 1727–1746, 2008.

[313] F. Rabier, H. Jarvinen, E. Klinker, J. F. Mahfouf, and A. Simmons, "The ECMWF operational implementation of four-dimensional variational assimilation. I: Experimental results with simplified physics," *Q J R Meteorol Soc*, vol. 126, no. 564, pp. 1143–1170, 2000.

[314] J. L. Anderson, "An Ensemble Adjustment Kalman Filter for Data Assimilation," *Mon Weather Rev*, vol. 129, pp. 2884–2903, 2001.

[315] G. Evensen, "The Ensemble Kalman Filter: Theoretical formulation and practical implementation," vol. 53, no. 4, pp. 343–367, 2003.

[316] M. S. S. Arulampalam, S. Maskell, N. Gordon, and T. Clapp, "A tutorial on particle filters for online nonlinear/non-Gaussian Bayesian tracking," *IEEE Trans Signal Process*, vol. 50, no. 2, pp. 174–188, 2002.

[317] C. De Bernardis, F. Vicente-Guijalba, T. Martinez-Marin, and J. Lopez-Sanchez, "Particle Filter Approach for Real-Time Estimation of Crop Phenological States Using Time Series of NDVI Images," *Remote Sens*, vol. 8, no. 7, p. 610, 2016.

[318] Y. Zhou, D. McLaughlin, and D. Entekhabi, "Assessing the performance of the ensemble Kalman filter for land surface data assimilation," vol. 134, no. 8, pp. 2128–2142, 2006.

[319] Y. Liu and H. V Gupta, "Uncertainty in hydrologic modeling : Toward an integrated data assimilation framework," *Water Resour Res*, vol. 43, pp. 1–18, 2007.

[320] G. van Delft, G. Y. El Serafy, and A. W. Heemink, "The ensemble particle filter (EnPF) in rainfall- runoff models," *Stoch Env Res Risk Assess*, vol. 23, pp. 1203–1211, 2009.

[321] N. Wanders, M. F. P. Bierkens, S. M. De Jong, A. De Roo, and D. Karssenberg, "The benefits of using remotely sensed soilmoisture in parameter identification of large-scale hydrologicalmodels," *Water Resour Res*, vol. 50, pp. 6874–6891, 2014.

[322] M. Bocquet, C. A. Pires, and L. Wu, "Beyond Gaussian Statistical Modeling in Geophysical Data Assimilation," *Mon Weather Rev*, vol. 138, pp. 2997–3023, 2010.

[323] C. Montzka, V. Pauwels, H.-J. Franssen, X. Han, and H. Vereecken, "Multivariate and Multiscale Data Assimilation in Terrestrial Systems: A Review," *Sensors*, vol. 12, no. 12, pp. 16291–16333, 2012.

[324] N. Wanders, D. Karssenberg, M. Bierkens, R. Parinussa, R. de Jeu, J. van Dam, and S. de Jong, "Observation uncertainty of satellite soil moisture products determined with physically-based modeling," *Remote Sens Environ*, vol. 127, pp. 341–356, 2012.

[325] I. D. Garcia, G. Y. El Serafy, A. Heemink, and H. Schuttelaars, "Towards a data assimilation system for morphodynamic modeling : bathymetric data assimilation for wave property estimation," *Ocean Dyn*, vol. 63, no. 5, pp. 489–505, 2013.

[326] N. van Velzen, M. U. Altaf, and M. Verlaan, "OpenDA-NEMO framework for ocean data assimilation," *Ocean Dyn*, vol. 66, no. 5, pp. 691–702, 2016.

[327] M. E. Ridler, N. Van Velzen, S. Hummel, I. Sandholt, A. K. Falk, A. Heemink, and H. Madsen, "Data assimilation framework: Linking an open data assimilation library (OpenDA) to a widely adopted model interface (OpenMI)," *Environ Model Softw*, vol. 57, pp. 76–89, 2014.

[328] A. Kurniawan, S. K. Ooi, S. Hummel, and H. Gerritsen, "Sensitivity analysis of the tidal representation in Singapore Regional Waters in a data assimilation environment," *Ocean Dyn*, vol. 61, no. 8, pp. 1121–1136, 2011.

[329] N. Serpoushan, M. Zeinoddini, and M. Golestani, "An Ensemble Kalman Filter Data Assimilation Scheme for Modeling the Wave Climate in Persian Gulf," in *ASME 2013 32nd International Conference on Ocean, Offshore and Arctic Engineering*, 2013, p. V005T06A028.

[330] M. Garcia, I. Ramirez, M. Verlaan, and J. Castillo, "Application of a three-dimensional hydrodynamic model for San Quintin Bay, B.C., Mexico. Validation and calibration using OpenDA," *J Comput Appl Math*, vol. 273, pp. 428–437, 2015.

[331] L. Nerger, W. Hiller, and J. Schröter, "PDAF - The Parallel Data Assimilation Framework: Experiences with Kalman Filtering," in *Use of High Performance Computing in Meteorology - Proceedings of the 11th ECMWF Workshop*, 2005, pp. 63–83.

[332] L. Nerger and W. Hiller, "Software for ensemble-based data assimilation systems - implementation strategies and scalability," *Comput Geosci*, vol. 55, pp. 110–118, 2013.

[333] W. Kurtz, G. He, S. J. Kollet, R. M. Maxwell, H. Vereecken, and H. J. Hendricks Franssen, "TerrSysMP-PDAF (version 1.0): A modular high-performance data assimilation framework for an integrated land surface-subsurface model," *Geosci Model Dev*, vol. 9, pp. 1341–1360, 2016.

[334] S. N. Losa, S. Danilov, J. Schröter, T. Janjić, L. Nerger, and F. Janssen, "Assimilating NOAA SST data into BSH operational circulation model for the North and Baltic Seas: Part 2. Sensitivity of the forecast's skill to the prior model error statistics," *J Mar Syst*, vol. 129, pp. 259–270, 2014.

[335] J. P. Hacker and W. M. Angevine, "Ensemble Data Assimilation to Characterize Surface-Layer Errors in Numerical Weather Prediction Models," *Mon Weather Rev*, vol. 141, no. 6, pp. 1804–1821, 2013.

[336] A. P. Mizzi, A. F. Arellano, D. P. Edwards, J. L. Anderson, and G. G. Pfister, "Assimilating compact phase space retrievals of atmospheric composition with WRF-Chem/DART: A regional chemical transport/ensemble Kalman filter data assimilation system," *Geosci Model Dev*, vol. 9, no. 3, pp. 965–978, 2016.

[337] Y. Zhang and T. Hoar, "Assimilation of MODIS Snow Cover through the Data Assimilation Research Testbed and the Community Land Model Version 4," *J Geophys Res Res*, pp. 1–13, 2014.

[338] J. A. Waller, S. L. Dance, A. S. Lawless, and N. K. Nichols, "Estimating correlated observation error statistics using an ensemble transform Kalman filter," *Tellus A*, vol. 66, no. 0, 2014.

[339] W. A. Lahoz and G. J. M. De Lannoy, *Closing the Gaps in Our Knowledge of the Hydrological Cycle over Land: Conceptual Problems*, vol. 35. 2014.

[340] G. B. M. Heuvelink and R. Webster, "Modelling soil variation: past, present, and future," *Geoderma*, vol. 100, pp. 269–301, 2001.

[341] M. Crosetto, J. A. Moreno Ruiz, and B. Crippa, "Uncertainty propagation in models driven by remotely sensed data," *Remote Sens Environ*, vol. 76, no. 3, pp. 373–385, 2001.

[342] K. Chokmani, M. Bernier, and Y. Gauthier, "Uncertainty analysis of EQeau, a remote sensing based model for snow water equivalent estimation," *Int J Remote Sens*, vol. 27, no. 19, pp. 4337–4346, 2007.

[343] K. Cockx, T. Van de Voorde, and F. Canters, "Quantifying uncertainty in remote sensing-based urban land-use mapping," *Int J Appl Earth Obs Geoinf*, vol. 31, pp. 154–166, 2014.

[344] N. Wanders, D. Karssenberg, A. De Roo, S. M. De Jong, and M. F. P. Bierkens, "The suitability of remotely

sensed soil moisture for improving operational flood forecasting," *Hydrol Earth Syst Sci*, vol. 18, no. 6, pp. 2343–2357, 2014.

[345] H. J. van der Woerd and R. Pasterkamp, "HYDROPT: A fast and flexible method to retrieve chlorophyll-a from multispectral satellite observations of optically complex coastal waters," *Remote Sens Environ*, vol. 112, no. 4, pp. 1795–1807, 2008.

[346] ESA, "MERIS Product Handbook," 2006.

[347] G. Desroziers, L. Berre, B. Chapnik, and P. Poli, "Diagnosis of observation, background and analysis-error statistics in observation space," *Q J R Meteorol Soc*, vol. 131, no. 613, pp. 3385–3396, 2005.

[348] J. A. Waller, S. L. Dance, and N. K. Nichols, "Theoretical insight into diagnosing observation error correlations using observation-minus-background and observation-minus-analysis statistics," *Q J R Meteorol Soc*, vol. 142, no. 694, pp. 418–431, 2016.

[349] K. Terasaki and T. Miyoshi, "Data assimilation with error-correlated and non-orthogonal observations: Experiments with the Lorenz-96 Model," *Sci Online Lett Atmos*, vol. 10, no. 1, pp. 210–213, 2014.

[350] A. R. Karspeck, "An Ensemble Approach for the Estimation of Observational Error Illustrated for a Nominal 1° Global Ocean Model," *Mon Weather Rev*, vol. 144, no. 5, pp. 1713–1728, 2016.

[351] L. M. Stewart, S. L. Dance, N. K. Nichols, J. R. Eyre, and J. Cameron, "Estimating interchannel observation-error correlations for IASI radiance data in the Met Office system," *Q J R Meteorol Soc*, vol. 140, no. 681, pp. 1236–1244, 2014.

[352] W. T. Crow and E. F. Wood, "The assimilation of remotely sensed soil brightness temperature imagery into a land surface model using Ensemble Kalman filtering: a case study based on ESTAR measurements during SGP97," *Adv Water Resour*, vol. 26, no. 2, pp. 137–149, 2003.

[353] C. Huang, X. Li, L. Lu, and J. Gu, "Experiments of one-dimensional soil moisture assimilation system based on ensemble Kalman filter," *Remote Sens Environ*, vol. 112, no. 3, pp. 888–900, 2008.

[354] S. Zhang, J. Shi, and Y. Dou, "A soil moisture assimilation scheme based on the microwave Land Emissivity Model and the Community Land Model," vol. 33, no. 9, pp. 2770–2797, 2012.

[355] R. H. Reichle, D. B. McLaughlin, and D. Entekhabi, "Variational data assimilation of microwave radiobrightness observations for land surface hydrology applications," *IEEE Trans Geosci Remote Sens*, vol. 39, no. 8, pp. 1708–1718, 2001.

[356] B. Jia, X. Tian, Z. Xie, J. Liu, and C. Shi, "Assimilation of microwave brightness temperature in a land data assimilation system with multi-observation operators," *J Geophys Res Atmos*, vol. 118, no. 10, pp. 3972–3985, 2013.

[357] L. Zhao, K. Yang, J. Qin, and Y. Chen, "Optimal exploitation of AMSR-E signals for improving soil moisture estimation through land data assimilation," *IEEE Trans Geosci Remote Sens*, vol. 51, no. 1, pp. 399–410, 2013.

[358] R. Boutin and O. Chertov, "Uncertainty analysis in carbon cycle models of forest ecosystems: Research needs and development of a theoretical framework to estimate error propagation," *Ecol Modell*, vol. 219, no. 3, pp. 400–412, 2008.

[359] E. Serpetzoglou, E. N. Anagnostou, A. Papadopoulos, E. I. Nikolopoulos, V. Maggioni, E. Serpetzoglou, E. N. Anagnostou, A. Papadopoulos, E. I. Nikolopoulos, and V. Maggioni, "Error propagation of remote sensing rainfall estimates in soil moisture prediction from a land surface model," *J Hydrometeorol*, vol. 11, no. 3, pp. 705–720, 2010.

[360] M. Dong, B. A. Bryan, J. D. Connor, M. Nolan, and L. Gao, "Land use mapping error introduces strongly-localised, scale-dependent uncertainty into land use and ecosystem services modelling," *Ecosyst Serv*, vol. 15, pp. 63–74, 2015.

[361] R. H. Reichle, "Data assimilation methods in the Earth sciences," *Adv Water Resour*, vol. 31, pp. 1411–1418, 2008.

[362] C. Piccolo and M. Cullen, "Ensemble Data Assimilation Using a Unified Representation of Model Error," *Mon Weather Rev*, vol. 144, no. 1, pp. 213–224, 2016.

[363] B. Revilla-Romero, H. E. Beck, P. Burek, P. Salamon, A. de Roo, and J. Thielen, "Remote Sensing of Environment Filling the gaps : Calibrating a rainfall-runoff model using satellite-derived surface water extent," *Remote Sens Environ*, vol. 171, pp. 118–131, 2015.

[364] H. Vereecken, J. A. Huisman, H. J. Hendricks Franssen, N. Bruggemann, H. R. Bogena, S. Kollet, M. Javaux, J. van der Kruk, and J. Vanderborght, "Soil hydrology: Recent methodological advances, challenges, and perspectives," *Water Resour Res*, vol. 51, no. 4, pp. 2616–2633, 2015.

[365] M. E. Ridler, H. Madsen, S. Stisen, S. Bircher, and R. Fensholt, "Assimilation of SMOS-derived soil moisture in a fully integrated hydrological and soil-vegetation-atmosphere transfermodel in Western Denmark," *Water Resour Res*, vol. 50, pp. 8962–8981, 2014.

[366] H. Lievens, G. J. M. De Lannoy, A. Al Bitar, M. Drusch, G. Dumedah, H.-J. Hendricks Franssen, Y. H. Kerr, S. K. Tomer, B. Martens, O. Merlin, M. Pan, J. K. Roundy, H. Vereecken, J. P. Walker, E. F. Wood, N. E. C. Verhoest, and V. R. N. Pauwels, "Assimilation of SMOS soil moisture and brightness temperature products into a land surface model," *Remote Sens Environ*, vol. 180, pp. 292–304, 2016.

[367] V. R. N. Pauwels, G. J. M. De Lannoy, H.-J. Hendricks Franssen, and H. Vereecken, "Simultaneous estimation of model state variables and observation and forecast biases using a two-stage hybrid Kalman filter," *Hydrol Earth Syst Sci*, vol. 17, no. 9, pp. 3499–3521, 2013.

[368] S. Quegan and T. Le Toan, "Embedding remote sensing data in models for forest carbon dynamics," in *Proceedings of the Third International Symposium on Retrieval of Bio- and Geophysical Parameters from SAR Data for Land Applications*, 2002, vol. 475, pp. 215–220.

[369] P. Peylin, C. Bacour, N. MacBean, S. Leonard, P. Rayner, S. Kuppel, E. Koffi, A. Kane, F. Maignan, F. Chevallier, P. Ciais, and P. Prunet, "A new stepwise carbon cycle data assimilation system using multiple data streams to constrain the simulated land surface carbon cycle," *Geosci Model Dev*, vol. 9, no. 9, pp. 3321–3346, 2016.

[370] M. Bagnara, M. Sottocornola, A. Cescatti, S. Minerbi, L. Montagnani, D. Gianelle, and F. Magnani, "Bayesian optimization of a light use ef fi ciency model for the estimation of daily gross primary productivity in a range of Italian forest ecosystems," *Ecol Modell*, vol. 306, pp. 57–66, 2015.

[371] H. S. Benavides Pinjosovsky, S. Thiria, C. Ottlé, J. Brajard, F. Badran, and P. Maugis, "Variational assimilation of land surface temperature within the ORCHIDEE Land Surface Model Version 1.2.6," *Geosci Model Dev*, vol. 10, no. 1, pp. 85–104, 2017.

[372] W. A. A. Dorigo, R. Zurita-Milla, A. J. W. J. W. de Wit, J. Brazile, R. Singh, and M. E. E. Schaepman, "A review on reflective remote sensing and data assimilation techniques for enhanced agroecosystem modeling," *Int J Appl Earth Obs Geoinf*, vol. 9, no. 2, pp. 165–193, 2007.

[373] K. P. Belyaev, C. A. S. Tanajura, and J. J. O'Brien, "A data assimilation method used with an ocean circulation model and its application to the tropical Atlantic," *Appl Math Model*, vol. 25, pp. 655–670, 2001.

[374] M. Blaas, G. Y. El Serafy, T. van Kessel, G. J. de Boer, M. A. Eleveld, and H. J. van der Woerd, "Data Model Integration of SPM transport in the Dutch coastal zone," in *Proceedings of the Joint 2007 EUMETSAT/AMS Conference*, 2007, pp. 1–8.

[375] M. Blaas, M. A. Eleveld, G. Y. El Serafy, J. Hans, V. Der Woerd, G. J. De Boer, and T. Van Kessel, "Integration of Remote Sensing and Modelling of Total Suspended Matter in the Dutch coastal zone," Delft, Netherlands, 2008.

[376] M. A. Eleveld, D. Van der Wal, T. Van Kessel, D. der Wal, and T. Van Kessel, "Estuarine suspended particulate matter concentrations from sun-synchronous satellite remote sensing: Tidal and meteorological effects and biases," *Remote Sens Environ*, vol. 143, pp. 204–215, 2014.

[377] F. J. H. Los, M. T. Villars, and M. W. M. Van Der Tol, "A 3-dimensional primary production model (BLOOM / GEM) and its applications to the (southern) North Sea (coupled physical - chemical - ecological model)," *J Mar Syst*, vol. 74, no. 1–2, pp. 259–294, 2008.

6. Annex 1

Author	Reference No.	Extent	Goal of the study	Opt. Sensor	Radar sensor	Map/output resolution	Technical algorithm of model
Gao et al. 2013	221	*local* (29 experimental plots; around 6000 m² each)	- Estimating Leaf Area Index, height, biomass and other plant variables of maize using optical and radar sensors	HJ-1 (30x30 m)	RADARSAT-2 (range: 5.2; azimuth: 7.9 m)	around 50 x 50 m (size of experimental plots)	- Linear regression analysis of optical reflectance values and SAR backscattering coefficients with plant variables of maize
Dusseux et al. 2014	222	*local* (catchement area of 61.5 km²)	- Dicriminating grassland and crop land -> comparing single use of optical data, SAR data and combined used for classification	SPOT 5 (5x5 m & 10x10 m) Landsat TM5 (30x30 m)	RADARSAT-2 (range: 12 m; azimuth: 8 m)	Field scale (different spatial resolution of input data have been harmonized using the boundaries of the fields determined by orthophotos)	- Classification of derived variable using the Support Vector Machine (SVM) - LAI and fCOVER retrieved using PROSAIL radiative transfer model (coupling of PROSPECT and SAIL models)
Koppe et al. 2012	223	*local* (four fields; average around 2.5 and 4.5 ha)	- Estimating winter wheat biomass using hyperspectral and SAR data -> comparing single use and combined use	EO-1 Hyperion (30x30 m)	Envisat ASAR (12.5x12.5 m)	Field scale (measured and extracted variables were averaged regarding parcels of homogenous management; around 6 parcels per field)	- Linear regression models between surface refelction as well as backscatter and wheat's standing biomass were established - multible regression analysis: combining hyperspectral indices and microwave backscatter as a function of crop parameters
Revill et al. 2013	227	*continental* (six different European field sites; field sizes varied from 1.5 to 97.6 ha)	- Improvement of carbon cycling model using LAI values estimated by optical and radar data -> singel and combined use tested	Combined SPOT-2 and SPOT-4 data (20x20 m)	ERS-2 (12.5 m)	Field scale (model improvement was tested at the six different fields)	- C cycle simulated using the Soil-Plant-Atmosphere (SPA) model modified for carbon allocation and croplands - updating of SPA model using LAI estimates via an Ensemple Kalman Filter approach
Attarchi & Gloaguen 2010	228	*local* (99 plots having a size of 60x60 m in the study area approximately 20x26 km)	- Improving the estimation of above ground biomass in mountaineous areas using optical and radar data	Landsat ETM+ (30x30 m)	ALOS/PALSAR (12.5x12.5 m) SRTM (90x90 m)	30 m	- Linear regression models including corrected spectral and SAR data and their derived products to estimate above ground biomass

Huang et al. 2014	229	*regional* (non-forested areas in Yellowstone National Park; 107 circular plots with a radius of 17 m)	- Estimation of sagebrush, herbaceous and bare ground cover by fusing optical and radar data	AVIRIS (17x17 m) Landsat ETM (30x30 m)	AirSAR (10x10 m)	10 m	- optical and radar data as well as derived products used for land cover classification based on threshold values, decision trees, linear interpolation and local knowledge
Xing et al. 2014	230	*local* (size of study area: 1.174 km²; 92 sample sites: 30x30 m; 3 sample plots per site: 0.5x0.5 m)	- Estimation of above ground biomass in a mixed vegetation area using optical and radar data (arid region)	Landsat-5 TM (30x30 m)	Envisat ASAR (range: 30 m, azimuth: 30 m, pixel size: 12.5 m)	30 m	- modified water cloud model (WCM) - radar data provide soil information and optical data measure vegetation coverage
Svoray & Shoshany 2003	233	*local* (study area: size unknown; 16 sample sites: 5 ha; 100 sample plots per site: 0.625 m²)	- Estimation of above ground biomass of herbaceous vegetation in a heterogenous semiarid region	Landsat TM (30x30 m)	ERS-2 SAR (no information)	30 m	- modified water cloud model (WCM) - radar data provide soil information and optical data measure vegetation coverage
Chakraborty et al. 2014	235	*regional* (2 sites a 3375.1 and 6420.6 km²)	- Monitoring submerging of vegetation biomass due to floods using radar and optical data	MODIS (500x500 m)	AMSR-E (C-band: 75x43 km, X-band: 51x29 km)	Resolution of radar data	- radar data have been employed in a radiative transfer model - optical data provided information on dominant land cover fractions
Rangoonwala et al. 2016	236	*regional* (204 km Atlantic Ocean cosatline of New Jersey; research focused on central and southern zones - no exact data on extent)	- Assessing linkages of Hurican Sandy surge persistence and changes in marsh conditions along the cosatline by combining radar and optical data	SPOT 5 (10x10 m) MODIS (232x232 m)	TerraSAR-X (up to 18x18 m) COSMO-SkyMed (30 m)	SPOT 5, TerraSAR-x and COSMO-Sky Med images were registered to USGS digital orthophote quarter quadrangles (resolution: 1x1 m); probably these data have also been downscaled to the 1-m ground resolution	- SPOT data were converted using the Atmospheric and Topographic Reduction (ATCOR) radiative transfer model to determine marsh canopy reflectance - MODIS data used to determine vegetation indice (NDVI) - radar data have been employed in the National Oceanic and Atmospheric Administration (NOAA) model to determine surge extent and persistence - different outputs have been spatially associated using a cross-correlation procedure

7. Annex 2

Author	Reference No.	Extent	Goal of the study	Opt. Sensor	Radar sensor	Map/output resolution	Technical algorithm of model
Gao et al. 2013	221	*local* (29 experimental plots; around 6000 m² each)	- Estimating Leaf Area Index, height, biomass and other plant variables of maize using optical and radar sensors	HJ-1 (30x30 m)	RADARSAT-2 (range: 5.2; azimuth: 7.9 m)	around 50 x 50 m (size of experimental plots)	- Linear regression analysis of optical reflectance values and SAR backscattering coefficients with plant variables of maize
Dusseux et al. 2014	222	*local* (catchement area of 61.5 km²)	- Dicriminating grassland and crop land -> comparing single use of optical data, SAR data and combined used for classification	SPOT 5 (5x5 m & 10x10 m) Landsat TM5 (30x30 m)	RADARSAT-2 (range: 12 m; azimuth: 8 m)	Field scale (different spatial resolution of input data have been harmonized using the boundaries of the fields determined by orthophotos)	- Classification of derived variable using the Support Vector Machine (SVM) - LAI and fCOVER retrieved using PROSAIL radiative transfer model (coupling of PROSPECT and SAIL models)
Koppe et al. 2012	223	*local* (four fields; average around 2.5 and 4.5 ha)	- Estimating winter wheat biomass using hyperspectral and SAR data -> comparing single use and combined use	EO-1 Hyperion (30x30 m)	Envisat ASAR (12.5x12.5 m)	Field scale (measured and extracted variables were averaged regarding parcels of homogenous management; around 6 parcels per field)	- Linear regression models between surface refelction as well as backscatter and wheat's standing biomass were established - multible regression analysis: combining hyperspectral indices and microwave backscatter as a function of crop parameters
Revill et al. 2013	227	*continental* (six different European field sites; field sizes varied from 1.5 to 97.6 ha)	- Improvement of carbon cycling model using LAI values estimated by optical and radar data -> singel and combined use tested	Combined SPOT-2 and SPOT-4 data (20x20 m)	ERS-2 (12.5 m)	Field scale (model improvement was tested at the six different fields)	- C cycle simulated using the Soil-Plant-Atmosphere (SPA) model modified for carbon allocation and croplands - updating of SPA model using LAI estimates via an Ensemple Kalman Filter approach
Attarchi & Gloaguen 2010	228	*local* (99 plots having a size of 60x60 m in the study area approximately 20x26 km)	- Improving the estimation of above ground biomass in mountaineous areas using optical and radar data	Landsat ETM+ (30x30 m)	ALOS/PALSAR (12.5x12.5 m) SRTM (90x90 m)	30 m	- Linear regression models including corrected spectral and SAR data and their derived products to estimate above ground biomass

Huang et al. 2014	229	*regional* (non-forested areas in Yellowstone National Park; 107 circular plots with a radius of 17 m)	- Estimation of sagebrush, herbaceous and bare ground cover by fusing optical and radar data	AVIRIS (17x17 m) Landsat ETM (30x30 m)	AirSAR (10x10 m)	10 m	- optical and radar data as well as derived products used for land cover classification based on threshold values, decision trees, linear interpolation and local knowledge
Xing et al. 2014	230	*local* (size of study area: 1.174 km²; 92 sample sites: 30x30 m; 3 sample plots per site: 0.5x0.5 m)	- Estimation of above ground biomass in a mixed vegetation area using optical and radar data (arid region)	Landsat-5 TM (30x30 m)	Envisat ASAR (range: 30 m, azimuth: 30 m, pixel size: 12.5 m)	30 m	- modified water cloud model (WCM) - radar data provide soil information and optical data measure vegetation coverage
Svoray & Shoshany 2003	233	*local* (study area: size unknown; 16 sample sites: 5 ha; 100 sample plots per site: 0.625 m²)	- Estimation of above ground biomass of herbaceous vegetation in a heterogenous semiarid region	Landsat TM (30x30 m)	ERS-2 SAR (no information)	30 m	- modified water cloud model (WCM) - radar data provide soil information and optical data measure vegetation coverage
Chakraborty et al. 2014	235	*regional* (2 sites a 3375.1 and 6420.6 km²)	- Monitoring submerging of vegetation biomass due to floods using radar and optical data	MODIS (500x500 m)	AMSR-E (C-band: 75x43 km, X-band: 51x29 km)	Resolution of radar data	- radar data have been employed in a radiative transfer model - optical data provided information on dominant land cover fractions
Rangoonwala et al. 2016	236	*regional* (204 km Atlantic Ocean cosatline of New Jersey; research focused on central and southern zones - no exact data on extent)	- Assessing linkages of Hurican Sandy surge persistence and changes in marsh conditions along the cosatline by combining radar and optical data	SPOT 5 (10x10 m) MODIS (232x232 m)	TerraSAR-X (up to 18x18 m) COSMO-SkyMed (30 m)	SPOT 5, TerraSAR-x and COSMO-Sky Med images were registered to USGS digital orthophote quarter quadrangles (resolution: 1x1 m); probably these data have also been downscaled to the 1-m ground resolution	- SPOT data were converted using the Atmospheric and Topographic Reduction (ATCOR) radiative transfer model to determine marsh canopy reflectance - MODIS data used to determine vegetation indice (NDVI) - radar data have been employed in the National Oceanic and Atmospheric Administration (NOAA) model to determine surge extent and persistence - different outputs have been spatially associated using a cross-correlation procedure